ABSTRACT

AVRAHAMI, HAVIV MOSHE. Paleobiodiversity of a New Microvertebrate Locality from the Upper Cretaceous Mussentuchit Member, Cedar Mountain Formation, Utah: Testing Morphometric Multivariate Approaches for Quantifying Shape Variation in Microvertebrate Specimens. (Under the direction of Dr. Lindsay Zanno).

When animals die, they can be preserved in a number of ways. It is often the case that the fossils of large-bodied animals receive the greatest attention and mainstream focus. However, vertebrate microfossil localities (localized concentrations of diminutive vertebrate hard parts usually comprised of isolated teeth, bones, scales, and shells) offer the opportunity to collect large amounts of data that can be used to rapidly reconstruct terrestrial vertebrate paleofaunas and determine the relative abundances of species. Here I report on a newly sampled site with the highest microfossil density yet discovered from the Mussentuchit Member of the Cedar Mountain Formation in Utah, a poorly understood interval in the early Late Cretaceous. The Cliffs of Insanity (COI) locality is one of the most taxonomically rich microvertebrate localities in the Mussentuchit Member and preserves osteichthyan, lissamphibian, testudinatan, mesoeucrocodylian, dinosaurian, metatherian, and trace fossil remains. Here I use a series of qualitative and quantitative approaches to refine taxonomic identifications of microfossils and analyze biodiversity. Multivariate analyses on a series of theropod teeth add new data on theropod tooth morphodiversity. I also provide the first descriptions of tyrannosauroid premaxillary teeth from the Mussentuchit Member. Additionally, I document the earliest occurrence of the ancestrally Asian adocid turtles, extending the earliest known appearance of this clade in North America by 5 million years. This adds support to studies documenting a pre-Cenomanian Laurasian faunal exchange across Beringia.

The majority of vertebrate remains from the COI are isolated teeth. This is in concordance with many other microvertebrate fossil localities. Because of their abundance and

high preservation likelihood, isolated teeth have the potential to serve as excellent indicators of biodiversity. However, the distribution of tooth traits across various taxonomic divisions is often not well understood and without associated skeletal material, it can be difficult to confidently refer teeth to the genus or species level. Many previous studies have conducted multivariate statistical analyses, utilizing series of linear measurements, in order to discriminate between tooth morphologies for the purpose of taxonomic identifications. The traditional method of using linear measurements has proven relatively effective at parsing out tooth morphotypes; however, this approach often fails to account for a number of morphological tooth features predicted to be important indicators of similarity. For example, characteristics such as curvature, regions of convexity and concavity, carinae orientation, and other nuances of shape are usually excluded from these analyses, or may require additional calculations and arbitrary measurements that may not be homologous across all samples. In contrast, geometric morphometrics offers the ability to statistically compare the shape of teeth with more refinement, potentially improving taxonomic identifications. Unfortunately, geometric morphometric analysis of isolated teeth is challenged by the simplicity of archosaurian teeth, which yield few discrete homologous points, and the often diminutive size of specimens, which has proven difficult to capture in 3D. Here, I characterize the shape of 32 archosaurian (theropodan, phytosaurian, mosasaurid, mesocrocodillian) and two osteichthyan teeth using traditional linear measurements, 2D and 3D geometric morphometrics, as well as combinations of these techniques, and analyze shape data using various multivariate techniques. I compare the effectiveness of these diverse protocols based on accuracy (correct placement of teeth in known taxonomic groups), data discrimination (ability to reduce convex hull overlap, identify ontogenetic differences, and account for preservation quality), and the amount of time, labor, complexity, and investment necessary.

Although data collection effort is significantly higher, I find optimum accuracy and data discrimination of isolated archosaurian teeth when traditional methods are combined with geometric methods, especially when linear measurements are combined with 3D landmarks.

Paleobiodiversity of a New Microvertebrate Locality from the Upper Cretaceous Mussentuchit Member, Cedar Mountain Formation, Utah: Testing Morphometric Multivariate Approaches for Quantifying Shape Variation in Microvertebrate Specimens

by
Haviv Moshe Avrahami

A thesis submitted to the Graduate Faculty of
North Carolina State University
in partial fulfillment of the
requirements for the degree of
Master of Science

Biology

Raleigh, North Carolina
2018

APPROVED BY:

Dr. Andrew Heckert	Dr. Adrian Smith

Dr. Lindsay Zanno
Chair of Advisory Committee

DEDICATION

To Mom

BIOGRAPHY

Haviv Avrahami was born in Los Angeles, CA where he lived for eleven years before moving to Winston-Salem, NC. He attended Appalachian State University and graduated with a BS in Geology in 2016. He decided to pursue an MS in Biology at North Carolina State University and upon graduation, he intends to remain at North Carolina State University to pursue a PhD in Biology.

ACKNOWLEDGMENTS

This study would not have been possible without the cooperation and assistance of so many people. However, first and foremost, I would like to thank my graduate advisor, Dr. Lindsay Zanno, who saw the potential in me before I could see it in myself. She stands as my highest role model, and has provided me with unending guidance, insight, encouragement, and support. I would also like to thank my undergraduate research advisor Dr. Andrew Heckert, who gave me the training, confidence, opportunities and passion to pursue a career in vertebrate paleontology. I would also like to extend my gratitude to Dr. Adrian Smith for agreeing to be on my committee. Additionally, I would like to thank Dr. Terry Gates and Lisa Herzog for their mentoring and fellowship throughout the many years field work together. I extend my gratitude to Dr. Allison Moyer, B. Rodgers, and C.Thomas for undertaking the strenuous duty of hauling sediment down from the Cliffs of Insanity and Lisa Herzog for specimen transportation and databasing. I thank Larry Martin, who first suggested I screenwash with paint sieves. I extend my appreciation to volunteers from the Finding Fossils on Friday (FFF) team at Appalachian State University's Department of Geological and Environmental Sciences including J. Humphrey, D. Hoffman, N. Brand, K. Bynum, A. Deans, Y. Delgado, A. Hendrix, J. Voris and others for sorting and picking fossils. Special thanks to K. Whitteker for providing a total count of all COI fossils. I also thank Dr. Richard Cifelli, Dr. Don Brinkman, Dr. Christophe Hendrickx, and Benjamin Pomidor for email correspondence. Additionally, I thank Dr. Aurore Canoville for training me how to prepare histological thin sections, Dr. David Button for teaching me how to perform multivariate analyses, and Khai Button for helping me investigate how to capture accurate 3D models of diminutive objects. For funding, I would like to thank the Undergraduate Research Assistantship from the Appalachian State University Office of Student Research and

The Canyonlands Natural History Association. I would like the thank the Bureau of Land Management for permits and the Utah Geological Survey for enabling this research. I extend my loving appreciation to the Romedys for their loyalty and protection when I was young, and the 'Gurkha Squad', who never lost faith in me and inspired me to become the person I am today. I would be nowhere without the support of my family: to Zoran for saving us, my brother for giving me reason to live, my grandmother for her prayers, and my uncle for his strength. Lastly, I thank my mother, who planted the seeds of curiosity in my heart long ago, and who has remained my most beloved ally and dearest friend.

TABLE OF CONTENTS

LIST OF TABLES

CHAPTER 1

CHAPTER 2:

LIST OF FIGURES

CHAPTER 1:

CHAPTER 2:

Chapter 1

A new microvertebrate assemblage from the Mussentuchit Member, Cedar Mountain Formation: insights into the paleoecology and paleobiogeography of early Late Cretaceous ecosystems in western North America

ABSTRACT

The vertebrate fauna of the Upper Cretaceous Mussentuchit Member of the Cedar Mountain Formation has been studied for nearly three decades, yet this fossil-rich rock unit continues to produce new faunal information about life in western North America approximately 98 million years ago. Here I report on the composition of the Cliffs of Insanity (COI) microvertebrate locality, a newly sampled site with the highest microfossil density yet discovered from the Mussentuchit Member. The COI locality preserves osteichthyes, lissamphibia, testudinatan, mesoeucrocodylian, dinosaurian, metatherian, and trace fossil remains and is among the most taxonomically rich microvertebrate localities in the Mussentuchit Member. Quantitative analyses of theropod teeth from the COI were combined to comprehensive databases on theropod tooth measurements in order to refine taxonomic identifications, expanding our understanding of theropod tooth morphodiversity during this poorly understood interval. Additionally, I provide the first descriptions of tyrannosauroid premaxillary teeth, and document the earliest occurrence of North American adocid remains. This extends the earliest known appearance of the ancestrally Asian testudinatan clade by 5 million years in western North America and adds support to studies of a pre-Cenomaninan Laurasian faunal exchange across Beringia. The extreme overabundance of mesoeucrocodylian remains at the COI locality produces a comparatively low measure of relative biodiversity when compared to other microvertebrate sites in the Mussentuchit and likely records a true paleoenvironmental signal that may be linked to transgression of the Western Interior Seaway or microhabitat variation.

INTRODUCTION

The Lower through Upper Cretaceous Cedar Mountain Formation records an important interval in the history of life coinciding with global climatic changes (Beherensmeyer et al. 1992) such as globally high sea levels (Hallam 1992, and Haq et al.1987; Frakes, 1999; Fassell and Bralower. 1999), global warming (Barclay et al. 2010), and the emergence of flowering plants (Crepet & Friis 1987; Upchurch and Wolfe 1987; Saward 1992). On a more regional scale, the Cenomanian of North America records a dynamically changing biodiversity with immigration of new species from other continents and increasingly complex topography caused the beginning of the Sevier Orogeny.

Subduction of the Farallon Plate beneath North America's west coast initiated the Sevier Orogeny resulting in the formation of a north-south mountain range from Canada to Mexico. Additionally, accessory topographic changes resulted in an eastward migrating forebulge (Currie, 1998; White et al., 2002; Eberth et al. 2006) followed by the full inception of the foreland basin that lead to the formation of the North American Cretaceous Western Interior Seaway (WIS; Dickinson & Snyder, 1978; DeCelles, 1986; Neilson, 1986; Kauffman et al., 1993). The flooding of North America's interior during the medial Cretaceous provides a dynamic backdrop to paleoecological studies of the Cedar Mountain Formation. In particular, the Mussentuchit Member gains progressively more coastal influence throughout its deposition as the KWIS transgresses westward across the depositional basin. This is evidenced by the erosional contact between the Mussentuchit Member and the overlying Naturita Formation (Young, 1965). Though never studied in detail, the faunas living throughout the Mussentuchit Member depositional time would have experienced a habitat shift from drier more highland-type environs, recorded in the underlying Yellow Cat through Ruby Ranch members (Suarez et al. 2014;

Hatzell, 2015), towards more humid and ultimately coastal ecosystems (Cifelli et al. 1997; Suarez et al. 2012, 2014).

In addition to the drastic change in habitat, many authors have documented changes to the standing biodiversity attributed to replacement of the indigenous North American fauna with Asiatic animals migrating via the Alaskan land bridge (Ostrom 1970; Russell 1993, 1995; Cifelli et al. 1997; Kirkland et al. 1997, 1999; Sereno 1999; Ji et al. 2003, 2009; Kobayashi and Azuma 2003; Carpenter 2006; McDonald et al. 2010; Zanno & Makovicky 2011). This immigration resulted in a reorganization of terrestrial fauna at the highest trophic levels and set the stage for the iconic Late Cretaceous assemblages and adds great complexity the study of Albian-Turonian faunas across North America.

The Mussentuchit Member (Albian-Cenomanian) of the Cedar Mountain Formation is one of the most diverse Mesozoic assemblages in North America to date. Previous studies have recognized over 90 species (Gardner 1994, 1996, 1999b; Cifelli et al. 1997, 1999; Fiorillo 1999; Gardner & Cifelli 1999; Kirkland et al. 1999, 2016; Nydam 1999, 2000a,b, 2002; Goldberg 2000; Nydam & Cifelli 2002; Cifelli 2004; Garrison et al. 2007; McDonald et al. 2017); however, as documented in this paper, more species are still being discovered (e.g., Makovicky et al., 2014; Zanno and Makovicky, 2016; Fredrickson and Cifelli, 2017). The fauna of this unit is similar to that of the older Cloverly Formation (Oreska et al. (2013).

A large proportion of paleoecological data contained in the fossil record is derived from vertebrate microfossil bonebeds (defined by Rogers et al. [2017] as “localized concentrations of small resilient vertebrate hard parts”), including the majority of vertebrate species known from the Mussentuchit Formation (Cifelli & de Muizon 1997; Cifelli 1993, 1999, 2004; Cifelli et al. 2016, 1997, 1999; Eaton & Cifelli 2001; Fiorillo 1999; Garrison et al. 2007; Goldberg 2000;

Kirkland et al. 1999; McDonald et al. 2017; Nydam 2002; Nydam & Cifelli 2002). These are concentrations of small fossils, typically 12.5 mm or smaller (Heckert 2004), that reveal broader taxonomic sampling of ancient ecosystems because microfossil sites tend to preserve the remains of small-bodied vertebrates often overlooked or not preserved in macrovertebrate sites (i.e., those fossil sites containing larger animals such as dinosaurs) (Sankey & Baszio, 2008). Extensive screen-washing and microvertebrate sampling has been conducted in the Cedar Mountain Formation between 1990 and 2000 by the Oklahoma Museum of Natural History (Cifelli 1996; Cifelli et al. 1996, 1997, 1999) with a smaller effort aimed at studying the microvertebrates from a dinosaur locality by the College of Eastern Utah (Garrison et al., 2007). Microvertebrate data collection continues through ongoing research by the North Carolina Museum of Natural Sciences and the Field Museum of Natural History. For the first time in over a decade I report on a new microvertebrate locality in the Mussentuchit Member—the Cliffs of Insanity (COI) microsite. This site adds critical information to the standing biodiversity during this transition period as well as provides new insights into immigration patterns of Asian species. Finally, the methods used herein combine those from various fields of ecology in order to apply a more wholesale quantitative approach to microvertebrate paleoecology.

Abbreviations

Institutional abbreviations: NCSM = North Carolina Museum of Natural Sciences; OMNH = Sam Noble Museum of Natural History, University of Oklahoma.

Anatomical abbreviations and terminology: ADM = anterior denticles per millimeter, AL = apical length, BW = basal width, CBL = crown basal length, CBR = crown base ratio, CBW = crown basal width, CH = tooth crown height, CHR = crown height ratio, DC = distocentral

denticle density, FABL = fore aft basal length, MC = mesiocentral denticle density, MCL = mid-crown length, MCR = mid-crown ratio, MCW = mid-crown width, PDM = posterior denticles per millimeter. Anatomical terminology follows Hendrickx (2015).

Geologic Setting

The Cedar Mountain Formation was deposited during the medial Cretaceous in eastern and central Utah and is stratigraphically bounded by the Upper Jurassic Brushy Basin Member of the Morrison Formation below and by the Upper Cretaceous Naturita Formation above (Kirkland et al. 1997, 1999; Carpenter 2014). The Cedar Mountain Formation is divided into six members that range from the Barremian/Aptian through the Cenomanian. The five members underlying the Mussentuchit record an interval of increasing aridity linked to the rise of the Sevier Mountains (Suarez et al. 2014; Hatzell 2015). By contrast, the capping Mussentuchit Member, records a rapidly changing paleoclimatic shift toward warmer, more humid conditions resulting from the transgression of the Western Interior Seaway (Cifelli et al. 1997; Suarez et al. 2012, 2014).

Sedimentologically, the Mussentuchit Member consists predominantly of highly smectitic mudstone (formed from altered volcanic ash), containing localized, low grade coal beds (Kirkland et al. 1997, 1999) and has been interpreted as either a wet, lacustrine environment (Stokes 1944, 1952; Craig 1981; Garrison et al. 2007) or a fluvial environment (Kirkland 1997; Goldberg 2000); more specifically, as a distal delta system (Sorenson 2011; Holmes 2017) at the western margin of the Western Interior Seaway in what is now central Utah (Figure 1.1 A). Radioistopic dates reported by Cifelli et al. (1997), Garrison et al. (2007), and Tucker et al. (in press) support a Cenomanian – early Turonian age (98.2 ± 0.6 to 93 Ma) for the Mussentuchit Member.

The microvertebrate fossils described here were recovered from a fine-grained sandstone sandwiched between siltstone-dominated units, approximately 5 meters below the contact with the overlying Naturita Formation. Five geologic samples above, within, and below the fossil layer were collected along a section ~1 m high (Figure 1.1 E). These samples indicate the COI microfossil assemblage displays a coarsening upwards sequence from siltstone below the fossil-bearing layer to a bentonitic, fine-grained sandstone within it and then a transition back to siltstone above the fossil-bearing layer, possibly representing an oxbow lake with an adjacent river migrating towards the lake. Precise locality information for this site is recorded at the NC Museum of Natural Sciences.

Figure 1.1: Index map with stratigraphic and geographic context.
(A) Map of North America during the Cenomanian showing migration path of Asian Fauna (modified from Early Cenomanian 1 (*Neogastroplites haasi*) -- 98.3 Ma [Blakey 2014]). **(B)** Map of Emery County and part of Sevier County, showing the relative locations of the COI and eleven OMNH localities. Colored squares represent inferred depositional environments. Map modified and derived from Cifelli et al. (1999) and Goldberg (2000). **(C)** Simplified stratigraphic cross section of the Cedar Mountain Formation with overlying and underlying formations. **(D)** Relative stratigraphic positions of the COI and nine OMNH localities. (1) Near the top, just below the Naturita Formation (2) Above the ash layer (3) Immediately below the ash layer (4) Near the bottom, above the contact with the Ruby Ranch Member. Colored squares represent inferred depositional environments. **(E)** Stratigraphic section of COI ~1m high, represented by five geologic samples. (1) Above fossil-bearing layer. (2) Top of fossil-bearing layer. (3) Middle of fossil-bearing layer. (4) Lower transition layer. (5) Below fossil-bearing layer. Scale bar equals 1 mm.

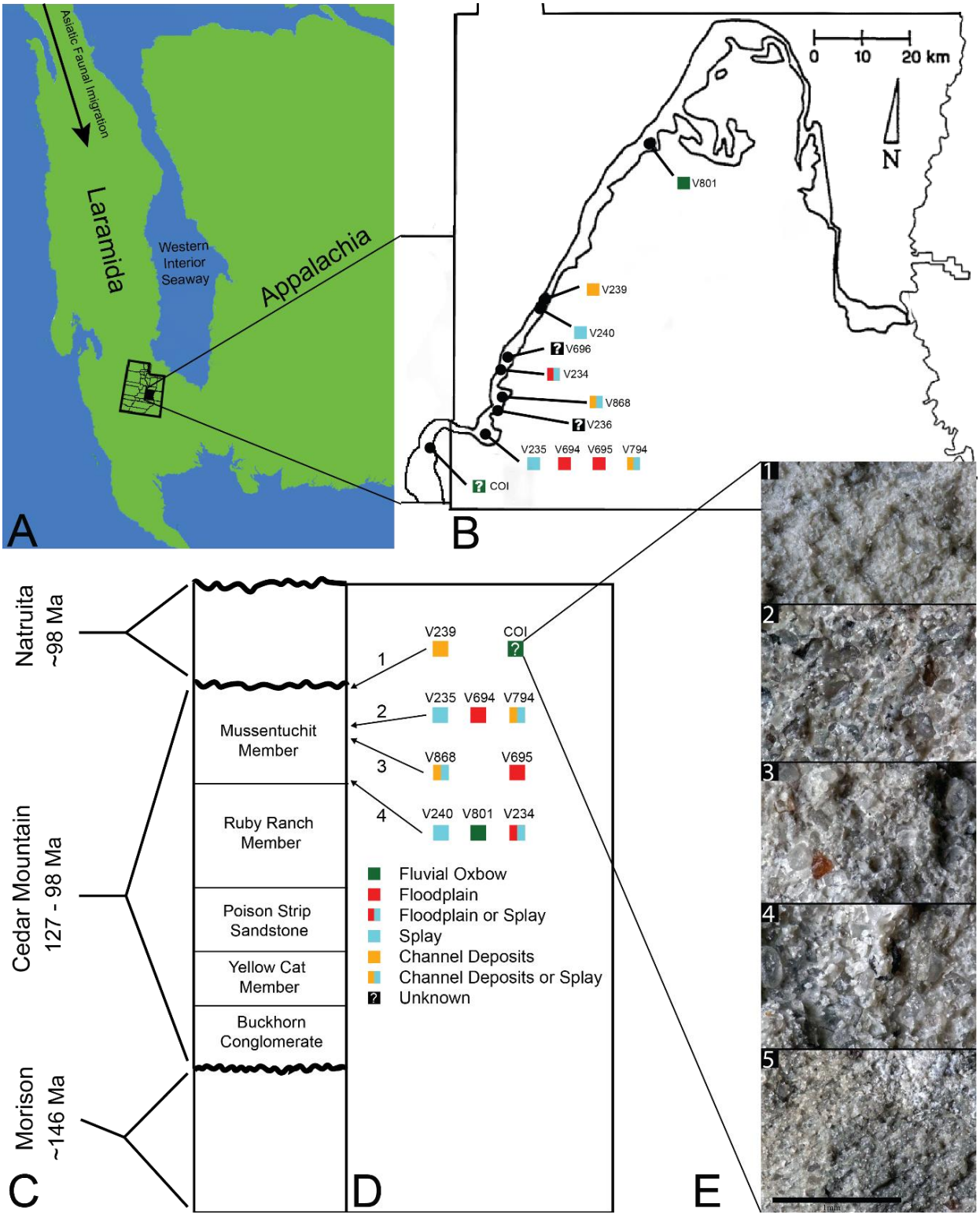
Asiatic Faunal Imigration
Laramida
Western Interior Seaway
Appalachia
A
0 10 20 km
N
V801
V239
V240
V696
V234
V868
V236
V235 V694 V695 V794
COI
B
1
2
3
4
5
Natruita ~98 Ma
Cedar Mountain 127 - 98 Ma
Morison ~146 Ma
Mussentuchit Member
Ruby Ranch Member
Poison Strip Sandstone
Yellow Cat Member
Buckhorn Conglomerate
C
D
E
Fluvial Oxbow
Floodplain
Floodplain or Splay
Splay
Channel Deposits
Channel Deposits or Splay
Unknown

The Early Cretaceous Laurasian Interchange Event

Two major dispersal events during the Cretaceous are thought to be responsible for the establishment of North America's Late Cretaceous dinosaur megafauna, which is dominated by clades with phylogenetically optimized Asian origins. This is in contrast to the endemic assemblages of the Jurassic. The Late Cretaceous Campano-Maastrichtian event has received much attention and is well supported (Gates & Sampson 2007; Godefroit et al. 2001; Ji et al. 2003; Longrich & Currie 2008; Longrich et al. 2010; Makovicky 2001; Maryanska et al. 2004; Sereno 1997). However, a number of asiatic taxa were already present in North America prior to the Campanian, emplaced during an Early Cretaceous Aptian/Albian dispersal event. (Carpenter 2006; Cifelli et al. 1997; Ji et al. 2009; Ji et al. 2003; Kirkland et al. 1997; Kirkland et al. 1999; Kobayashi & Azuma 2003; McDonald et al. 2010; Ostrom 1970; Russell 1993; Russell 1995; Sereno 1999). This interval coincides with the first occurrences of taxa bearing asian affinities and is considered one of the major factors leading to the extinction and replacement of much of North America's endemic dinosaur clades (Kirkland et al. 1997, 1999).

Two possible dispersal routes have been proposed to explain a pre-Cenomanian migration of Asiatic taxa into North America: (1) A westward dispersal route via Europe (Chinnery et al. 1998; Jerzykiewicz & Russell 1991; Russell 1993), and/or (2) a direct connection via the Beringian land bridge (Carpenter 2006; Cifelli et al. 1997; Gangloff 1998; Ji et al. 2009; Ji et al. 2003; Kirkland et al. 1997; Kirkland et al. 1999; Kobayashi & Azuma 2003; Makovicky et al. 2014; McDonald et al. 2010a; Russell 1993; Sereno 1999; Zanno & Makovicky 2011).

The Beringian and trans-European hypotheses are not necessarily mutually exclusive. however, the latter would have incurred a number of obstacles. For example, paleogeographic

reconstructions of Eastern North America and Western Europe indicate that a connection between the two continents probably did not exist during the Aptian (Doré 1991). Additionally, during the Aptian (Hay et al. 1999), or possibly as early as the Barremian (Smith et al. 1994), much of Europe became a fragmented series of islands and shallow inland seaways. Furthermore, the Western Interior Seaway divided North America during the late Albian and would have acted as an additional obstacle for westward faunal dispersals (Elder & Kirkland 1994). Faunal similarities between eastern North America and Europe vary. The presence of European aquatic vertebrates in eastern North America, such as paracryptodiran turtles (Lipka et al. 2006), does suggest there was some faunal mixing, however Cifelli et al. (1999) note that the mammalian fossil record of eastern North America is a mostly endemic composition, and the dinosaurian fossil record does not support a large scale dispersal route between these two continents (see Zanno & Mackovicky (2011) for citations on the dinosaurian paleobiogeography between eastern North America and Europe).

An Aptian/Albian age, high-latitude connection between eastern Asia and western North America has strong paleotectonic support (Plafker & Berg 1994), however, agreement on the exact timing of the EKLInE varies due to the region's complex tectonic history (Dumitru et al. 1995; Fiorillo 2008; Golonka et al. 2003; Toro et al. 2003; Yakubchuk 2008), which may be concurrent with globally low sea levels (Haq et al. 1987) and a sudden cooling event at the end of the Aptian (Mutterlose et al. 2009). Nonetheless, a suite of paleontological evidence favors a Beringian dispersal route. This includes strong phylogenetic relationships between a number of Asian and North American hadrosauroids (McDonald et al. 2010b; Norman 2004), the sudden appearance of pachycephalosaurians in the late Albian/Cenomanian (Cifelli et al. 1997; Gangloff 1998; Garrison et al. 2007), neoceratopsians from the middle to late Albian (Farke et al. 2014),

and the first appearance of several Asiatic theropods clades, during the Aptian/Albian (e.g. tyrannosaurids [Zanno & Mackovicky 2011], ornithomimids [Longrich 2008], and oviraptorosaurids [Makovicky & Sues 1998; Ostrom 1970]).

MATERIALS AND METHODS

Screen Washing and Recovery

Approximately 183 kg of in situ sediment was collected from a fossiliferous horizon ~15 m in width and 30 cm thick. The sediment, composed principally of a grey, highly bentonitic mudstone, was screenwashed in loads of 1000 grams using nylon paint sieves and traditional nested sieves (Avrahami et al. 2015). A series of aquarium air bubblers was used in conjunction with the sieves to expedite breakdown of the matrix. Approximately 95% of the matrix broke down in water (99%–100% breakdown of bentonite, with any remaining weight usually constituting fossils or sand). Concentrate from the paint sieves was size-sorted in nested sieves (4, 2, 1 and 0.5 mm aperture). The smallest mesh size used during screenwashing was number 35 mesh, with aperture diameters of 0.50 mm. This dimension is similar to the mesh size used to screen the 12 microvertebrate fossil assemblages considered in the comparative biodiversity analyses (0.59 mm, Cifelli 1996), thus I suggest that the assemblages are broadly comparable with regard to size of specimens sampled. Additionally, some surface collecting did occur at the COI; however, the vast majority of fossil material was obtained via quarrying-disaggregation methods. Specimens were imaged on a Keyence VHX-1000E microscope. A total of ~6339 fossils were recovered in the year 2014 from state lands in Utah under permit Utah 2014-447 and are reposited at the North Carolina Museum of Natural Sciences.

It should be noted that the fossil density analyses may not reflect a true assessment of each locality due to institutional variation in specimen recovery. One hundred percent of the recovered fossils from the COI were counted and catalogued by the NCSM, whereas this same approach was not applied for the specimen counts reported in Goldberg (2000). In other words, no full, actual accounting of individual fossils exists for the OMNH sites (R. Cifelli, personal communication 2018). However, in the biodiversity analyses of the COI locality I did not include materials unidentifiable to family level, such as vertebrate bone fragments, and specimens unidentifiable to family level were also likely to have been discarded during collection of the OMNH sites, rendering the biodiversity sampling more comparable.

Taxonomic Referral and Morphometrics

Taxonomic referrals are based on comparisons with previously collected specimens from the Mussentuchit Member of the Cedar Mountain Formation housed at the OMNH and a variety of comprehensive microfaunal studies. I take a conservative approach, using apomorphy-based identifications to assign specimens to the most inclusive taxonomic level possible. Fragmentary or poorly preserved material lacking autapomorphies was referred using morphological similarities and assigned to higher taxonomic levels. Dental terminology follows a number of authors depending on faunal group. These can be found in supporting descriptions and references therein.

Paleoecological studies of theropods are often difficult to conduct due to the lack of multiple specimens. This can be attributable to the propensity for theropod skeletons to be osteologically weak and fragile. Theropod teeth, however, are far more mechanically and chemically resistant, and often occur in abundance at microfossil localities. Therefore,

paleobiological and faunal studies that document the occurrence of isolated teeth is more practical than those which rely strictly on skeletal elements (Currie et al. 1990; Fiorillo 1999; Sankey 2001; Sankey 2008a; Sankey 2008b; Vullo et al. 2007). Furthermore, due to the wide morphological diversity of theropod teeth, they can be used to identify new taxa (Currie et al., 1990; Baszio 1997a, 1997b; Sankey 2001; Sankey et al. 2002; Larson 2008; Gates et al. 2015). Some theropod clades that were present in the Mussentuchit Member such as oviraptorosaurs (Makovicky et al. 2015), or likely present such as ornithomimosaurs, were toothless and thus would not be represented in microvertebrate samples.

To better constrain the diversity of theropod species represented in the sample, I followed the approach of several recent studies (Gates & Scheetz 2015; Hendrickx et al. 2014; Larson & Currie 2013; Smith et al. 2005; Williamson & Brusatte 2014) by performing principal component analyses (PCA) and linear discriminant analyses (LDA) in the program PAST version 3.19 (Hammer, Ø et al. 2001) on two, independently derived, taxonomically comprehensive databases of theropod tooth measurements including the eight theropod teeth from the COI. Measurements follow Smith et al. (2005) and Larson and Currie (2013) (Figure 1.2) and were taken in the program ImageJ (Rasband, W. S. 2011).

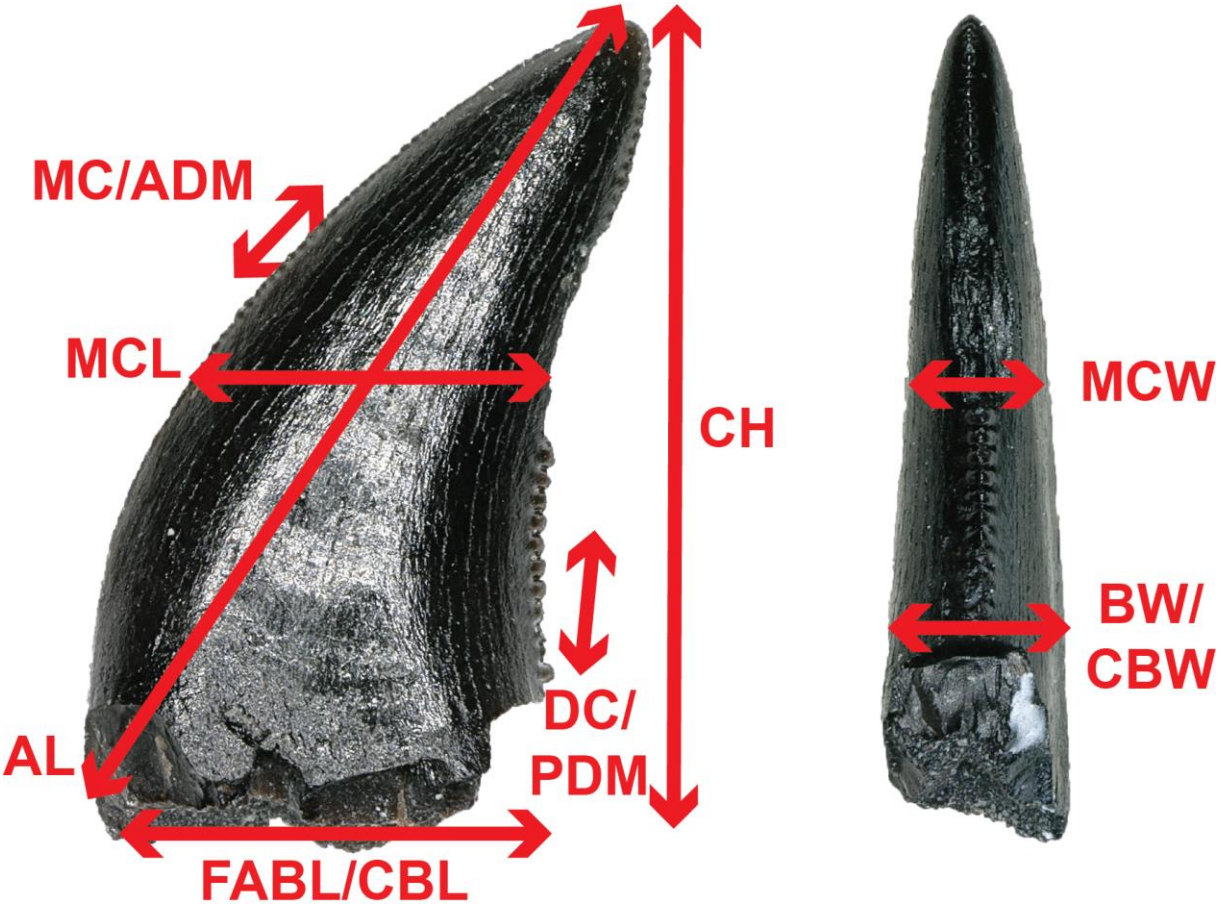

Figure 1.2: Anatomical Abbreviations:
All linear measurements and ratios used in the multivariate analyses. (**ADM**) anterior denticles per millimeter, (**AL**) apical length, (**BW**) basal width, (**CBL**) crown basal length, (**CBR**) crown base ratio, (**CBW**) crown basal width, (**CH**) tooth crown height, (**CHR**) crown height ratio, (**DC**) distocentral denticle density, (**FABL**) fore aft basal length, (**MC**) mesiocentral denticle density, (**MCL**) mid-crown length, (**MCR**) mid-crown ratio, (**MCW**) mid-crown width, (**PDM**) posterior denticles per millimeter.

Both PCA and LDA identify the hypothetical variables (components) that account for the majority of variation in a multivariable dataset by transforming the new variables into linear combinations of the original variables (Davis 1986; Harper 1999). An LDA is a supervised analysis, which discriminates according to class, whereas a PCA is an unsupervised analysis that ignores class labels (Martínez & Kak 2001).

I performed an LDA using a taxonomically extensive dataset (Hendrickx et al. 2014) that includes eight linear measurements (CBL, CBW, CH, AL, MCL, MCW, MC, DC,) and three ratios (CBR, CHR, and MCR). The Hendricks et al. (2014) dataset comprises 995 teeth belonging to one of 16 qualitative morphotype categories each representing a clade, family, paraphyletic group, or a theropod species of uncertain affinity. All values were log-transformed to better reflect a normally distributed multivariate dataset. Three theropod teeth from the COI were recovered with missing apices. To account for this uncertainty, I estimated a maximum CH for each tooth. Estimated maximum CHs were plotted in independent analyses in order to maintain statistical integrity, and resultant data points were then superimposed onto the output of prior analyses. Thus, the true point resides somewhere along the line, most likely close to the estimated CH point.

I performed a second series of PCA and LDA using a novel combination of numerical data derived from Larson and Currie (2013) and Williamson and Brusatte (2014), modified to remove samples missing a measured FABL, CH, or BW. The five principal measurements included in the combined database are FABL, CH, BW, PDM, and ADM. The modified dataset consists of 1027 teeth belonging to one of six qualitative morphotypes identified to species by previous authors. These categories include Dromaeosauridae, *Paronychodon*, *Richardoestesia*, Saurornitholestinae, Troodontidae, and Tyrannosauroidea. Teeth were further separated into a

total of 14 categories based on lithostratigraphic unit and numerical data was log-transformed to better reflect a normally distributed multivariate dataset. This independent analysis was performed in order to check and contrast the results of the LDA using the Hendricks et al. (2014) database. However, the Hendricks et al. (2014) database is superior in terms of theropod diversity, tooth completeness, confidence of taxonomic identifications, and number of measured principal components. Therefore, I consider the LDA results using the Hendricks et al. (2014) database more heavily in my taxonomic identifications than those of the other analyses.

Histology

I produced and examined paleohistological sections of isolated turtle shell to corroborate taxonomic referrals made from gross morphology. Three specimens of adocids and three specimens of helochelydrids, formerly referred to as Solemyidae (Joyce et al. 2014) were sampled. Specimens were embedded in synthetic resin and ten thin sections were produced following standard procedures for the preparation of petrographic thin sections (Scheyer et al., 2007). Sections were cut using a Buehler IsoMet 1000 Precision Saw and studied using a Nikon Eclipse Ci POL microscope equipped with an Iphone 7 camera.

Paleoecology

In order to contrast taphonomic and ecologic signals between microvertebrate localities within the Mussentuchit Member I added the faunal information from the Cliffs of Insanity locality to the Goldberg (2000) dataset of 12 sites, then reduced taxonomic data to family-level and higher using actual counts as opposed to simple presence-absence. Next, we used this database to calculate three quantities: fossil densities, the proportion of the total number of fossils that each locality contributed to the dataset, and the Shannon-Wiener biodiversity index

(Shannon & Weaver 1949; Spellerberg & Fedor 2003). Fossil density for each site was calculated as the *total number of fossils from a locality divided by the total sediment weight sampled from that site*. This is not, strictly speaking, a density because volume was not in the equation, but total weight of sediment is the most often provided measurement for the amount of sediment sampled from a microvertebrate locality. The proportion of fossils in the dataset was calculated as the *total number of fossils from each locality divided by the total number of fossils included in the entire database*. The proportion of fossils provides a measure of influence for each site when assessing the pie chart of total diversity from microvertebrate localities, rarefaction curves, and Shannon-Wiener biodiversity index calculated for the entire dataset.

Lastly, rarefaction curves were produced to assess the likelihood of recovering additional higher-level taxa from each locality. As mentioned, the database used for this calculation is based on family-level taxonomy and above. As such, the rarefaction is calculating the likelihood of finding new taxa at those taxonomic levels, not at the species level. Both the Shannon-Wiener diversity indices and the rarefaction curves were produced using PAST (version 3.19; Hammer et al. 2001).

It should be noted that the fossil density analyses may not reflect a true assessment of each locality due to institutional variation in specimen curation. One hundred percent of the recovered fossils from the COI were counted and catalogued by the NCSM, whereas this same approach was likely not applied for the specimen counts reported in Goldberg (2000). In other words, no full, actual accounting of individual fossils exists for the OMNH sites (R. Cifelli, personal communication 2018). Additionally, materials unidentifiable to family level, such as vertebrate bone fragments, were not included in the biodiversity analyses.

Finally, to assess the impact of geology and stratigraphic position on the preserved fauna, I used multivariate techniques to draw comparisons with the other vertebrate microfossil sites in the Mussentuchit Member. I produced a correspondence analysis (CA) in PAST version 3.19 (Hammer et al. 2001), using the same faunal data from the paleoecology analyses. CA is a multivariate ordinal technique used to explore relationships among a matrix of categorical or continuous variables (Hammer et al. 2001) and has been used by other studies to understand diversity changes across gradients (e.g., Gates et al. 2010), because of the method's robust nature to missing data (Hirsch and Jackson 2007). Eleven of the twelve OMNH microsites were associated with one of four types of depositional environment, categorized by Goldberg (2000) as either fluvial oxbow, floodplain, crevasse splay, or channel deposits. In my analysis, each site was categorized according to Goldberg's assessment whereas COI was categorized as an ox-bow lake according to my geologic interpretation.

RESULTS

First, we present our taxonomic assessment of the assemblage in a traditional "Systematic Paleontology" format, followed by subsequent analyses of biodiversity, paleoecology, and paleoenvironmental influences, based on comparisons of the COI assemblage with other microvertebrate assemblages from the Mussentuchit Member.

SYSTEMATIC PALEONTOLOGY
OSTEICHTHYES Huxley, 1880
ACTINOPTERYGII Klein, 1885
NEOPTERYGII Regan, 1923

Approximately 112 teeth (Figure 1.3 A–Z6), 53 complete or partial scales (Figure 1.3 Z10–Z12), and skeletal and vertebral fragments were recovered representing Osteichthyes.

Amiiform and lepisosteiform teeth constitute the majority of material, whereas only three teeth represent pycnodontids. Fish material unidentifiable to lower taxonomic levels are shown in Figure 1.3 Z7–Z12.

AMIIFORMES Hay, 1929 (sensu Grande and Bemis, 1998)
AMIINAE Bonaparte, 1838

Amiid teeth from the COI possess a suite of characteristics typical of Amiidae as outlined by Estes & Sanchíz (1982), including a styliform morphology with a rounded crown situated atop a bony pedestal (Figure 1.3 A–E). Well-developed carinae extend from the crown base to the apex and the teeth become increasingly transparent towards the apex similar to those described by Bryant (1988).

LEPISOSTEIFORMES Hay, 1929
LEPISOSTEIFORMES indent

Over 56 partial scales attributable to gars were discovered at the COI site, as is common for many nonmarine Cretaceous microvertebrate fossil concentrations. For taxonomic assignment I followed Grande (2010) and Brinkman et al. (2013, 2014) in considering isolated scales as generically indeterminate.

LEPISOSTEIDAE Cuvier, 1825

There are three morphotypes of lepisosteiform teeth from the COI. Two of these were originally described by Bilelo (1969; but see also Estes & Sanchíz, 1982; Fiorillo, 1999) as dentary and palatal teeth of lepisosteids from the Paluxy Formation of north-central Texas, and a third, lanceolate tooth type was described by Brinkman et al. (2013) from the Kaiparowits Formation and the John Henry Member of the Straight Cliffs Formation. McDonald et al. (2017) illustrated the first gar tooth from the Mussentuchit Member, which has striking similarities to

specimens in the COI such as those in Figure 1.3 L-P. Dentary (marginal?) teeth are short, broad, and conical with a smooth, translucent crown, and are occasionally falcate (Figure 1.3 F–H). Teeth of the palatine are hemispherical with a smooth, convex crown (Figure 1.3 I–K). The third tooth type accounts for the majority of recovered lepisosteiform material and is similar to the first type in that they are conical and translucent. However, the crowns possess elongated, narrow peduncles that constrict below the apex (Figure 1.3 L–P). The apex is distinguished by short, well-developed, mesio-distal carinae.

PYCNODONTIFORMES Berg, 1940

Pycnodontiform teeth from the COI are strongly falcate, with a smooth, translucent crown (Figure 1.3 Q–Z). They are strongly labiolingually compressed and lack any striations or a carinae. They are identical to pycnodont teeth recovered at the Cifelli #2 *Eolambia caroljonesa* Quarry in Mussentuchit Wash of Utah (Garrison et al. 2007) as well as other localities across the Cretaceous of North America (Brinkman et al. 2013).

SALMONIFORMES Greenwood, Rosen, Weitzman, and Myers, 1966
cf. ENCHODONTIDAE Lydekker, 1889

NCSM 33308 may represent an Enchodus tooth fragment (Figure 1.3 Z1–Z6), sharing a suite of features with those described in Fiorillo (1999) and Winkler et al. (1990). The tooth fragment is slender and labiolingually compressed with a lenticular cross section in basal view. It is slightly recurved, and the apex is blunt and rounded. The enamel is smooth and thin, lacking striations, and there are weakly defined carinae on the mesial and distal margins. The fragmentary nature of NCSM 33308 makes an accurate referral to Enchodus tenuous, however the presence of three *Enchodus* teeth that have been previously reported from the Mussentuchit Member (OMNH 026333, 026983, and 032537) may add support for this referral.

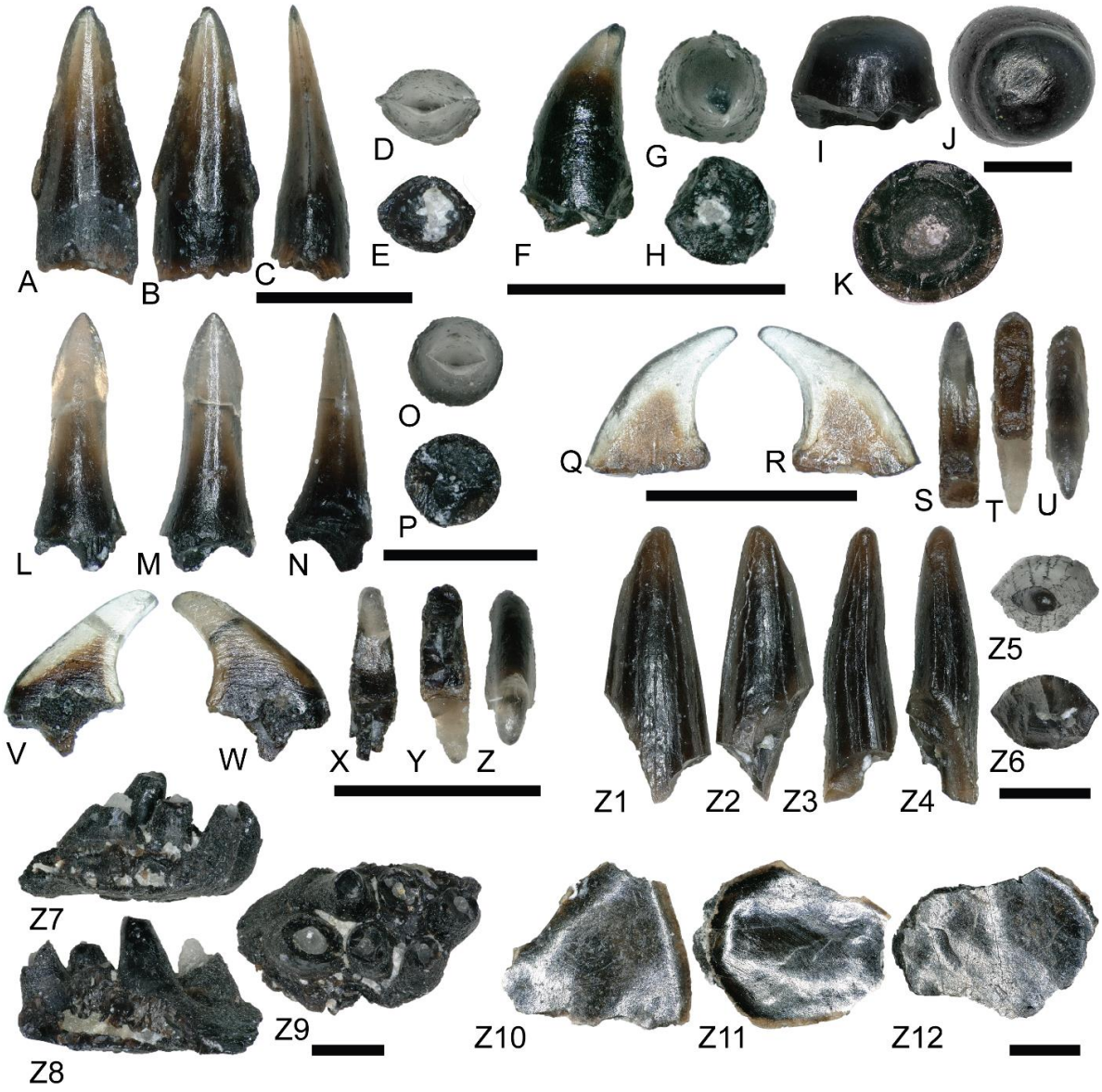

Figure 1.3: Osteichthyan teeth.
(A–E) (NCSM 33292) Amiid tooth in (A) lingual, (B) labial, (C) mesial?/distal?, (D) occlusal, and (E) basal views. **(F–G)** (NCSM 33279) Lepisosteiform marginal tooth in (F) mesial?/distal?, (G) occlusal, and (H) basal views. **(I–K)** (NCSM 33280) Lepisosteiform vomerine tooth in (I) mesial?/distal?, (J) occlusal, and (K) basal views. **(L–P)** (NCSM 33282) Lepisosteiform tooth in (L) labial, (M) lingual, (N) mesial?/distal?, (O) occlusal, and (P) basal views. **(Q–U)** (NCSM 33304) Pycnodontiform tooth in (Q–R) labial?/lingual?, (S) distal, (T) basal, and (U) occlusal views. **(V–Z)** (NCSM 33303) Pycnodontiform tooth in (V–W) labial?/lingual?, (X) distal, (Y) basal, and (Z) occlusal views. **(Z1–Z6)** (NCSM 33307) Enchodontid tooth fragment in (Z1) labial, (Z2) lingual, (Z3–Z4) mesial?/distal?, (Z5) occlusal, and (Z6) basal views. **(Z7–Z9)** (NCSM 33297) Fish spines in (Z7–Z8) mesiodistal/labiolingual and (Z9) dorsal views. **(Z10–Z12)** (NCSM 33361) fish scales. Scale bars equal 1 mm.

LISSAMPHIBIA indet. Haeckel, 1866
ALLOCAUDATA Fox and Naylor, 1982
ALBANERPETONTIDAE Fox and Naylor, 1982
ALBANERPETON Estes and Hoffstetter, 1976
ALBANERPETON, n. sp.

NCSM 33278 (Figure 1.4) is a lissamphibian dentary bearing three complete teeth and one tooth fragment. Much of the jaw is missing and the lack of diagnostic elements makes assigning it to a lower taxonomic level difficult. However, Gardner (1999a) describes several dental characteristics of *Albanerpeton arthridion* that NCSM 33278 shares. These include teeth with strong labiolingual compression that are non-pedicellate, chisel shaped, and with strong pleurodont implantation. Additionally, teeth are straight and arranged closely together along the parallel orientations of their lengths. Oreska et al. (2013) describe *Albanerpeton* material from the Cloverly Formation resembling NCSM 33278.

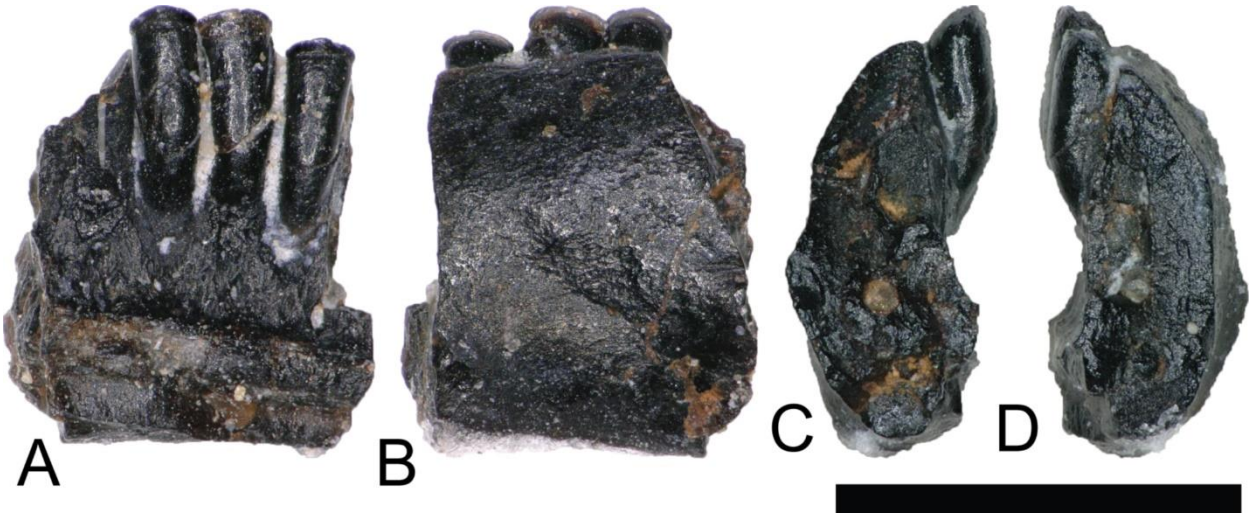

Figure 1.4: *Albanerpeton* dentary
(NCSM 33278) Lisamphibian dentary fragment likely belonging to a species of *Albanerpeton* in **(A)** medial, **(B)** lateral, and **(C–D**) cross section views. Scale bar equals 1 mm.

REPTILIA Linnaeus, 1758
TESTUDINATA Klein, 1760
HELOCHELYDRIDAE (SOLEMYDIDAE) Lapparent de Broin and Murelaga, 1996

The majority of turtle materials from the COI are referable to a new species of helochelydrid, previously referred to *Naomichelys speciosa* (Herzog et al. 2015). Helochelydrid shell fragments, characterized by a dense arrangement of raised, cylindrical tubercles, are common throughout the Mussentuchit Member (Herzog et al. 2015). Tubercles are typically 0.5–1 mm tall with planar apices and constricted bases (Figure 1.5 A–B). Microstructurally, COI helochelydrid shell samples are similar to *Solemys vermiculata* and *Solemys sp.* previously reported from Spain, and *Naomichelys sp.* previously reported from Canada and USA (Scheyer et al. 2015). All samples possess a dipole structure with cortices of relatively equal thickness (Figure 1.5 C). The external cortex is characterized by an outer zone of ornamental tubercles composed of parallel-fibered bone (Figure 1.5 D). The lower zone of the external cortex is composed of coarse, interwoven structural bone fibers (Figure 1.5 E). The cancellous bone is comprised of long slender trabeculae with large intertrabecular regions (Figure 1.5 F). Secondary lamellar bone is often present along the walls of the trabeculae. The internal cortex is made of parallel fibered bone and occasionally grades into lamellar zonal bone (Figure 1.5 G).

ADOCIDAE Cope, 1870

The COI contains shell fragments likely representing a new species of adocid (Figure 1.5 H–O). Danilov et al. (2011) describes adocid shell sculpturing as having a diagnostic arrangement of small and regular grooves and pits or dots. COI shell fragments ascribed to Adocidae are similar to those described by Danilov et al. (2011, 2013) and are characterized by a smooth surface with small pits and rhomboidal sulci. A few shell fragments are sculptured,

bearing small grooves and pits (Figure 1.5 H–J). The identification of these specimens as adocid is supported by similarities of internal microstructure (Scheyer et al. 2017). All samples possess thick, densely packed external and internal cortical bone with well-developed interior cancellous bone (Figure 1.5 K). The external cortex is divided into upper and lower zones. The lower zone (bordering the internal cancellous bone) is made of interwoven structural fibers and is characterized by a reticular vascular pattern. The upper zone (bordering the external surface) is characterized by highly birefringent growth marks exhibiting a wavy pattern, and diagonally oriented Sharpey's fibers (Figure 1.5 L). The cancellous bone is less spongy than found in *Helochelydra*, and is made of coarse, dense, short trabeculae with round to oval intertrabecular regions (Figure 1.5 N). Secondary lamellar bone is often present along the walls of the trabeculae. The internal cortex is made of parallel-fibered bone and occasionally grades into lamellar zonal bone (Figure 1.5 O).

Figure 1.5: Helochelydra and adocidae shell histology
(A–G) Helochelydra. (**H–O),** Adocidae. (**A–B)** (NCSM 33383) shell fragment showing external ornamentation pattern. **(C)** (NCSM 33380) Sectioned Helochelydra specimen in polarized light and thresholded indicating internal bone density. **(D)** Close-up of ornamentation in polarized light. **(E)** (NCSM 33388) Close-up of the ECO in polarized light. **(F)** (NCSM 33380) close-up of the CB showing trabeculae and SO, in polarized light. **(G)** (NCSM 33388) close-up of the internal cortex showing PFB, in polarized light. **(H–J),** shell fragments showing external sculpting pattern (NCSM 33387, NCSM 33382). (**K)** (NCSM 33381) Sectioned Adocidae specimen in polarized light and thresholded indicating internal bone density. **(L)** (NCSM 33387) Close-up of ECO in polarized light with ISF in the lower zone and GM and ShF in the upper zone. **(M)** close-up of the RVP in normal transmitted light and polarized light. **(N)** (NCSM 33381) close-up of the CB showing SO with lamellar bone around the internal walls, in polarized light. **(O)** (NCSM 33387) close-up of the internal cortex showing PFB, in polarized light. Abbreviations: **CB**, cortical bone; **ECO**, external cortex; **GM**, growth mark; **ISF**, interwoven structural fiber bundles; **OP**, ornamentation pattern; **PC**, primary vascular canal; **PFB**, parallel-fibred bone; **RVP**, reticular vascularization pattern; **SO**, secondary osteon; **ShF**, Sharpey's fibers. Scale bars equal 1 mm unless otherwise noted.

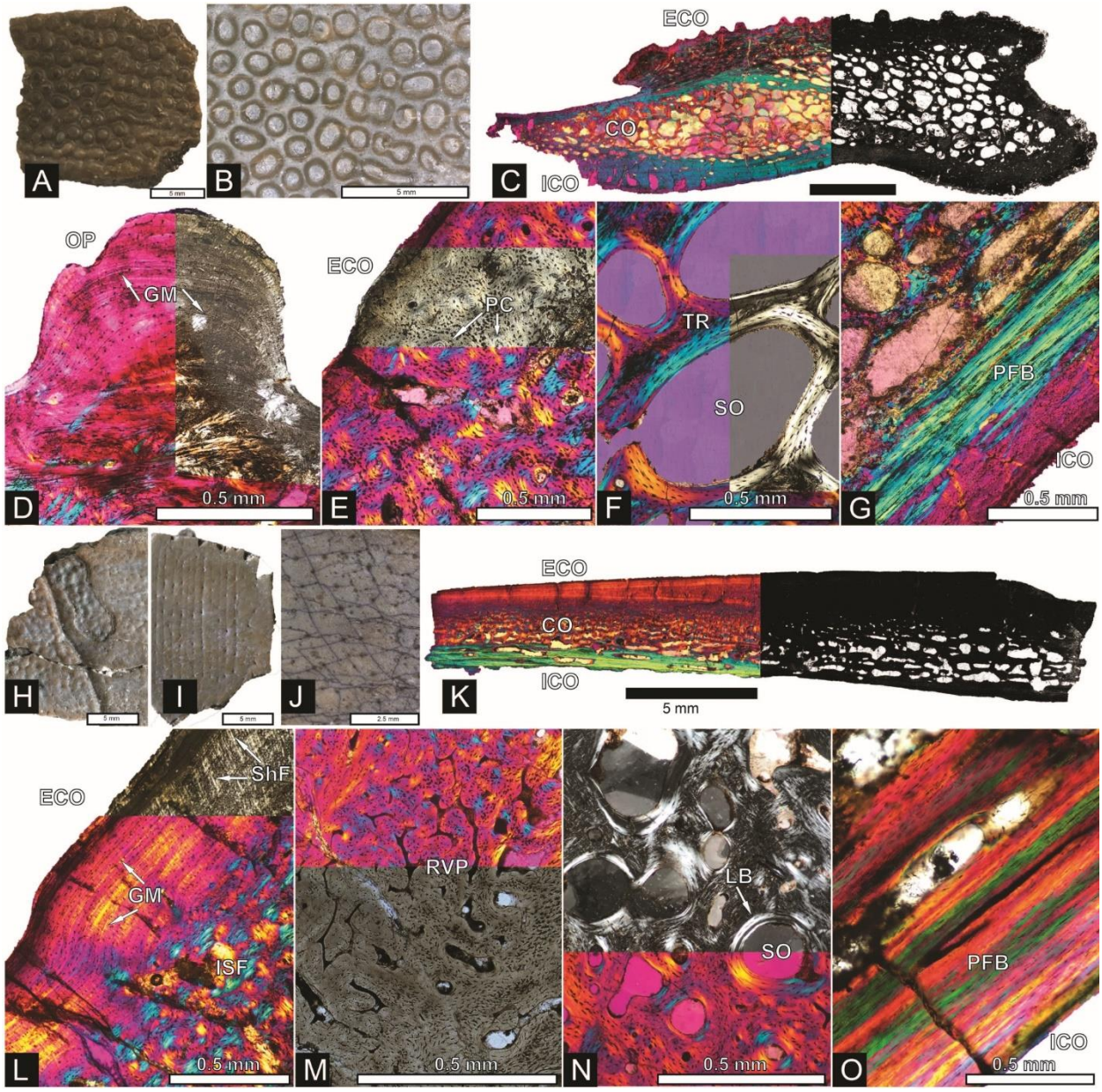
A
B
5 mm
C
ECO
CO
ICO
5 mm
OP
GM
D
0.5 mm
ECO
PC
E
0.5 mm
TR
SO
F
0.5 mm
PFB
ICO
G
0.5 mm
H
I
J
2.5 mm
ECO
CO
ICO
K
5 mm
ECO
ShF
GM
ISF
L
0.5 mm
RVP
M
0.5 mm
LB
SO
N
0.5 mm
PFB
ICO
O
0.5 mm

SQUAMATA Oppel, 1811

Squamata is represented by two isolated teeth (Figure 1.6 A–J) and a jaw fragment bearing two teeth (Figure 1.6 K–M). The poorly preserved and fragmentary condition of these specimens makes confident referrals to lower taxonomic levels difficult, however they share a suite of characteristics with squamate dental material described from the Mussentuchit Member (Nydam 2002) and other Cretaceous-age sedimentary rocks (Nydam, 2013).

SCINCOMORPHA Camp, 1923

NCSM 33293 is a scincomorphan (paramacellodid–cordylid grade) (R. Nydam, personal communication 2018) with subpleurodont implantation and deposits of cementum at the base (Figure 1.6 A–E). The tooth is tall, narrow, conical, slightly recurved distally, with a weakly defined carina and several weakly developed striations on the lingual crown surface.

SQUAMATA indet.

NCSM 33295 is a poorly preserved, isolated tooth possibly belonging to Squamata (Figure 1.6 F–J). The tooth is tall, narrow, conical, lacks curvature, and is subpleurodont with heavy deposits of cementum at the base.

SQUAMATA indet.

NCSM 33296 is a possible scincomorphan jaw fragment with two closely placed teeth (R. Nydam, personal communication 2018) (Figure 1.6 K–M). The complete tooth is tall, conical, lacks curvature, has heavy deposits of cementum at the base. The enamel is poorly preserved, improving slightly toward the tooth crown. The tooth crown is rounded and blunt, with a weakly defined carina.

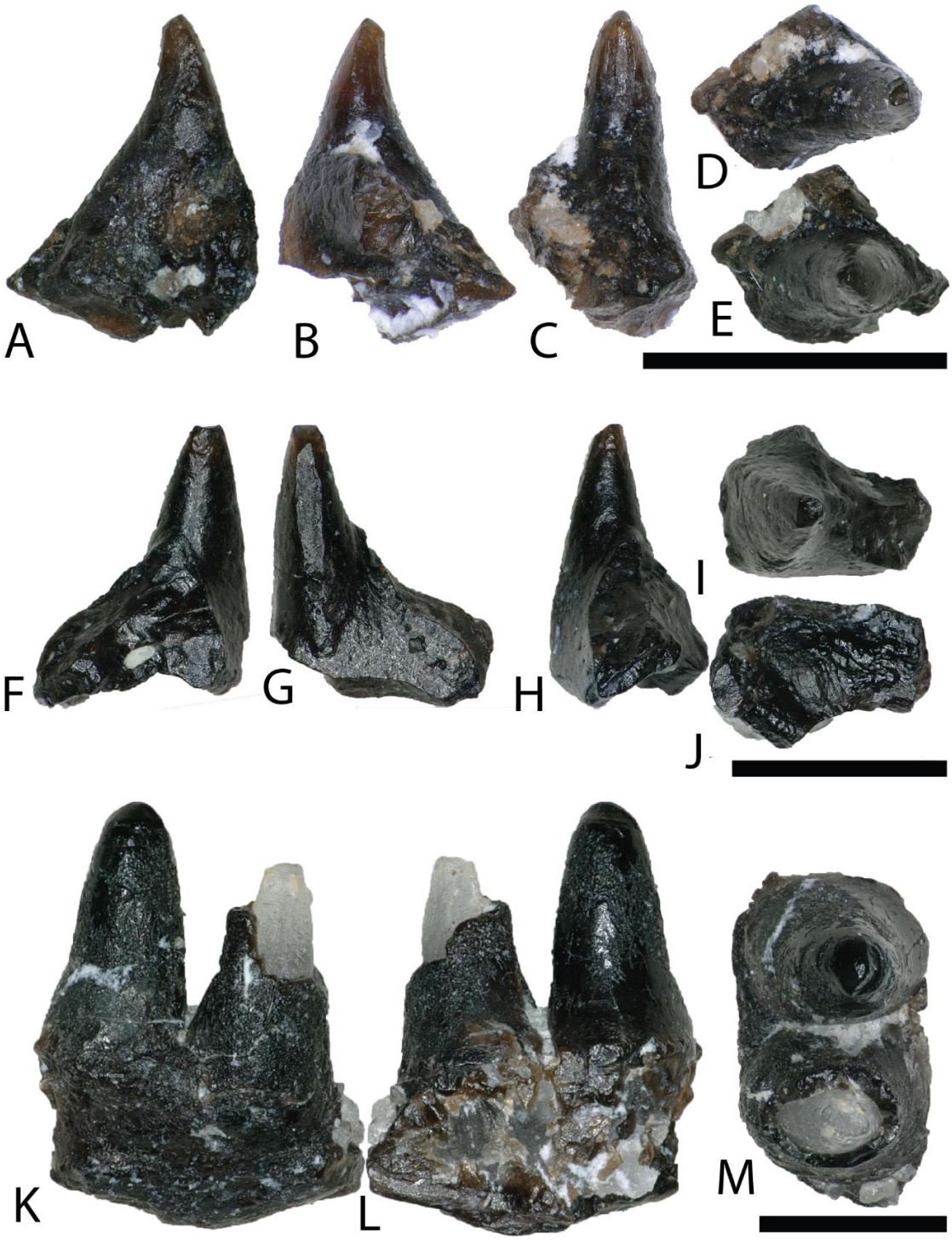

Figure 1.6: Squamata teeth
(A–E) (NCSM 33293) scincomorphan tooth in (A) mesial?/distal?, (B) mesial?/distal?, (C) lingual, and (D–E) occlusal views. **(F–J)** (NCSM 33295) Possible squamata tooth in (F–H) mesiodistal?/labiolingual?, (I) occlusal view, and (J) basal view **(K–M)** (NCSM 33296) Possible scincomorphan jaw fragment in (K–L) medial?/lateral? view, and (M) dorsal view. Scale bars equal 1 mm.

ARCHOSAURIA Cope, 1869
CROCODYLIFORMES Hay, 1930, sensu Benton and Clark, 1988
MESOEUCROCODYLIA Whetstone and Whybrow, 1983

By far the most abundant identifiable material from the COI is crocodyliform (Figure 1.7), constituting approximately 94% of teeth as well as abundant osteoderm fragments. I note similarities of these teeth to four Late Cretaceous groups (bernissartids, atoposaurids, pholidosaurids, and cf. *Dakotosuchus*). However, these assignments should be considered tentative as there is a great variability within and between tooth morphologies, with many teeth possessing a suite of characteristics along a gradational spectrum (Buscalioni et al. 2008). Following the example of McDonald et al. (2017), I simply consider the morphotypes under Mesoeucrocodylia with no further speculation to their taxonomic framework.

MESOEUCROCODYLIA indet.

Teeth I identify as similar in morphology to bernissartids are apico-basally short, mesio-distally elongate, labiolingually compressed, and slightly reniform in occlusal view (Figure 1.7 A–J). The crowns often possess an elliptical apical wear facet. The mesial and distal margins have poorly defined carinae and the labial and lingual faces are ornamented with widely spaced, well-defined, apicobasally oriented striations that converge towards the apex. Teeth matching this description have been recovered from the Lower Cretaceous Cloverly Formation of Wyoming and Montana and the Rabekke, Jydegård, and Annero formations of Scandinavia (Schwarz-Wings et al. 2009; Oreska et al. 2013).

Teeth resembling atoposaurids from the COI are proportionately taller, labiolingually compressed, and reniform in occlusal view (Figure 1.7 K–T). They are constricted toward the crown base and have well-developed, sometimes crenulated, mesial and distal carinae. They are

typically triangular in mesio-distal view, with a strongly convex labial face and a weakly convex lingual face. Tooth crowns range from strongly rounded to moderately acuminate and have varying degrees of recurvature. Striations run apicobasally, are sometimes anastomosing, and are typically more pronounced on the lingual face. Recent descriptions of similar teeth have come from the Cloverly Formation of Wyoming and Montana and other sites in the Mussentuchit Member of the Cedar Mountain Formation (Garrison et al. 2007; Oreska et al. 2013; McDonald et al. 2017).

Teeth morphologically similar to those of pholidosaurids are considerably taller, strongly conical, and have nearly circular bases (Figure 1.7 Z–Z14). Smaller teeth are tall and slender, with slight lingual recurvature and sharp apices (Figure 1.7 Z–Z9). Larger teeth tend to be more stout with rounded apices (Figure 1.7 Z10–Z14). Mesial and distal carinae extend from the base to the apex and are weakly defined. Striations are strongly defined and run apicobasally, sometimes anastomosing towards the apex. Larger, stouter teeth have numerous, thin, well defined striations that run apicobasally (Figure 1.7 Z10–Z14). These larger teeth have been previously reported from the Cedar Mountain Formation as a fifth group of teleosaurid teeth similar to *Machimosaurus* (Cifelli et al. 1997), which display a nearly complete sinusoidal curve outlined by the primary carinae in apical view (R. Nydam, personal communication 2018).

NCSM 33362 and NCSM 33384 are mesoeucrocodylian osteoderms (Figure 1.7 Z15–Z16). Due to breakage there is no evidence of an anterior bar or posterior suture to aid identification and so I assign these osteoderms to Mesoeucrocodylia indet. NCSM 33384 possesses a random array of approximately equal-sized round pits, generally similar to the morphology on pholidosaurids and goniopholids. One feature on NCSM 33362 is a low median keel that barely rises above the level of the dermal body (Figure 1.7 Z15).

cf. *DAKOTASUCHUS* sp. Mehl (1941)

Teeth I identify as similar to *Dakotasuchus* are conical, sometimes slightly lingually recurved, and typically sub-circular in occlusal view (Figure 1.7 U–Y) (Frederickson 2017). They are somewhat labiolingually compressed, with the labial side slightly more convex than the lingual. Tooth bases are circular to somewhat elliptical and the crown apices are strongly pointed. Both the mesial and distal carinae extend from the base to the apex and are less pronounced than those of similar to atoposaurid-like teeth. Enamel ornamentation is characterized by multiple, weakly defined, apicobasally oriented, parallel striations. Teeth of *Dakotasuchus* are morphologically similar to goniopholid and pholidosaurid teeth (Garrison et al. 2007; Puértolas-Pascual et al. 2015; Frederickson 2017).

Figure 1.7: Mesoeucrocodylia teeth and osteoderms
(A–E) (NCSM 33284) Bernissartid-like tooth in (A) labial, (B) lingual, (C) mesial?/distal?, (D) occlusal, and (E) basal views. (**F–J)** (NCSM 33286) Bernissartid-like tooth in (F) labial, (G) lingual, (H) mesial?/distal?, (I) occlusal, and (J) basal views. **(K–O)** (NCSM 33305) atoposaurid-like tooth in (K) labial, (L) lingual, (M) mesial?/distal?, (N) occlusal, and (O) basal views. **(P–T)** (NCSM 33315) atoposaurid-like tooth in (P) labial, (Q) lingual, (R) mesial?/distal?, (S) occlusal, and (T) basal views. **(U–Y)** (NCSM 33269) *Dakotasuchus* teeth in (U) labial, (V) lingual, (W) mesial?/distal?, (X) occlusal, and (Y) basal views. **(Z–Z4)** (NCSM 33290) Pholidosaurid-like tooth in (Z) labial, (Z1) lingual, (Z2) mesial?/distal?, (Z3) occlusal, and (Z4) basal views. **(Z5–Z9)** (NCSM 33289) Pholidosaurid-like tooth in (Z5) mesial?/distal?, (Z6) lingual, (Z7) mesial?/distal?, (Z8) occlusal, and (Z9) basal views. **(Z10–Z14)** (NCSM 33270) Pholidosaurid-like teleosaurid tooth in (Z10) labial, (Z11) lingual, (Z12) mesial?/distal?, (Z13) occlusal, and (Z14) basal views. (**Z15–Z16),** (NCSM 33362, NCSM 33384) mesoeucrocodylia osteoderms. Scale bars equal 1 mm unless otherwise noted.


A
B
C
D
E
F
G
H
I
J
K
L
M
N
O
P
Q
R
S
T
U
V
W
X
Y
5 mm
Z
Z1
Z2
Z3
Z4
Z5
Z6
Z7
Z8
Z9
Z10
Z11
Z12
Z13
Z14
5 mm
Z15
Z16
5 mm

DINOSAURIA Owen, 1842
SAURISCHIA Seeley, 1887
THEROPODA Marsh, 1881

Theropods from the COI are represented by 8 complete to partially complete teeth, 20 tooth fragments, and 11 bone fragments. Tooth and bone fragments are too poorly preserved to allow for confident lower level taxonomic identifications. Therefore, only the 8 well-preserved teeth are described here. These 8 teeth are identified to varying degrees of taxonomic confidence based on qualitative features and the results of the morphological analyses (Figure 1.8). Qualitative tooth descriptions are based on Hendrickx (2015).

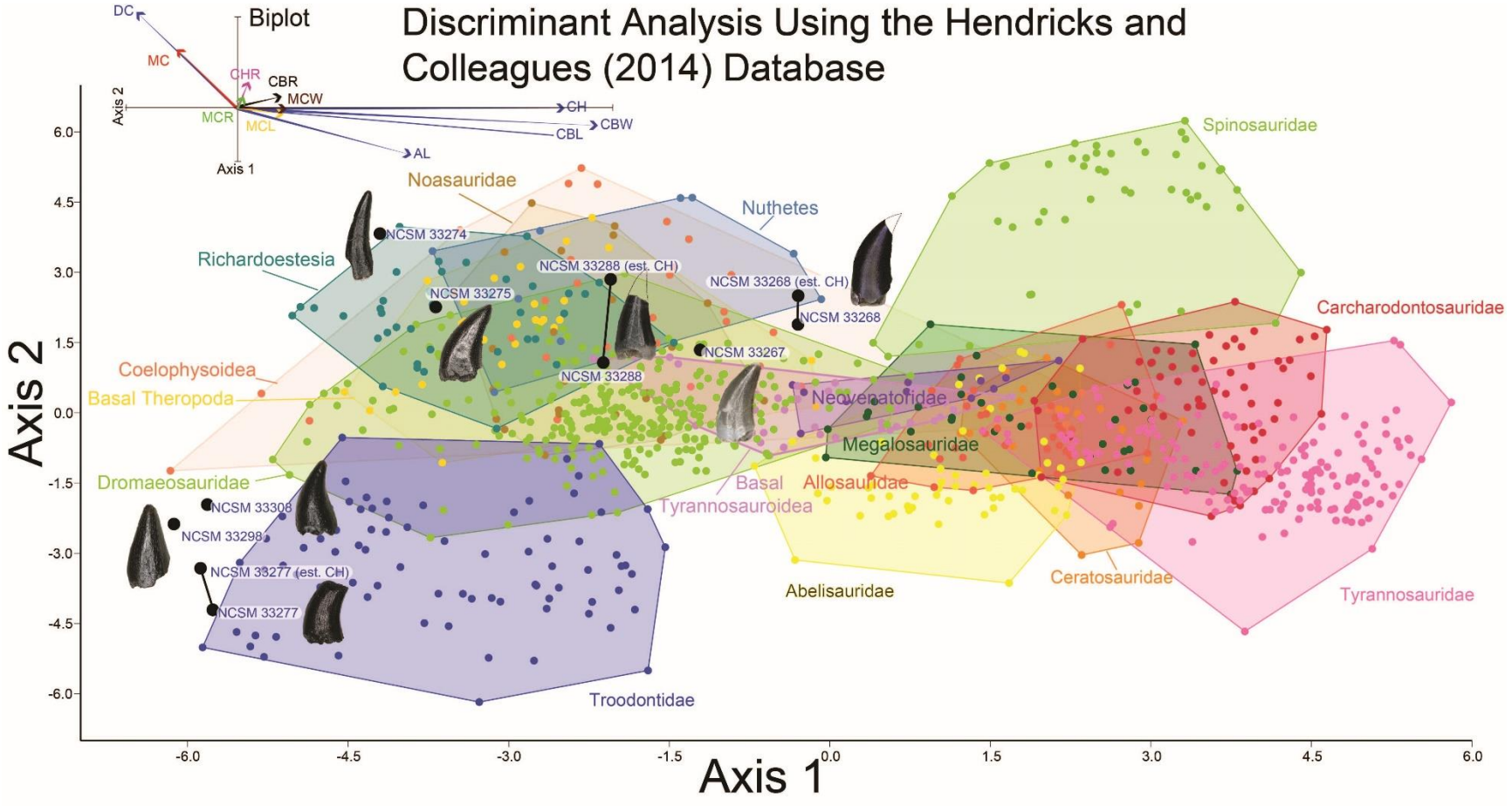

Figure 1.8: Linear discriminant analysis of theropod teeth
Multivariate analysis of eight theropod teeth from the COI and 994 theropod teeth from Hendrickx et al. (2014). All linear measurements were log-transformed. The biplot and eigenvectors represent the direction and magnitude of each linear measurement and ratio.

COELUROSAURIA von Huene, 1914
COELUROSAURIA indet.

NCSM 33268 (Figure 1.9 G–N) is the largest theropod tooth recovered from the COI, with a preserved crown height of 17.5mm, an estimated crown height of ~20 mm, a FABL of 8.39 mm, and a basal width of 4.5 mm. The exact crown height is unknown because the apical portion of the tooth is missing. The tooth is robust, lacks recurvature in mesial view, and possesses a wide elliptical basal cross section. The enamel texture is veined and apicobasally oriented. Both the anterior and posterior denticles are subrectangular in shape and centrally positioned. The mesial carinae becomes unserrated towards the base as is typical with tyrannosaurids (Buckley 2010). When considered as part of the Hendrickx et al. (2014) database (Figure 1.8), NCSM 33268 plots within the Coelophysoidea and *Nuthetes* morphospaces, the former being an improbable identification for a Late Cretaceous theropod and the latter, an enigmatic theropod of indeterminate affinity, but likely referable to dromaeosaurids or tyrannosauroids (Sweetman 2004; Rauhut et al. 2010). However, in the PCA and LDA performed with the combined (Larson & Currie 2013; Williamson & Brusatte 2014) database NCSM 33268 consistently plots within or adjacent to Tyrannosauroidea and Dromaeosauridae.

TYRANNOSAUROIDEA Osborn, 1906

NCSM 33276 (Figure 1.9 A–F) is a premaxillary tooth and the only specimen that can be confidently referred to as a tyrannosauroid based on a suite of diagnostic characteristics (e.g., Currie et al. 1990; Baszio 1997b; Carr & Williamson 2004; Zanno & Makovicky 2011; Williamson & Brusatte 2014). These include a D-shaped cross section, a lingually oriented carina that arches around the lingual side of the tooth, a greater arc length along the labial face than the lingual face, a lack of denticles and serrations, and a prominent ridge on the lingual

surface. The tooth has a crown height of 6 mm and part of the lingual surface, near the apex is worn away.

MANIRAPTORA Gauthier, 1986
DROMAEOSAURIDAE Matthew and Brown, 1922

Two teeth are assigned to Dromaeosauridae from the COI. Diagnostic characteristics of dromaeosaurid teeth are outlined in Currie et al. (1990) and Sankey et al. (2002). Maxillary and dentary teeth are laterally compressed and recurved in lateral view, lack basal constriction, and possess a flattened, oval cross section. Distal denticles are thin, sometimes point apically, and larger than mesial serrations, and the distal carina is often positioned towards the lingual margin. In both datasets, the dromaeosaurid convex hulls have wide regions that overlap with Tyrannosauridae and *Richardoestesia*. Thus, several teeth may in fact belong to other groups and should be considered tentatively assigned.

NCSM 33267 (Figure 1.9 O–U) has a crown height of 10.15 mm, a FABL of 5.03 mm, and a basal width of 3.32 mm. The tooth lacks recurvature in mesial view and has an incrassate figure-eight-shaped cross section (sensu Hendrickx [2015]). Wear facets extend along the apical portion of the distal carina and across the smooth enamel of the labial surface. The mesial carina lacks serrations and twists lingually near the base. The distal denticles are subrectangular and the distal carina is positioned towards the lingual margin. When considered as part of the Hendrickx et al. (2014) database, NCSM 33267 plots exclusively within Dromaeosauridae (Figure 1.8).

NCSM 33275 (Figure 1.9 V–Z3) has a crown height of 5.83 mm, a FABL of 3.23 mm, and a basal width of 1.36 mm. The tooth is strongly compressed laterally, lacks recurvature in mesial view, and has a weakly figure-eight-shaped cross section. The enamel texture is smooth and a depression is present on the lingual face. The mesial carina is centrally positioned and the

distal carina is positioned centrally at the apex, turning towards the lingual margin near the base. Both mesial serrations and distal denticles are subrectangular. When plotted with the Hendrickx et al. (2014) database NCSM 33275 plots within *Richardoestesia* and close to Dromaeosauridae (Figure 1.8). However, NCSM 33275 is assigned to Dromaeosauridae because it possesses strong recurvature in lateral view, a characteristic of dromaeosaurid teeth that is not accounted for in the dataset.

Figure 1.9: Tyrannosaur and dromaeosaur teeth
(A–F) (NCSM 33276) tyrannosaurid premaxillary tooth in (A) mesial?/distal?, (B) labial, (C) mesial?/distal?, (D) lingual, (E) occlusal, and (F) basal views. (**G–H)** (NCSM 33268) tyrannosaurid? tooth in (G) lingual, (H) labial, (I) distal, (J) mesial, (K) occlusal, and (L) basal views, with close-ups of mesial (M) and distal (N) denticles. (**O–U)** (NCSM 33267) dromaeosaur tooth in (O) lingual, (P) labial, (Q) distal, (R) mesial, (S) occlusal, and (T) basal views, with close-up of mesial (U) denticles. (**V–Z3)** (NCSM 33275) dromaeosaur tooth in (V) lingual, (W) labial, (X) distal, (Y) mesial, (Z) occlusal, and (Z1) basal views, with close-ups of mesial (Z2) and distal (Z3) denticles. Scale bars equal 1 mm unless otherwise noted.

RICHARDOESTESIA Currie, Rigby, and Sloan, 1990
RICHARDOESTESIA sp.

NCSM 33274 (Figure 1.10 A–G) is complete and includes part of the root. NCSM 33274 is ascribed to *Richardoestesia* based on a suite of characteristics outlined in Currie et al. (1990; see also Sankey et al. 2002) and from the results of the LDA (Figure 1.8). NCSM 33274 has a crown height of 4.21 mm, a FABL of 1.65 mm, and a basal width of 0.98 mm. The tooth is tall and slender, lacks curvature in mesial view, is weakly recurved in lateral view, and has an oval to figure-eight-shaped cross section in basal view. The mesial carina lacks serrations and is centrally positioned, whereas the distal carina is positioned centrally at the apex, turning towards the lingual margin near the base. Distal denticles are small and sub rectangular. There is a depression near the base on both the lingual and labial surfaces and the enamel has a weakly braided texture (sensu Hendrickx [2015]). When considered as part of the Hendrickx et al. (2014) database, NCSM 33274 plots slightly outside of the *Richardoestesia* convex hull.

NCSM 33288 (Figure 1.10 H–N) has a crown height of 6.58 mm, an estimated crown height of ~9.00 mm, a FABL of 4.05 mm, and a basal width of 1.9 mm. The exact crown height is unknown because the apical ~third of the tooth crown is missing. The tooth is laterally compressed, weakly recurved in lateral view, lacks recurvature in mesial view, and has an elliptical cross section. The enamel texture is smooth and a subtle longitudinal depression is present on the lingual face. The mesial carina is centrally positioned, lacks serrations, and is worn away except near the base. The distal carina is positioned centrally at the apex, turning slightly towards the lingual margin near the base. Denticles along the distal carina are sub-rectangular to weakly apically oriented. When considered as part of the Hendrickx et al. (2014) database, NCSM 33288 plots along a line representative of reconstructed crown height. Nearly

all points along the line fall within the overlapping morphospace of *Richardoestesia*, *Nuthetes*, and Dromaeosauridae (Figure 1.8).

PARONYCHODON Cope, 1876
PARONYCHODON sp.

Three teeth are referred to *Paronychodon* based on a suite of characters outlined by Currie et al. (1990; see also Rauhut 2002; Sankey et al. 2002). These teeth are recurved in lateral view, with a flattened lingual face, a convex labial face, numerous longitudinal ridges, oval cross section, and lacking denticles or serrations. Previous studies have tentatively referred *Paronychodon* to Dromaeosauridae (Antunes & Sigogneau-Russell 1991), Troodontidae (Osmólska & Barsbold 1990), and Aves (Rauhut 2002).

NCSM 33277 (Figure 1.10 O–T) has a crown height of 2.4 mm, an estimated crown height of ~3.3 mm, a FABL of 1.57 mm, and a basal width of 1.00 mm. The exact height is unknown because part of the tooth crown is missing. NCSM 33277 is laterally compressed, recurved in lateral view, and has an elliptical cross section in basal view. The labial face is convex and the lingual face is flattened with a weakly defined longitudinal ridge. The distal carina is positioned lingually and lacks denticles. The mesial carina is worn away except at the base, positioned lingually, and lacks serrations. The enamel texture is smooth and ornamented by numerous longitudinal striations along the lingual and labial surface. When considered as part of the Hendrickx et al. (2014) dataset, NCSM 33277 plots slightly outside of the troodontid morphospace (Figure 1.8).

NCSM 33298 (Figure 1.10 U–Z) has a crown height of 2.11 mm, a FABL of 1.16 mm, and a basal width of 0.77 mm. It is recurved in lateral view and has an asymmetrically salinon cross section (sensu Hendrickx [2015]) in basal view. The labial face is strongly convex and the lingual face is flattened with a well-defined longitudinal ridge. Both the distal and mesial carinae

are positioned lingually and lack denticles or serrations and the distal carina is deflected inward. The enamel texture is smooth and there is a slight constriction at the base. When considered as part of the Hendrickx et al. (2014) database, NCSM 33298 plots slightly outside of the troodontid morphospace (Figure 1.8).

NCSM 33308 (Figure 1.10 Z1–Z5) has a crown height of 2.75 mm, a FABL of 1.39 mm, and a basal width of 0.85 mm. It is laterally compressed, lacks recurvature, and has a lenticular cross-section in basal view. The labial and lingual faces are convex, and the lingual face has a weakly defined medial depression near the base. The distal and mesial carinae lack denticles or serrations and the mesial carina twists lingually at the base. The enamel texture is ornamented by numerous longitudinal striations with no real relief extending baso-apically along the lingual and labial surfaces. When considered as part of the Hendrickx et al. (2014) database, NCSM 33308 plots slightly outside of the troodontid morphospace (Figure 1.8). NCSM 33308 may belong to Aves based on a series of characteristics specific to this tooth morphotype that are not accounted for in the analysis such as recurvature, flattened lingual surface, absence of denticles, and an oval cross section. Therefore, NCSM 33308 may be a morphologically distinct bird tooth or possibly a mesially positioned theropod tooth.

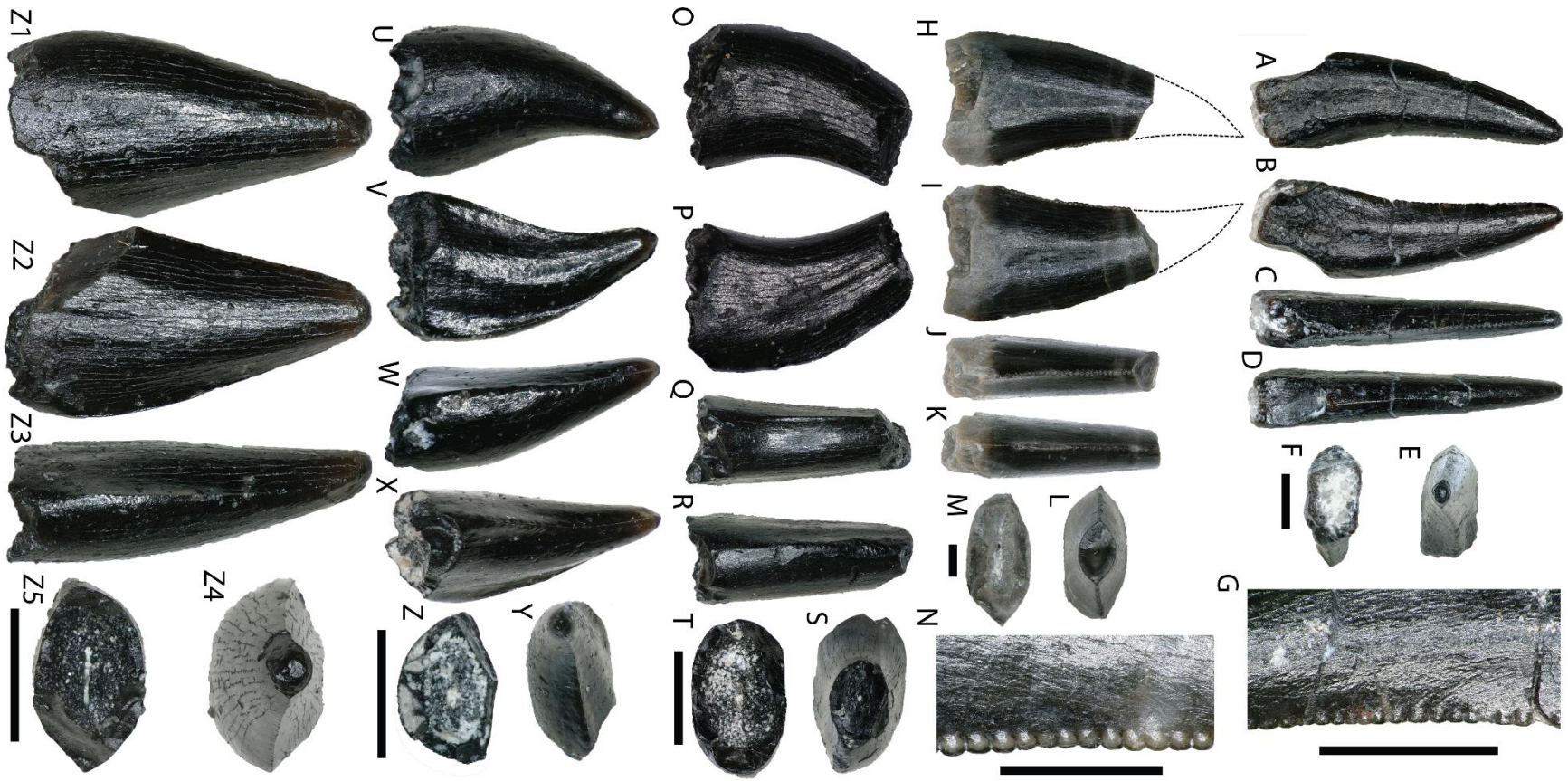

Figure 1.10: *Richardoestesia* and *Paronychodon* teeth
(A–G) (NCSM 33274) *Richardoestesia* tooth in (A) lingual, (B) labial, (C) distal, (D) mesial, (E) occlusal, and (F) basal views, with close-up of mesial (G) denticles. (**H–N)** (NCSM 33288) *Richardoestesia* tooth in (H) lingual, (I) labial, (J) distal, (K) mesial, (L) occlusal, and (M) basal views, with close-up of mesial (N) denticles. **(O–T)** (NCSM 33277) *Paronychodon* tooth in (O) lingual, (P) labial, (Q) distal, (R) mesial, (S) occlusal, and (T) basal views. **(U–Z)** (NCSM 33298) *Paronychodon?* tooth in (U) labial, (V) lingual, (W) mesial, (X) distal, (Y) occlusal, and (Z) basal views. **(Z1–Z5)** (NCSM 33308) *Paronychodon?* tooth in (Z1) labial, (Z2) lingual, (Z3) mesial, (Z4) occlusal, and (Z5) basal views. Scale bars equal 1 mm.

AVES Linnaeus, 1758
Gen. et sp. indet.

Bird material from this locality is difficult to properly discern, as no complete skeletal material has been documented and teeth vary widely in morphology (Sankey et al. 2002; Mayr et al. 2007; Larson & Currie 2013; Wilson et al. 2016). Two morphologically distinct teeth from the COI are tentatively ascribed to Avialae.

NCSM 33299 (Figure 1.11 A–E) and NCSM 33300 (Figure 1.11 F–J) are similar in morphology and size to three teeth from the OMNH referred to Aves: OMNH 28735, 28736, and 28737. These teeth are very small, measuring ~1 mm in height, are constricted at the base, and have circular cross sections. The crowns are asymmetrical, have weakly defined carinae on both anterior and posterior edges, and lack serrations or denticles. The enamel is smooth and moderately worn, and the crown apex is usually worn flat.

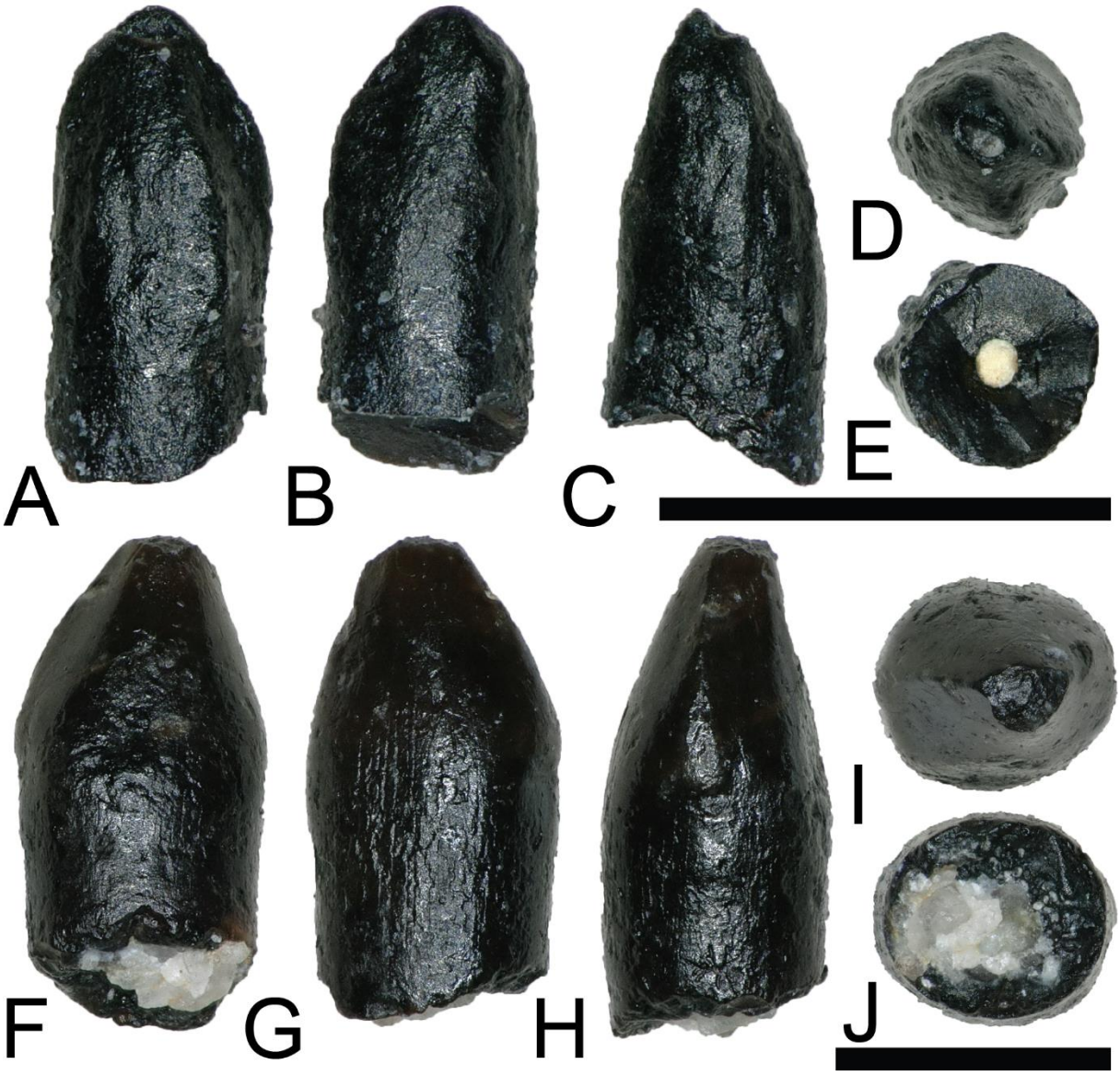

Figure 1.11: Possible avian teeth
(A–E) (NCSM 33299) Bird tooth? in (A) lingual?, (B) labial?, (C) mesial?, (D) occlusal, and (E) basal views. **(F–J)** (NCSM 33300) Bird tooth? in (F) labial, (G) lingual, (H) distal, (I) occlusal, and (J) basal views. Scale bars equal 1 mm.

DINOSAURIA Owen, 1842
ORNITHISCHIA Seeley, 1887
ORNITHISCHIA indet.

NCSM 33322 (Figure 1.12 A–E) is a heavily worn tooth with a CH of 7.31 mm, a FABL of 9.59 mm, and a BW of 5.71 mm. There is a large wear facet that extends across the apical portion of the labial surface. Even after accounting for wear, the tooth is mesio-distally elongate and apico-basally short. The tooth is constricted below the crown and several worn ridges run apicobasally along the lingual surface. Due to the poor preservation, NCSM 33322 cannot be confidently referred to a lower taxonomic level. However, NCSM 33322 compares favorably with illustrations of worn ankylosaur teeth (e.g., Coombs 1978, fig. 20.6d). Based on the megaherbivore clades known to have inhabited the Western Interior Basin of North America during the Late Cretaceous, a referral to Ankylosauridae is the most plausible.

NCSM 33318 (Figure 1.12 F–G) is a 6.8 mm long tooth fragment, preserving five large denticles. NCSM 33318 compares most favorably with ankylosaurid teeth (Coombs 1978).

NCSM 33316 (Figure 1.12 H–L) is a small, triangular tooth with a CH of 1.4 mm, a FABL of 1.49 mm, and a BW of 0.79 mm, possibly pertaining to Neornithischia, Ankylosauria, or Pachycephalosauria. It has seven cusps, a typical characteristic of premaxillary teeth of basal euornithopods (Oreska et al. 2013), and lacks an elevated rim along with the primary and secondary ridges present in ornithopod teeth such as *Zalmoxes* (Virág & Ősi 2017).

NCSM 33312 (Figure 1.12 M–Q) is possibly the premaxillary tooth of a neornithischian (Fanti & Miyashita 2009), with a CH of 0.95 mm, a FABL of 1.18 mm, and a BW of 0.73 mm. It is a small, triangular, scoop-shaped tooth with a constriction below the crown. The labial face is smooth and strongly convex. The lingual face is concave and possesses ~15 well defined, apicobasally oriented ridges.

NCSM 33314 (Figure 1.12 R–W) may represent a small ornithischian tooth, with a CH of 0.45 mm, a FABL of 0.55 mm, and a BW of 0.34 mm. It has a triangular crown that is weakly constricted between the base and root, and appears to have seven weakly defined denticles and apicobasally oriented striations.

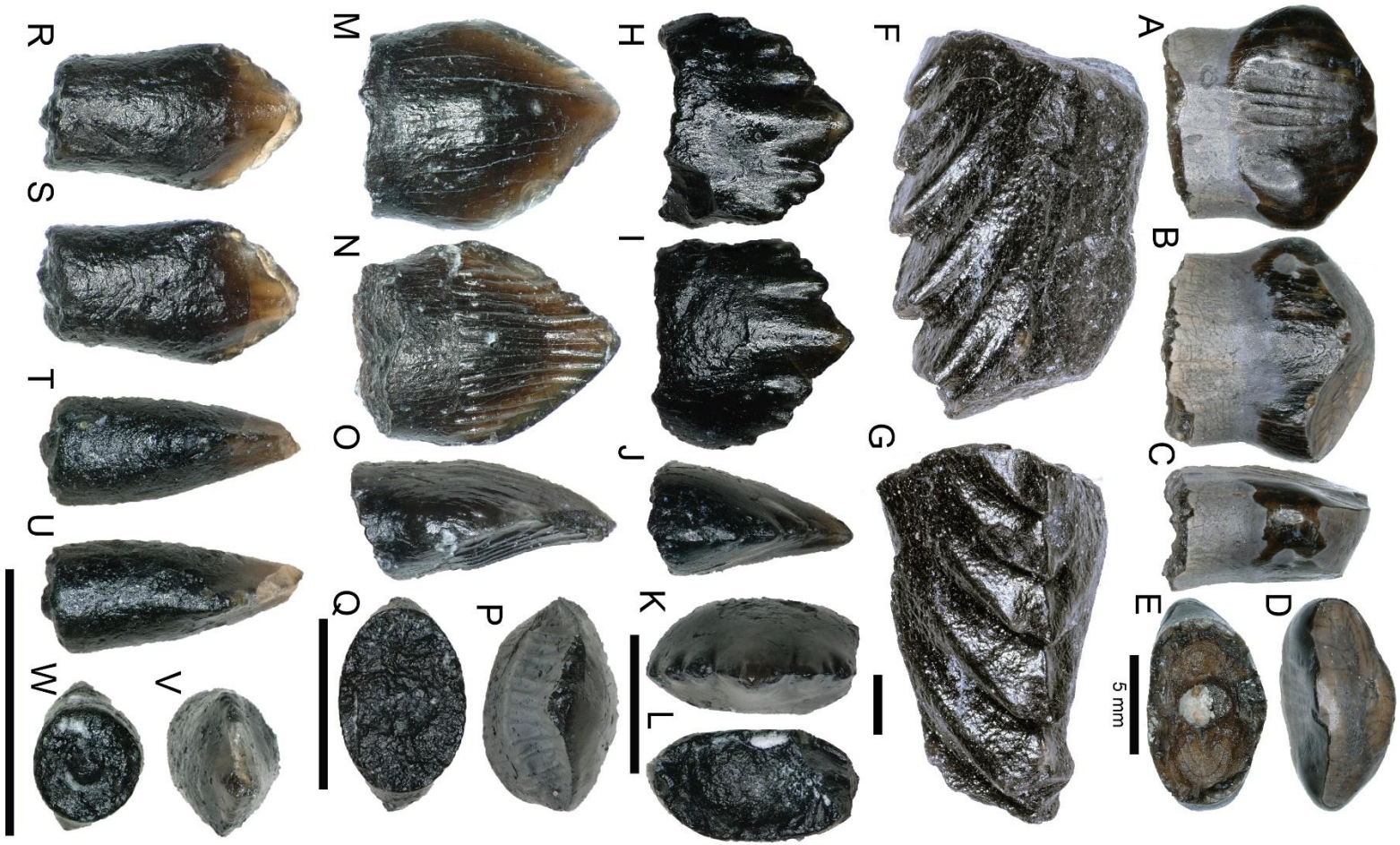

Figure 1.12: Ankylosaur and basal ornithischian teeth
(A–E) (NCSM 33322) Ankylosaur tooth in (A) lingual?, (B) labial?, (C) mesial?/distal?, (D) occlusal, and (E) basal views. **(F–G)** (NCSM 33318) Ankylosaur? tooth fragment in (F) labial?/lingual? and (G) mesial?/distal? views. **(H–L)** (NCSM 33316) Neornithischian tooth in (H) lingual, (I) labial, (J) mesial?/distal?, (K) occlusal, and (L) basal views. **(M-Q)** (NCSM 33312) Neornithischian? tooth in (M) labial, (N) lingual, (O) mesial?/distal?, (P) occlusal, and (Q) basal views. Scale bars equal 1 mm. **(R–W)** (NCSM 33314) Ornithischian tooth? in (R) labial?, (S) lingual?, (T-U) mesial?/distal?, (V) occlusal, and (W) basal views. Scale bars equal 1 mm unless otherwise noted.

ORNITHOPODA Marsh, 1881
HADROSAUROIDEA Cope, 1863

NCSM 33320, NCSM 33321, and NCSM 33323 (Figure 1.13 A–O) are hadrosauroid teeth possibly referable to *Eolambia caroljonesa*, the only hadrosauroid yet described from the Mussentuchit Member (Cifelli et al. 1997; Kirkland 1998; McDonald et al., 2017)). The teeth show considerable wear and are marked by linear and branched tubule ridges along the transverse cross section. These tubules produce multiple shearing faces along the chewing surface (Erickson et al. 2012). Each tooth possesses a prominent main keel, and NCSM 33321 (Figure 1.13 F–J) shows two additional smaller ridges running nearly parallel to the primary keel. Remnants of denticles on the apical edge of NCSM 33320 and NCSM 33321 demonstrate the presence of these features, but they are too worn to make comparisons.

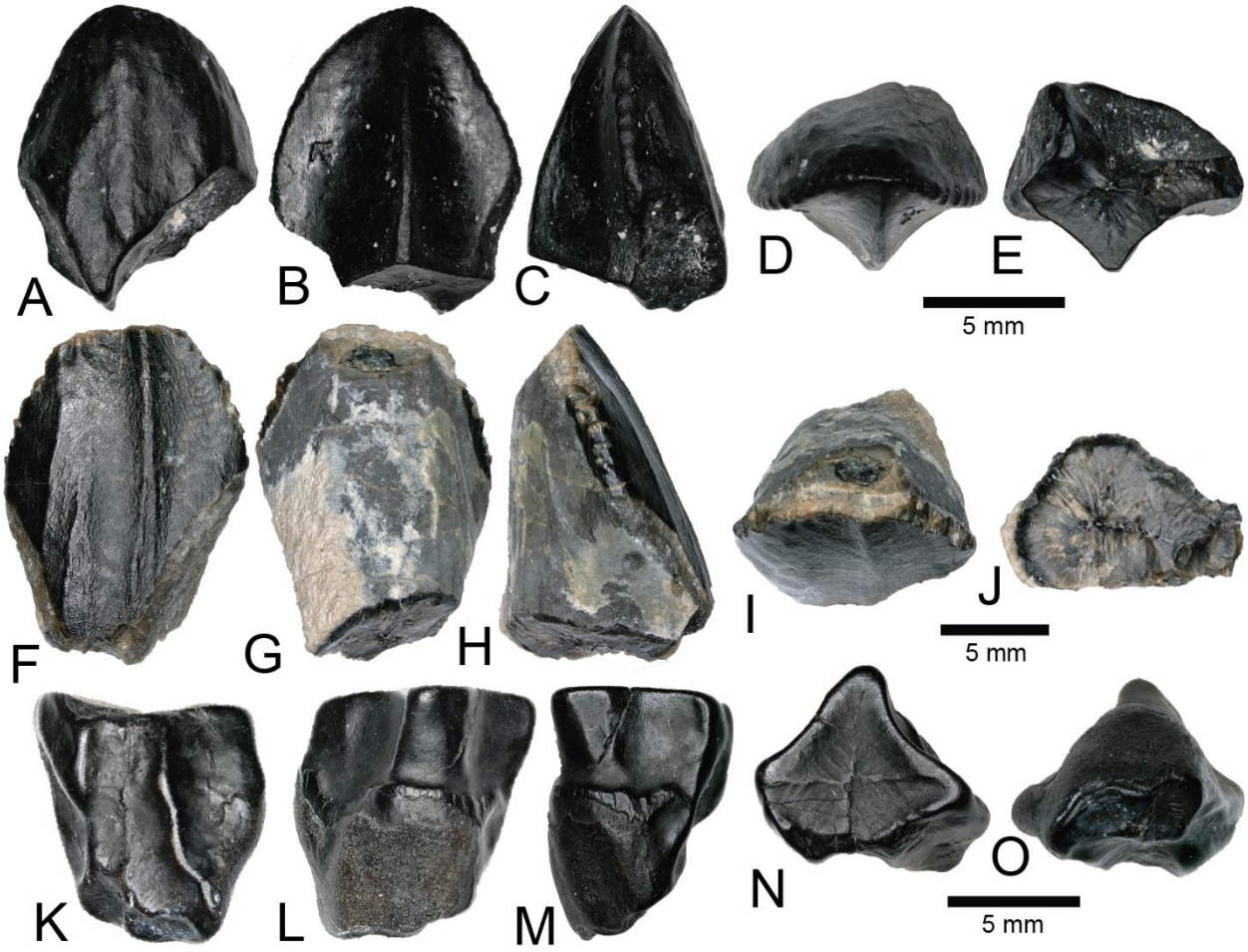

Figure 1.13: Hadrosaurid teeth
(A–E) (NCSM 33320) Possible *Eolambia* tooth in (A) labial, (B) lingual, (C) mesial?/distal?, (D) occlusal, and (E) basal views. **(F–J)** (NCSM 33321) Possible *Eolambia* tooth in (F) labial, (G) lingual, (H) mesial?/distal?, (I) occlusal, and (J) basal views. **(K–O)** (NCSM 33323) Possible *Eolambia* tooth in (K) labial?, (L) lingual?, (M) mesial?/distal?, (N) occlusal?, and (O) basal? views. Scale bars equal 5 mm.

MAMMALIA Linnaeus, 1758
METATHERIA Thomas Henry Huxley, 1880
MARSUPIALIA Illiger, 1811
SINBADELPHYS SCHMIDTI Cifelli 2004

NCSM 33354 (Figure 1.14 A–C) appears to be the mesial half of a right upper molar at the second locus, possibly belonging to *Sinbadelphys schmidti* but also similar to *Adelodelphys muizoni* (Cifelli 2004). NCSM 33354 lacks a number of dental features except for the ectoflexus, post-metacrista, and metacone. This makes its precise taxonomic assignment on the basis of dental features difficult. Nonetheless, the dimensions of NCSM 33354 compare favorably to those of *S. schmidti*. The second molar of *S. schmidti* (OMNH 26451) has an anteroposterior length of 1.5 mm, and another possible second molar (OMNH 33088) has an anteroposterior length of 1.89 mm. NCSM 33354 has a predicted anteroposterior length ranging from 1.5–1.6 mm. Therefore, *S. schmidti* is the most appropriate known taxon to ascribe to NCSM 33354.

MARSUPIALIA indet.

NCSM 33355 (Figure 1.14 D–G) is the incomplete upper, second premolar of a marsupial, most likely belonging to *A. muizoni*. This assignment to a marsupial clade is based on comparisons with illustrations in Lillegraven (1969) and Clemens (1966). The dimensional proportions of NCSM 33355 compare favorably with Cretaceous marsupial teeth at the second locus, and the height of the principal cusp indicates it is a maxillary tooth. The length of the second premolar of Cretaceous marsupials is approximately 80% the length of the first lower molar (Lillegraven 1969; Cifelli 2004). If NCSM 33355 was complete it would be approximately 1.1 mm in length, 0.2 mm smaller than the estimated length of the M1 of *A. muizoni* (1.3 mm). Therefore, NCSM 33355 is mostly likely referable to *A. muizoni* although the specimen could

also belong to the slightly larger *S. schmidti*, which has lower molars lengths between 1.4–1.7 mm and estimated premolar lengths between 1.2–1.4 mm.

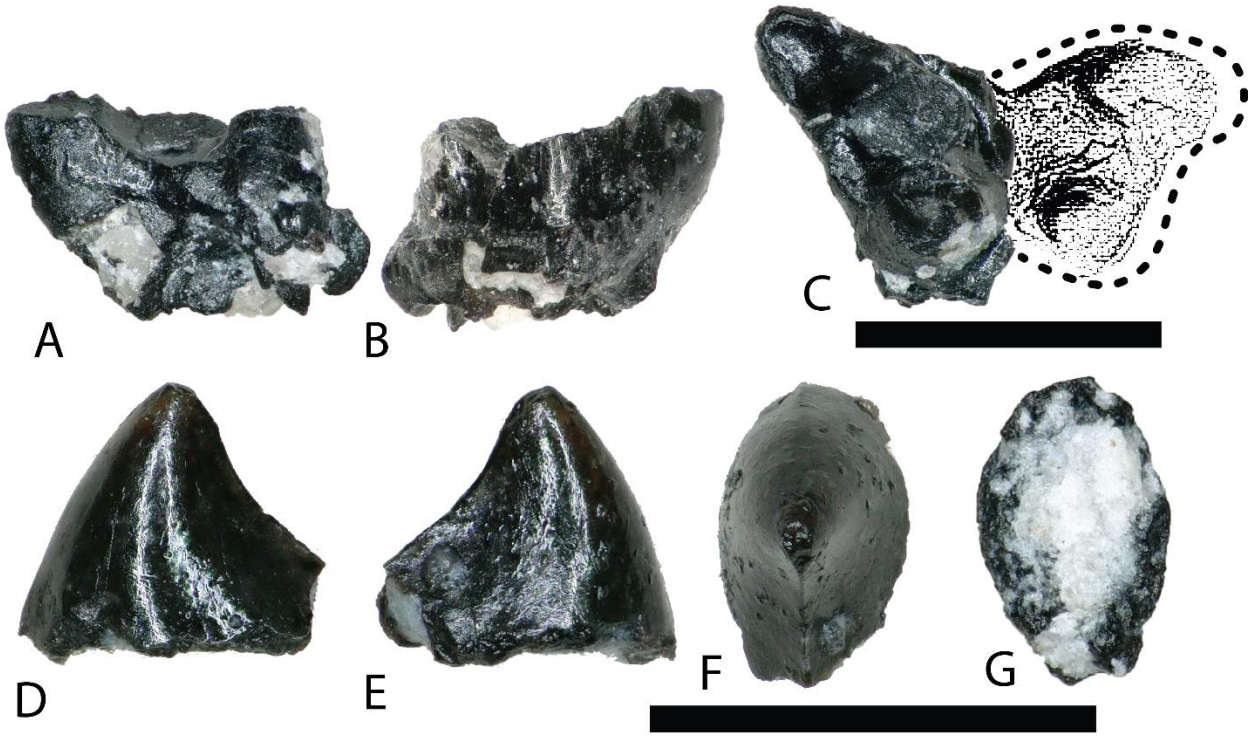

Figure 1.14: Mammalian teeth
(A–C) (NCSM 33354) mesial half of a right M2 upper molar belonging to a small marsupial, in (A) lingual view (showing plane of fracture), (B) labial view, and (C) occlusal view. Dotted line and shaded area represent estimated dimensions of complete tooth, based on complete upper left M2 molar of *Sinbadelphys schmidti* (Cifelli 2004). **(D–G)** (NCSM 33355) marsupial upper premolar in (D–E) labial?/lingual?, (F) occlusal, and (G) basal views. Scale bars equal 1 mm.

Ichnofossils

ELONGATOOLITHIDAE Zhao, 1975
MACROELONGATOOLITHUS Li, Yin, and Liu, 1995
MACROELONGATOOLITHUS SP.

Twenty-eight fragments of eggshell, belonging to the oogenus *Macroelongatoolithus*, were recovered from the COI. These fragments exhibit varying degrees of wear and range between 6–20 mm^2 and 1–3 mm thick (Figure 1.15 A–C). Fragments usually possess a subtle curvature along a single axis, suggesting an elongated egg morphology (Zelenitsky 2000). Shell material displays variation in ornamentation, similar to material previously collected material in the Mussentuchit Member (Zelenitsky 2000). These include dispersituberculate and linearituberculate ornamentation, with some fragments having well-defined, bulbous nodes and tubercles.

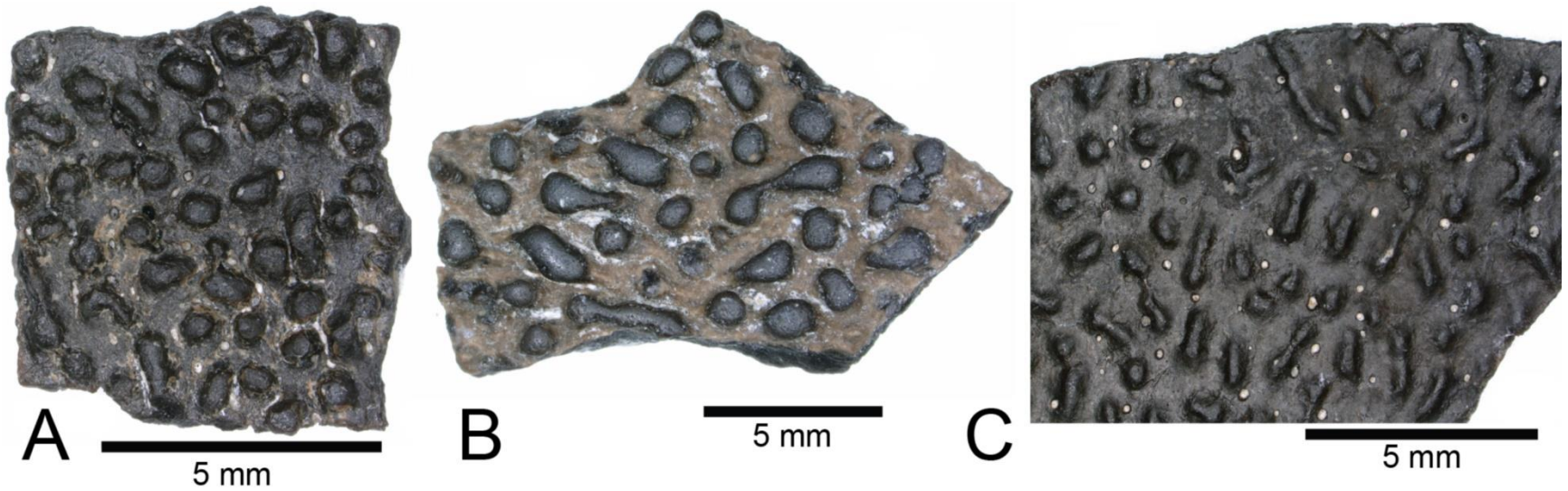

Figure 1.15: *Macroelongatoolithus* egg shell
A-C, (NCSM 33364, NCSM 33363, NCSM 33365) *Macroelongatoolithus* egg shell fragments. Scale bars equal 5 mm.

Biodiversity and Paleoecology

I compared the faunal assemblage of the COI sight to 12 OMNH microvertebrate localites from the Mussentuchit. Faunal abundances were sourced from Goldberg (2000) and compiled into a database for analyses.

The results of the analysis reveal that the total proportions of all specimens from all sites are skewed toward crocodylomorphs and osteichthyans, which constitute the majority of material at 31.7% and 39.3%, while mammals are the third most abundant at 12.6%. Dinosaurian material makes up 12.9%, with saurischia at 9.4% and ornithischia at 3.5%. Squamata, Chondrichthyes, Chelonia, and Urodela have the lowest abundances, together making up the final 3.4% (Figure 1.16 and 1.17). There are a number of consistent themes and outliers between sites (Figure. 1.16 and 1.17). In four sites (COI, 694, 801, and another site not included in this analyses by McDonald et al. (2017)) crocodylomorphs are by far the most abundant faunal group. Two sites (240 and 695) are dominated by osteichthyan material, while 213 is the only site dominated by chondrichthyans at 34.4% and also has the highest abundance of saurischian material at 21.9%.

Eight of the 13 Mussentuchit sites analyzed are dominated by mesoeucrocodylian remains. This pattern is also present at a site not included in this study (McDonald et al. 2017), raising that value to nine of 14 sites. The most second most common taxon in mesoeucrocodylian-dominated localities are osteichthyan fish, although this proportion is nearly equal with sites containing a secondary abundance of mammalian remains (Goldberg 2000; McDonald et al. 2017). A large percentage of sites are dominated by fish fossils, principally osteichthyans, with secondary abundances represented by mammals, mesoeucrocodylians, and saurischian dinosaurs.

Three sites (COI, 695, and 794) account for the majority of fossil material, each providing nearly a quarter of the total specimens (Figure 1.18). While the COI provides the most specimens to the dataset, it is the least sampled site, with only 183 kg of sediment processed. This gives the COI a fossil density of 22.4 fossils per kg, 53.3 times higher than the next densest site (OMNH 240), with a fossil density of 0.42 fossils per kg (Table 1.1; Figure 1.18).

Figure 1.19 shows the rarefaction curves of all 13 sites. The curves that have plateaued represent the sites that likely will not produce any new vertebrate clades. Conversely, curves that have not plateaued represent sites where more vertebrate clades are likely to be found if more sampling is conducted. Four sites (OMNH 239, 694, 695, 794) have plateaued and nine sites have not. The COI is among those that have not plateaued, however it does appear close to leveling off.

The rarefaction of over 4000 specimens was estimated, and the COI appears equal to OMNH V695 in clade representation. The direction of the rarefaction line for the COI locality is quite different from the OMNH localities, rising gradually towards the end of the graph. This pattern is due to the high number of mesoeucrocodylian and osteichthyes teeth in the sample, along with the rarer individual numbers of additional clades. In other words, the rarefaction of the COI database continuously provides excessive individuals of mesoeucrocodylians and fish, along with occasional other clades, which when considered across the entire resampling protocol produces the slowly increasing line. Compared to other OMNH localities there are key clades that are missing from the COI site, and recalculation of rarefaction curves at lower taxonomic levels may produce different outcomes, yet more refined taxonomic classifications are not yet possible. Given the higher potential for COI to yield additional clades through further sampling,

the COI locality could be one of the most taxonomically rich microsites yet described from the Mussentuchit Member.

In contrast, the biodiversity calculated via the Shannon-Wiener index produces a low value of 0.41 (Table 1.1) compared to other OMNH sites. The Shannon-Wiener index evaluates the evenness of a site by considering the number of individuals of each clade in relation to the total number of clades present. In other words, the unevenness of a site corresponds to a lower the biodiversity. Sampling localities that have a larger number of clades and a relatively equal number of individuals per clade will receive a higher biodiversity score than those with either low number of clades or sites possessing a large number of clades, yet a very few of those clades possess nearly all of the individual abundance. By this measure the COI has the lowest biodiversity because 90% of the fossils are mesoeucrocodylia, a similar theme seen with OMNH V801, which also has a large skew towards crocodylomorphs. Locality OMNH V868 is the most diverse site by this measure, with a biodiversity index of 1.61.

There appears to be no correlation between the number of fossils collected and the Shannon-Wiener biodiversity index. The slope of the correlation was essentially zero (-5.77x10-5). The four sites with plateaued rarefaction curves (OMNH V239, OMNH V694, OMNH V695, and OMNH V794) ranged in biodiversity from 1.05 to 1.40, which are lower than the highest biodiversity of 1.61 (OMNH V868). This indicates that extensive sampling and fossil abundance are not adequate predictors of the biodiversity of an individual site.

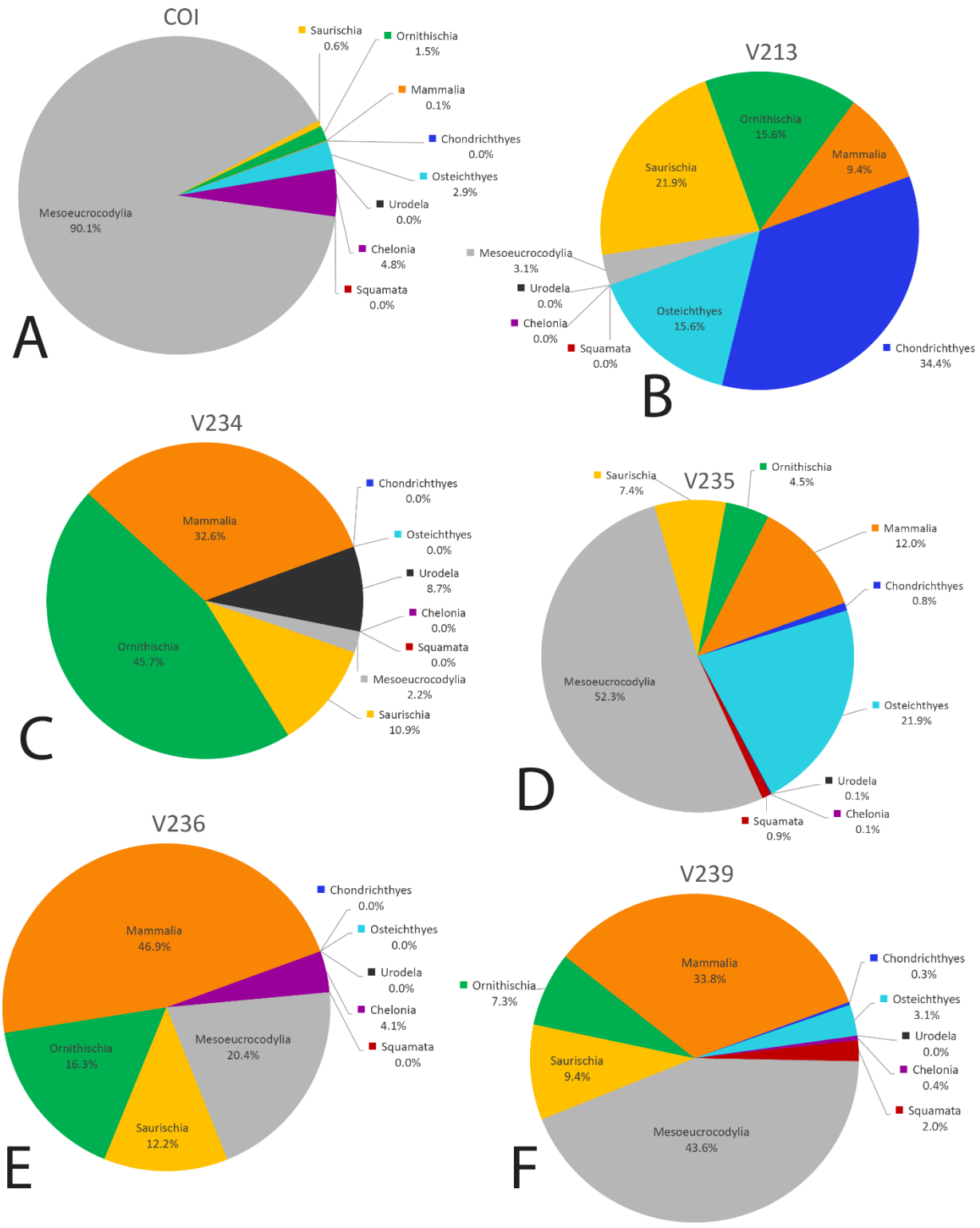

Figure 1.16: Biodiversity pie charts of the COI and 5 OMNH microfossil localities
Pie charts representing the biodiversity from (**A**) COI, (**B**) OMNH V213, (**C**) OMNH V234, (**D**) OMNH V235, (**E**) OMNH V236, and (**F**) OMNH V239.

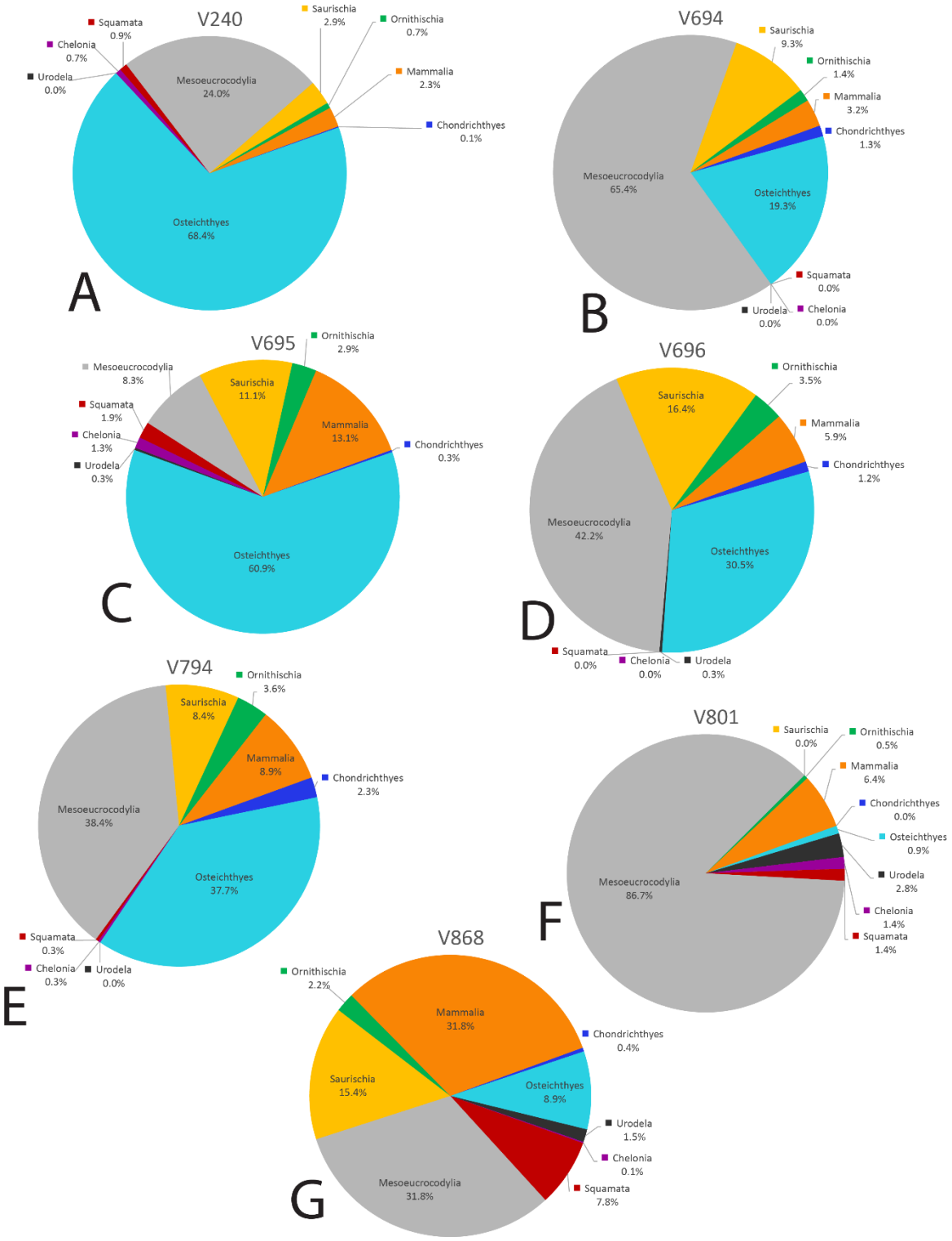

Figure 1.17: Biodiversity pie charts of 7 OMNH microfossil localities localities
Pie charts representing the biodiversity from (**G**) OMNH V240, (**H**) OMNH V694, (**I**) OMNH V695, (**J**) OMNH V696, (**K**) OMNH V794, (**L**) OMNH V801, and (**M**) OMNH V868.

Table 1.1: Microfossil locality compilation
Specimen abundances, quantity of processed matrix, fossil density, and biodiversity indexes from all 13 localities.

Site	COI	213	234	235	236	239	240	694	695	696	794	801	868	Total
Total specimens	4100	37	46	1413	64	695	808	632	3979	364	3877	218	710	16943
Matrix processed (kg)	183	775	1825	4690	910	1960	1915	3645	14580	955	11390	1820	2780	47428
Fossil density per kg	22.4	0.05	0.03	0.3	0.07	0.35	0.42	0.17	0.27	0.38	0.34	0.12	0.26	
Proportion	0.24	0.002	0.003	0.08	0.004	0.04	0.05	0.04	0.23	0.02	0.23	0.01	0.04	
Shannon-Wiener index	0.45	1.61	1.26	1.35	1.36	1.37	0.91	1.05	1.29	1.38	1.40	0.58	1.61	

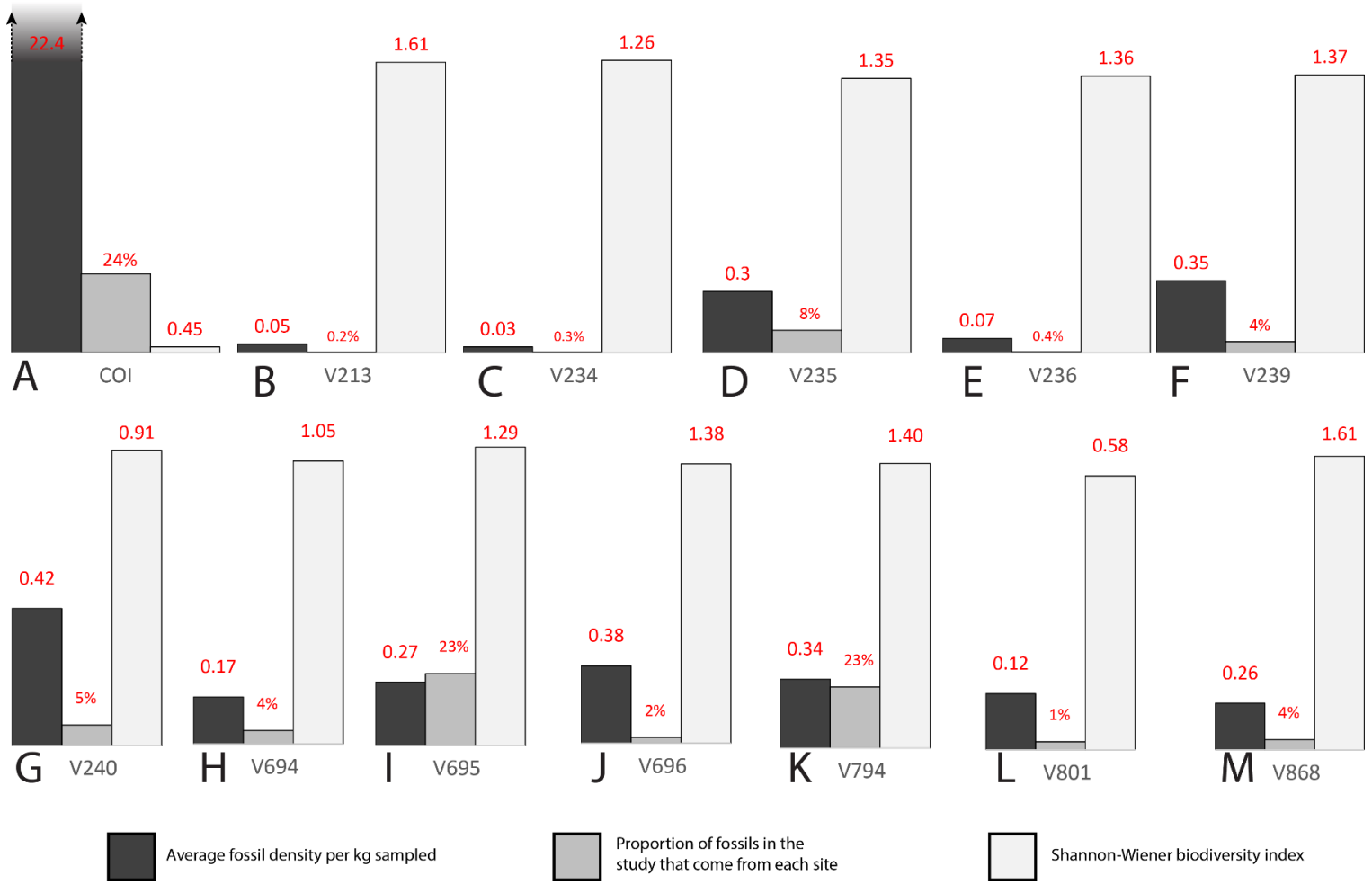

Figure 1.18: Biodiversity bar charts of the COI and 12 OMNH microfossil localities
Barcharts representing the biodiversity from (**A**) COI, (**B**) OMNH V213, (**C**) OMNH V234, (**D**) OMNH V235, (**E**) OMNH V236, (**F**) OMNH V239, (**G**) OMNH V240, (**H**) OMNH V694, (**I**) OMNH V695, (**J**) OMNH V696, (**K**) OMNH V794, (**L**) OMNH V801, and (**M**) OMNH V868. The dark grey line represents the density of fossils from a single kilogram of sediment at each locality, the medium grey line shows the proportion of fossils in this study that come from each site, and the light grey line is the Shannon-Wiener biodiversity index for each site.

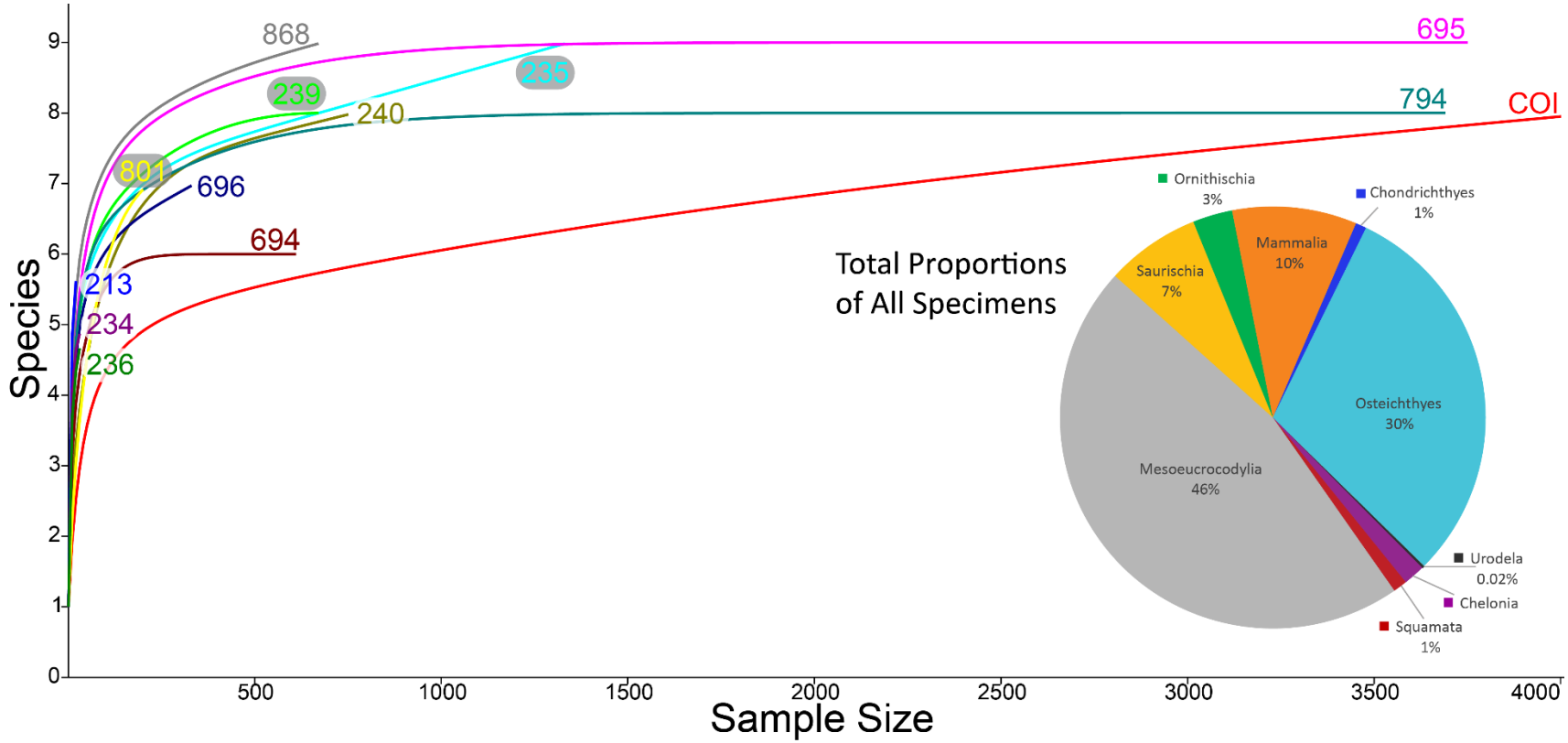

Figure 1.19: Rarefaction curves for all microfossil localities and biodiversity pie chart of all 13 localities combined
Rarefaction curves for the 12 OMNH microfossil localities listed in the Goldberg (2000) dataset and the Cliffs of Insanity locality. Colors of site names correspond to the rarefaction line of the same color. The pie chart represents the combined percentage of all 13 site abundances used in the present study.

Paleoenvironmental Influences

Goldberg (2000) characterized 11 of the 12 OMNH sites as either fluvial oxbow, floodplain, crevasse splay, or channel deposits, basing these inferences on a number of sedimentary features such as clast size, lag deposits, clay balls, slickensides, and plant debris. Among these localities, OMNH V236 and OMNH V239 were interpreted as channel deposits, OMNH V235 and OMNH V240 as splay environments, OMNH V694 and OMNH V695 as floodplain deposits, and OMNH V801 as an abandoned oxbow channel. Some uncertainty was noted for select sites including OMNH V794 and OMNH V868, which were interpreted as either channel deposits or splays, and OMNH V234, which was interpreted as either a floodplain or splay deposit.

Correspondence analysis (CA) of all 13 sites, using faunal data as a predictor of depositional environment (Figure 1.20), shows that site faunal compositions can be associated with specific depositional environments; this ordination plots the COI close to OMNH V801, both of which are interpreted as representing oxbow lake environments. These sites trend to the bottom left of the ordination space due to their high concentration of Mesoeucrocodylia and Chelonia material. However, for the majority of sites taxonomic content is a poor predictor of depositional environment. These include channel or splay deposits and floodplain deposits.

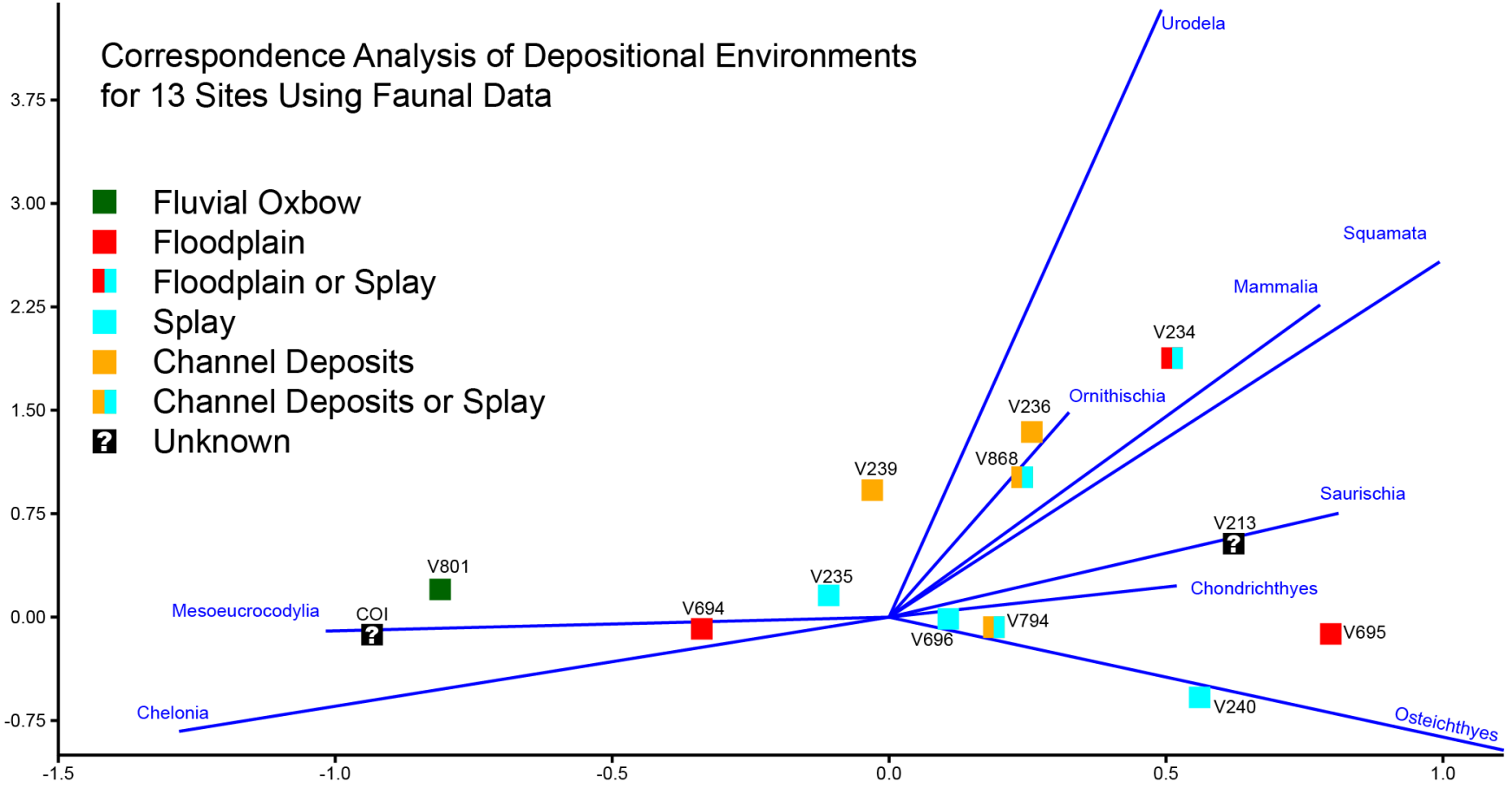

Figure 20: Correspondence Analysis of Depositional Environments for 13 Sites Using Faunal Data.
Correspondence analysis of all 13 sites, using simplified faunal data as a predictor of depositional environment. Blue eigenvectors represented by faunal groups.

Stratigraphic and Geographic Context

Goldberg (2000) noted that determining the exact stratigraphic position of the OMNH localities in the Mussentuchit Member is challenged by difficult terrain, distances between sites, and frequently obscured bedding. Nonetheless, Cifelli et al. (1999) and Goldberg (2000) were able to place ten of the microsites in relative positions to one another both stratigraphically (Figure 1.1 D) and geographically (Figure 1.1 B). The relative stratigraphic positions were based on the proximity of a site to the upper or lower contacts of the Mussentuchit Member, or its position above or below a specific ash layer used as a marker bed. To this framework, I added the stratigraphic position of the COI as determined from the contact with the Naturita Formation.

The COI and OMNH V239 are the stratigraphically highest units, located in the uppermost strata of the Mussentuchit Member. OMNH V235, OMNH V694, and OMNH V794 are located above the ash layer, whereas OMNH V868 and OMNH V695 are located directly below the ash layer. OMNH V240, OMNH V801, and OMNH V234 are all located near the bottom of the Mussentuchit Member, just above the contact with the Ruby Ranch Member. Geographically, OMNH V801 represents the Northeastern-most locality, while the COI represents the Southwestern-most.

DISCUSSION

Biodiversity

Prior studies of microvertebrate localities in the Mussentuchit Member of the Cedar Mountain Formation reportedly processed 49,295 kg of matrix in total, with individual sites contributing between 775–14,580 kg of matrix. These studies have resulted in a total of 13,036 identifiable specimens (Goldberg 2000). By comparison, the Cliffs of Insanity microvertebrate

locality preserves a uniquely high density of fossils, with over 6342 specimens recovered from only 183 kg of sediment.

The majority of Mussentuchit sites sampled, including the COI locality, are dominated by mesoeucrocodylian teeth (Goldberg 2000; McDonald et al. 2017), with a large percentage of sites alternatively dominated by osteichthyan and chondrichthyan material. The remarkably high abundance of mesoeucrocodylia material (90% of recovered fossils) warrants further investigation as a potential paleoenvironmental signal within the Mussentuchit Member itself. I hypothesize that the general predominance of mesoeucrocodylians in the upper Cedar Mountain Formation may represent an authentic paleoecological signal associated with the transgression of the Western Interior Seaway during this interval. If specimen NCSM 33308 is indeed an enchodontid tooth, then this would support my hypothesis because members of Enchodontidae are predominantly marine (Silva & Gallo 2011). However, shed teeth can often over-represent a population density, and the fluvial nature of many of the sampled localities, (including the COI) can lead to the overrepresentation of aquatic faunal elements compared to terrestrial vertebrate elements.

While marsupial mammals are generally abundant in Mussentuchit localities (Goldberg 2000), they currently make up only a minor component of the COI diversity. The COI site thus far lacks chondrichthyan, and serpent remains; yet, rarefaction curves suggest additional sampling efforts will likely produce materials representative of these clades.

Baenid, helochelydrid (solemydid), glyptopsid, and trionychid turtles have been reported previously (Cifelli et al. 1997; Fiorillo 1999; Herzog et al. 2015) from the Mussentuchit Member. My histological analysis as well as qualitative assessment of turtle shell fragments from the COI add the presence of Adocidae, representing the first occurrence of this taxon from the

Cedar Mountain Formation and the earliest occurrence in North America.

Tooth Identifications

A diverse assemblage of dinosaurian species are known from the Mussentuchit Member based on previous microfaunal studies (Eaton 1987; Nelson & Crooks 1987; Cifelli et al. 1999; Fiorillo 1999; Kirkland et al. 1999). I find support for some of these identifications in the COI sample; however, I take a more conservative approach to isolated tooth identifications because the Mussentuchit represents a unique taxonomic diversity, composed predominantly of undescribed dinosaurian species (e.g. Makovicky et al. 2015; Zanno et al. 2016) and previous studies caution assigning isolated dinosaur teeth to refined taxonomic levels (e.g., Zanno et al. 2013). Importantly, I provide some of the first detailed descriptions and photographic documentation of dinosaurian teeth from the Mussentuchit Member.

A wide diversity of isolated dinosaurian teeth in the Mussentuchit have been documented following multiple screenwashing efforts (Cifelli et al. 1999; Eaton 1987; Fiorillo 1999; Kirkland et al. 1999; Nelson & Crooks 1987). Despite these extensive efforts, documentation of recovered dinosaurian teeth have been limited to biodiversity studies, and detailed analyses of the morphological diversity of dinosaurian teeth have yet to be conducted until this study.

The gross morphological examination of isolated theropod teeth suggests the presence of most major dentigerous coelurosaurian clades known to have inhabited the Western Interior Basin of North America during the Late Cretaceous including Tyrannosauroidea, Dromaeosauridae, Troodontidae, and Avialae, which is consistent with the diversity reported by previous workers. Tyrannosauroidea is definitively represented by the presence of a single

premaxillary tooth similar in morphology to tyrannosauroid premaxillary teeth from the Early Cretaceous of Asia and North America (Zanno and Makovicky 2011).

Several morphotypes of ornithischian teeth are represented at COI, suggesting a large diversity of herbivorous dinosaurs, most of which are already documented via published or undescribed macrovertebrate remains (Kirkland 1998; Carpenter et al. 1999; Makovicky et al. 2015; Zanno et al. 2016). A quantitative morphological analysis coupled with publication of these specimens will aid in producing more refined identifications.

Marsupial mammals are abundant in Mussentuchit localities generally (Goldberg 2000), yet make up only a minor component of the COI diversity. The COI site thus far lacks chondrichthyan, and serpent remains; yet, rarefaction curves (Figure 1.19) suggest the likelihood of recovering materials representative of these clades with additional sampling efforts.

It is still difficult to properly ascribe exact taxonomic identifications to many of these teeth due to the lack of associated skeletal material, and some tooth diversity may be explained by heterodonty and variation along the tooth row (Buckley 2009; Smith 2002; Smith 2005). Furthermore, it is still unclear the degree to which ontogeny contributes to dental variation among theropods. Ontogeny is noted to have only minor effects on the dental shape of *Coelophysis bauri* teeth, specifically the degree of tooth recurvature; however, variation is noted in the presence of discrete tooth traits such as denticles on premaxillary teeth or longitudinal ridges on tooth crowns (Buckley 2009), which can affect identifications.

Paleoenvironmental and Taphonomic Considerations

Taphonomic processes such as transport, sorting, winnowing, reworking, time averaging, and other hydrodynamic factors have been suggested to affect the comparability between sites

and perhaps introduce significant bias (Wilson 2008). However, Rogers et al. (2017) compared six intraformational vertebrate microfossil bonebeds in the Upper Cretaceous Judith River Formation, represented by three lacustrine settings and three channel-hosted settings, and found them to be largely comparable with regards to taphonomic bias.

We found little evidence among currently sampled microvertebrate localities in the Mussentuchit to support a relationship between depositional environment (Figure 1.20) or stratigraphic position (Figure 1.1 D) and faunal abundance data, with the exception of the two sites proposed to be oxbow lake environments (COI and OMNH V801). Although ambiguity in interpretations of depositional environment for some OMNH localities (e.g., V868, 794)(Goldberg 2000), if clarified, could extend this result to channel deposits as well.

The faunal composition of the COI plots closest to OMNH V801 in the correspondence analyses; both localities are characterized by a relatively high concentration of turtle and mesoeucrocodylian material. This raises the possibility that relative overabundance of semiaquatic taxa within these sites represents a true paleoenvironmental signal, yet I note that a sample size of two is insufficient to generate much confidence. Moreover, significant differences remain between these two localities suggesting that they may be non-isotaphonomic. OMNH V801 preserves an abundance of articulated fossils, including complete turtle shells, and freshwater invertebrates with mottled coloration, a feature proposed to indicate high biological activity (Goldberg 2000). In contrast, I have not recovered freshwater invertebrates or articulated fossils from the COI locality, and turtle shell material is fragmentary. These dissimilarities suggest that, although depositional environment may be broadly influencing the proportion of vertebrate clades preserved at these localities, different taphonomic factors are also at work and the sites may not be taphonomically equivalent.

Paleobiogeography

The late Early Cretaceous Laurasian Interchange Event, EKLInE, is marked the first occurrences of taxa bearing Asian affinities in North America during the Aptian-Cenomanian (Cifelli et al. 1999; Zanno and Makovicky 2011, 2013). These taxa include hadrosauroids (Norman 2004; McDonald et al. 2010b), pachycephalosaurians (Cifelli et al. 1997; Gangloff 1998; Garrison et al. 2007), neoceratopsians (Farke et al. 2014), and theropods (e.g., tyrannosauroids [Zanno & Makovicky 2011], ornithomimids [Longrich 2008], and oviraptorosaurs [Makovicky & Sues 1998]), mammals (Cuenca-Bescos and Canudo 2003), squamates (Nydam 2002, 2013), and trionychid turtles (Hirayama et al. 2000). The introduction of these faunal groups is considered one of the major factors leading to the extinction and replacement of much of North America's endemic dinosaur clades (Kirkland et al. 1997, 1999).

The previous oldest occurrence of adocid turtles in North America derives from the Smoky Hollow Member of the Straight Cliffs Formation (Eaton et al. 1999), dated to the Turonian (~92 Ma; Titus et al. 2013). Therefore, the presence of adocids in the Cenomanian aged (~97 Ma) Mussentuchit Member (Cifelli et al. 1997; Garrison et al. 2007) extends the presence of the clade in North America by approximately 5 million years and provides further evidence for a Laurasian interchange at or prior to the beginning of the Late Cretaceous.

The oldest records of adocids derive from the Late Jurassic of Asia (Syromyatnikova & Danilov 2009; Danilov et al. 2011), and the clade is notably absent in the fossil record of Europe during the Early Cretaceous, suggesting a Beringian dispersal route in concordance with the majority of other vertebrate records. It has been suggested that the high-latitude connection between eastern Asia and western North America acted as a climatic barrier, resulting in a dispersal filter that restricted smaller members of faunal assemblages such as turtles (Lipka et al.

2006). The appearance of adocids in North America by at least the Cenomanian, would seem to contradict this hypothesis, suggesting that at least some testudinatans were able to disperse across high latitude barriers in the Early Cretaceous. This is especially notable given that turtles have been suggested to exhibit a high degree of endemism and climatic zonation (Moody 1984; Gates et al., 2010; Hirayama et al. 2000), however extant turtles endemic to higher latitudes display broader geographic ranges compared to those at lower latitudes (Angielczyk et al. 2015).

CONCLUSION

The recovery and analyses of over 4000 new fossil specimens from the COI microvertebrate site has improved our understanding of the Cenomanian vertebrate fauna from Mussentuchit Member of the Cedar Mountain Formation. The site is diverse and is composed of the remains of Amiidae, lepisosteiforms, pycnodontiforms, salmoniforms, albanerpetontids, helochelydrids, adocids, mesoeucrocodylians, tyrannosauroids, dromaeosaurids, the theropods *Richardoestesia* and *Paronychodon*,avialans, a variety of ornithischians, metatherians, and trace fossils assigned to *Macroelongatoolithus*. The recovery of adocid turtle material marks a new addition to the Mussentuchit assemblage and adds to a growing body of evidence refining the pattern and tempo of faunal interchange between Asia and North America prior to and post the Early/Late Cretaceous boundary. Additionally, it represents the earliest occurrence of the Adocidae in North America, extending the record of this group by 5 million years. Documenting the fine-scale patterns of the Mussentuchit taxa can provide a better understanding of the effects of biogeographic complexity during the Cretaceous of North America.

The morphometric analysis of the eight theropod teeth from the COI using the Hendrickx et al. (2014) database was informative, yet limited in its ability to accurately predict taxonomic

associations. The inconsistencies between where a tooth may plot is likely due to the inability of existing databases to account for subtle shape variation and ambiguous taxonomic referrals due to their reliance solely on a limited series of linear measurements. Future attempts to refine this methodology will incorporate a larger sample set of theropod teeth from the Mussentuchit, utilizing landmark data and 3-Dimensional shape analyses.

Finally, I find no consistent relationship between depositional environment and the abundance of vertebrate clades between microvertebrate localities in the Mussentuchit Member (with the possible exception of oxbow environments, which may preserve an overabundance of semiaquatic taxa). Yet, also caution that detailed taphonomic studies are needed to parse out whether the lack of paleoenvironmental signal for most depositional environments is the result of non-isotaphonomy or is authentic.

REFERENCES

Angielczyk KD, Burroughs RW, and Feldman C. 2015. Do turtles follow the rules? Latitudinal gradients in species richness, body size, and geographic range area of the world's turtles. *Journal of Experimental Zoology Part B: Molecular and Developmental Evolution* 324:270-294.

Antunes M, and Sigogneau-Russell D. 1991. Nouvelles données sur les Dinosaures du Crétacé supérieur du Portugal. *Comptes rendus de l'Académie des sciences Série 2, Mécanique, Physique, Chimie, Sciences de l'univers, Sciences de la Terre* 313:113-119.

Avrahami HM, Heckert AB, and Martin L. 2015. Comparison of Nested Sieves, Traditional Screen Boxes, and Paint Sieves for The Recovery of Microvertebrate Fossils. *Journal of Vertebrate Paleontology Program Abstract*:81.

Barclay RS, McElwain JC, and Sageman BB. 2010. Carbon sequestration activated by a volcanic CO_2 pulse during Ocean Anoxic Event 2. *Nature Geoscience* 3:205.

Baszio S. 1997a. Palaeo-ecology of dinosaur assemblages throughout the Late Cretaceous of South Alberta, Canada. *Courier Forschungsinstitut Senckenberg* 196:1-31.

Baszio S. 1997b. Systematic palaeontology of isolated dinosaur teeth from the latest Cretaceous of south Alberta, Canada. *Courier Forschungsinstitut Senckenberg* 196:33-77.

Beherensmeyer A, Damuth J, DiMichele W, Potts R, Sues HD, and Wing S. 1992. Terrestrial ecosystems through time. University of Chicago Press, Chicago.

Bilelo MM. 1969. The fossil fish *Lepidotes* in the Paluxy Formation, north-central Texas. *American Midland Naturalist*:405-411.

Blakey RC. 2014. Paleogeography and paleotectonics of the Western Interior Seaway, Jurassic-Cretaceous of North America. *Search and Discovery* 30392:72.

Brinkman D, Newbrey M, Neuman A, and Eaton J. 2013. Freshwater Osteichthyes from the Cenomanian to Late Campanian of Grand Staircase—Escalante National Monument, Utah. *At the top of the grand staircase: the Late Cretaceous of southern Utah. Edited by AL Titus and MA Loewen Indiana University Press, Bloomington, Indiana*:195-236.

Brinkman DB, Newbrey MG, and Neuman AG. 2014. Diversity and paleoecology of actinopterygian fish from vertebrate microfossil localities of the Maastrichtian Hell Creek Formation of Montana. *Geological Society of America Special Papers* 503:247-270.

Bryant LJ. 1988. A new genus and species of Amiidae (Holostei; Osteichthyes) from the Late Cretaceous of North America, with comments on the phylogeny of the Amiidae. *Journal of Vertebrate Paleontology* 7:349-361.

Buckley LG. 2009. Individual and ontogenetic variation in theropod dinosaur teeth: a case study of *Coelophysis bauri* (Theropoda: Coelophysoidea) and implications for identifying isolated theropod teeth. University of Alberta.

Buckley LG, Larson DW, Reichel M, and Samman T. 2010. Quantifying tooth variation within a single population of *Albertosaurus sarcophagus* (Theropoda: Tyrannosauridae) and implications for identifying isolated teeth of tyrannosaurids. *Canadian Journal of Earth Sciences* 47:1227-1251. 10.1139/e10-029

Buscalioni A, Fregenal M, Bravo A, Poyato-Ariza F, Sanchíz B, Báez A, Moo OC, Closas CM, Evans S, and Lobón JM. 2008. The vertebrate assemblage of Buenache de la Sierra (Upper Barremian of Serrania de Cuenca, Spain) with insights into its taphonomy and palaeoecology. *Cretaceous Research* 29:687-710.

Carpenter K. 1999. Ankylosaurs (Dinosauria:Ornithischia) of the Cedar Mountain Formation, Utah, and their stratigraphic distribution. *Utah Geological Survey Miscellaneous Publications* 99-1:243-251.

Carpenter K. 2006. Assessing dinosaur faunal turnover in the Cedar Mountain Formation (Lower Cretaceous) of eastern Utah, USA. In: Barrett PM, and Evans SE, eds. *Ninth International Symposium on Mesozoic Terrestrial Ecosystems and Biota*. London: The Natural History Museum, 21-25.

Carpenter K. 2014. Where the sea meets the land: the unresolved Dakota Problem in Utah. *Utah Geological Association Publication* 43:357-372.

Carr TD, and Williamson TE. 2004. Diversity of late Maastrichtian Tyrannosauridae (Dinosauria: Theropoda) from western North America. *Zoological Journal of the Linnean Society* 142:479-523.

Cifelli RL. 1996. Techniques for recovery and preparation of microvertebrate fossils. Oklahoma Geological Survey Special Publication. Norman: Oklahoma Geological Survey. p 36.

Cifelli RL. 2004. Marsupial mammals from the Albian–Cenomanian (Early–Late Cretaceous) boundary, Utah. *Bulletin of the American Museum of Natural History* 285:62-79.

Cifelli RL, Kirkland JI, Weil A, Deino AL, and Kowallis BJ. 1997. High-precision 40Ar/39Ar geochronology and the advent of North America's Late Cretaceous terrestrial fauna. *Proceedings of the National Academy of Sciences* 94:11163-11167.

Cifelli RL, Madsen SK, and Larson EM. 1996. Screenwashing and associated techniques for the recovery of microvertebrate fossils. *Oklahoma Geological Survey Special Publications* 96-4:1-24.

Cifelli RL, Nydam RL, Gardner JD, Weil A, Eaton JG, Kirkland JI, and Madsen SK. 1999. Medial Cretaceous vertebrates from the Cedar Mountain Formation, Emery County, Utah: the Mussentuchit Local Fauna. In: Gillette DD, ed. *Vertebrate paleontology in Utah*. Salt Lake City: Utah Geological Survey, 219-242.

Clemens WA. 1966. *Marsupialia*: University of California Press.

Coombs Jr WP. 1978. The families of the ornithischian dinosaur order Ankylosauria. *Palaeontology* 21:143-170.

Craig LC. 1981. Lower Cretaceous rocks, southwestern Colorado and southeastern Utah.

Crepet W, and Friis E. 1987. The evolution of insect pollination in angiosperms. *Friis, E, M,, Chaloner, W, G,, Crane, P, R ed (s) Cambridge Univ Press: Cambridge, etc*:181-201.

Cuenca-Bescós G, and Canudo JI. 2003. A new gobiconodontid mammal from the Early Cretaceous of Spain and its palaeogeographic implications. *Acta Palaeontologica Polonica* 48.

Currie BS. 1998. Upper Jurassic-Lower Cretaceous Morrison and Cedar Mountain Formations, Ne Utah-Nw Colordo: Relationships between Nonmarine Deposition and Early Cordilleran Foreland-Basin Development. *Journal of Sedimentary Research* 68.

Currie PJ, Rigby JK, Jr., and Sloan RE. 1990. Theropod teeth from the Judith River Formation of southern Alberta, Canada. In: Carpenter K, and Currie PJ, eds. *Dinosaur systematics: Approaches and perspectives*. Cambridge: Cambridge University Press, 108-125.

Danilov I, Sukhanov V, and Syromyatnikova E. 2011. New Asiatic materials on turtles of the family Adocidae with a review of the adocid record in Asia. *Proceedings of the Zoological Institute RAS* 315:101-132.

Danilov IG, Syromyatnikova EV, Skutschas PP, Kodrul TM, and Jin J. 2013. The first 'true' *Adocus* (Testudines, Adocidae) from the Paleogene of Asia. *Journal of Vertebrate Paleontology* 33:1071-1080. 10.1080/02724634.2013.768254

Davis J. 1986. Statistics and Data Analysis in Geology. John Wiley & Sons.

Decelles PG. 1986. Sedimentation in a tectonically partitioned, nonmarine foreland basin: The Lower Cretaceous Kootenai Formation, southwestern Montana. *Geological Society of America Bulletin* 97:911-931.

Dickinson WR, and Snyder WS. 1978. Plate tectonics of the Laramide orogeny. *Geological Society of America Memoirs* 151:355-366.

Eaton JG. 1987. Stratigraphy, depositional environments, and age of Cretaceous mammal-bearing rocks in Utah, and systematics of the Multituberculata (Mammalia). University of Colorado.

Eaton JG, Cifelli RL, Hutchison JH, Kirkland JI, and Parrish JM. 1999. Cretaceous vertebrate faunas from the Kaiparowits Plateau, south-central Utah. In: Gillette DD, ed. *Vertebrate paleontology in Utah*. Salt Lake City: Utah Geological Survey, 345-353.

Eberth DA, Britt BB, Scheetz RD, Stadtman KL, and Brinkman DB. 2006. Dalton Wells: Geology and significance of debris-flow-hosted dinosaur bonebeds in the Cedar Mountain Formation (Lower Cretaceous) of eastern Utah, USA. *Palaeogeography, Palaeoclimatology, Palaeoecology* 236:217-245.

Erickson GM, Krick BA, Hamilton M, Bourne GR, Norell MA, Lilleodden E, and Sawyer WG. 2012. Complex dental structure and wear biomechanics in hadrosaurid dinosaurs. *Science* 338:98-101.

Estes R, and Sanchíz B. 1982. Early Cretaceous lower vertebrates from Galve (Teruel), Spain. *Journal of Vertebrate Paleontology* 2:21-39.

Fanti F, and Miyashita T. 2009. A high latitude vertebrate fossil assemblage from the Late Cretaceous of west-central Alberta, Canada: evidence for dinosaur nesting and vertebrate latitudinal gradient. *Palaeogeography, Palaeoclimatology, Palaeoecology* 275:37-53.

Farke AA, Maxwell WD, Cifelli RL, and Wedel MJ. 2014. A Ceratopsian Dinosaur from the Lower Cretaceous of Western North America, and the Biogeography of Neoceratopsia. *PLOS One* 9:e112055. 10.1371/journal.pone.0112055

Farlow JO, Brinkman DL, Abler WL, and Currie PJ. 1991. Size, shape, and serration density of theropod dinosaur lateral teeth. *Modern Geology* 16:161-198.

Fassell ML, and Bralower TJ. 1999. Warm, equable mid-Cretaceous: Stable isotope evidence. *Geological Society of America Special Papers*:121-142.

Fiorillo AR. 1999. Non-mammalian microvertebrate remains from the Robison Eggshell Site, Cedar Mountain Formation (Lower Cretaceous), Emery County, Utah. In: Gillette DD, ed. *Vertebrate paleontology in Utah*. Salt Lake City: Utah Geological Survey, 259-268.

Frakes LA. 1999. Estimating the global thermal state from Cretaceous sea surface and continental temperature data. *Geological Society of America Special Paper* 332:49-58.

Frederickson JA, Cohen JE, Hunt TC, and Cifelli RL. 2017. A new occurrence of Dakotasuchus kingi from the Late Cretaceous of Utah, USA, and the diagnostic utility of postcranial characters in Crocodyliformes. *Acta Palaeontologica Polonica* 62:279-286.

Gangloff RA. 1998. Arctic dinosaurs with emphasis on the Cretaceous record of Alaska and the Eurasian-North American connection. *Bulletin of the New Mexico Museum of Natural History and Science* 14:211-220.

Gardner J. 1994. Amphibians from the Lower Cretaceous (Albian) Cedar Mountain Formation, Emery Country, Utah. *Journal of Vertebrate Paleontology (supplement)* 14:26A.

Gardner J. 1996. The North American fossil record of Albanerpeton (Lissamphibia, Albanerpetontidae). *Journal of Vertebrate Paleontology* 16:36A.

Gardner J, and Cifelli R. 1999. A primitive snake from the Cretaceous of Utah. *Special Papers in Palaeontology*:87-100.

Gardner JD. 1999a. The amphibian *Albanerpeton arthridion* and the Aptian–Albian biogeography of albanerpetontids. *Palaeontology* 42:529-544.

Gardner JD. 1999b. New albanerpetontid amphibians from the Albian to Coniacian of Utah, USA—bridging the gap. *Journal of Vertebrate Paleontology* 19:632-638.

Garrison JR, Brinkman D, Nichols DJ, Layer P, Burge D, and Thayn D. 2007. A multidisciplinary study of the Lower Cretaceous Cedar Mountain Formation, Mussentuchit Wash, Utah: a determination of the paleoenvironment and paleoecology of the Eolambia caroljonesa dinosaur quarry. *Cretaceous Research* 28:461-494.

Gates T, Sampson S, Zanno L, Roberts E, Eaton J, Nydam R, Hutchison J, Smith J, Loewen M, and Getty M. 2010. Biogeography of terrestrial and freshwater vertebrates from the Late Cretaceous (Campanian) Western Interior of North America. *Palaeogeography, Palaeoclimatology, Palaeoecology* 291:371-387.

Gates TA, and Scheetz R. 2015. A new saurolophine hadrosaurid (Dinosauria: Ornithopoda) from the Campanian of Utah, North America. *Journal of Systematic Palaeontology* 13:711-725.

Goldberg P. 2000. Faunal composition, non-marine vertebrates, of the upper Cedar Mountain formation (Cretaceous: Albian-Cenomanian), central Utah.

Grande L. 2010. An empirical synthetic pattern study of gars (Lepisosteiformes) and closely related species, based mostly on skeletal anatomy. The resurrection of Holostei. *American Society of Ichthyologists and Herpetologists Special Publication* 6:1-871.

Hallam A. 1992. *Phanerozoic sea-level changes*: Columbia University Press.

Hammer Ø, Harper D, and Ryan P. 2001. Paleontological statistics software: Package for education and data analysis. *Palaeontologia Electronica*.

Haq BU, Hardenbol J, and Vail PR. 1987. Chronology of fluctuating sea levels since the Triassic. *Science* 235:1156-1167.

Harper DA. 1999. *Numerical palaeobiology: computer-based modelling and analysis of fossils and their distributions*: John Wiley & Sons Inc.

Hatzell GA. 2015. *Paleoclimate Implications from Stable Isotope Analysis of Sedimentary Organic Carbon and Vertebrate Fossils from the Cedar Mountain Formation, UT, USA*: University of Arkansas.

Heckert AB. 2004. Late Triassic microvertebrates from the lower Chinle Group (Otischalkian-Adamanian: Carnian), southwestern U.S.A. *New Mexico Museum of Natural History and Science Bulletin* 27:1-170.

Hendrickx C, Mateus O, and Araújo R. 2014. The dentition of megalosaurid theropods. *Acta Palaeontologica Polonica* 60:627-642.

Hendrickx C, Mateus O, and Araújo R. 2015. A proposed terminology of theropod teeth (Dinosauria, Saurischia). *Journal of Vertebrate Paleontology* 35:e982797.

Herzog LL, Zanno LE, and Makovicky PJ. 2015. New records of solemydid turtles in North America: Specimens from the Upper Cretaceous Mussentuchit Member of the Cedar Mountain Formation. *Society of Vertebrate Paleontology Program Abstract*:124.

Hirayama R, Brinkman DB, and Danilov IG. 2000. Distribution and biogeography of non-marine Cretaceous turtles. *Russian Journal of Herpetology* 7:181-198.

Hirst CN, Jackson DA. 2007. Reconstructing community relationships: the impact of sampling error, ordination approach, and gradient length. *Diversity and Distributions* 13:361-371.

Holmes, A.D., 2017. Sedimentology and Taphonomy of the *Abydosaurus mcintoshi* Quarry, (Naturita Formation, Early Cretaceous, Latest Albian), Dinosaur National Monument, Utah. Brigham Young University, Provo, UT.

Ji Q, Ji S-A, and Zhang L-J. 2009. First large tyrannosauroid theropod from the Early Cretaceous Jehol Biota in northeastern China. *Geological Bulletin of China* 28:1369-1374.

Ji Q, Norell MA, Makovicky PJ, Gao K-Q, Ji S, and Yuan C. 2003. An early ostrich dinosaur and implications for ornithomimosaur phylogeny. *American Museum Novitates* 3420:1-19.

Joyce WG, Sterli J, and Chapman SD. 2014. The skeletal morphology of the solemydid turtle *Naomichelys speciosa* from the Early Cretaceous of Texas. *Journal of Paleontology* 88:1257-1287. 10.1666/14-002

Kauffman E, and Caldwell W. 1993. The Western Interior Basin in space and time. *Evolution of the Western Interior Basin: Geological Association of Canada, Special Paper* 39:1-30.

Kirkland JI. 1998. A new hadrosaurid from the upper Cedar Mountain Formation (Albian-Cenomanian, Cretaceous) of eastern Utah—the oldest known hadrosaurid (lambeosaurine?). *Bulletin of the New Mexico Museum of Natural History and Science* 14:283-295.

Kirkland JI, Britt B, Burge DL, Carpenter K, Cifelli R, DeCourten F, Eaton J, Hasiotis S, and Lawton T. 1997. Lower to middle Cretaceous dinosaur faunas of the central Colorado

Plateau: a key to understanding 35 million years of tectonics, sedimentology, evolution and biogeography. *Brigham Young University Geology Studies* 42:69-103.

Kirkland JI, Cifelli RL, Britt BB, Burge DL, DeCourten FL, Eaton JG, and Parrish JM. 1999. Distribution of vertebrate faunas in the Cedar Mountain Formation, east-central Utah. In: Gillette DD, ed. *Vertebrate paleontology in Utah*. Salt Lake City: Utah Geological Survey, 201-217.

Kirkland JI, Suarez M, Suarez C, and Hunt-Foster R. 2016. The Lower Cretaceous in East-Central Utah—The Cedar Mountain Formation and its Bounding Strata (Field Trip Guide). *Geology of the Intermountain West* 3:101-228.

Kobayashi Y, and Azuma Y. 2003. A new iguanodontian (Dinosauria: Ornithopoda) from the Lower Cretaceous Kitadani Formation of Fukui Prefecture, Japan. *Journal of Vertebrate Paleontology* 23:166-175.

Larson DW. 2008. Diversity and variation of theropod dinosaur teeth from the uppermost Santonian Milk River Formation (Upper Cretaceous), Alberta: a quantitative method supporting identification of the oldest dinosaur tooth assemblage in Canada. *Canadian Journal of Earth Sciences* 45:1455-1468.

Larson DW, and Currie PJ. 2013. Multivariate analyses of small theropod dinosaur teeth and implications for paleoecological turnover through time. *PLOS One* 8:e54329.

Lillegraven JA. 1969. Latest Cretaceous mammals of upper part of Edmonton Formation of Alberta, Canada, and review of marsupial-placental dichotomy in mammalian evolution.

Lipka TR, Therrien F, Weishampel DB, Jamniczky HA, Joyce WG, Colbert MD, and Brinkman DB. 2006. A new turtle from the Arundel Clay facies (Potomac Formation, Early Cretaceous) of Maryland, U.S.A. *Journal of Vertebrate Paleontology* 26:300-307.

Longrich N. 2008. A new, large ornithomimid from the Cretaceous Dinosaur Park Formation of Alberta, Canada: Implications for the study of dissociated dinosaur remains. *Palaeontology* 51:983-997.

Ludvigson GA, Joeckel RM, Murphy LR, Stockli DF, Gonzalez LA, Suarez CA, Kirkland JI, Al-Suwaidi A. 2015. The emerging terrestrial record of Aptian-Albian global change. *Cretaceous Research* 56:1-24.

Makovicky PJ, and Sues H-D. 1998. Anatomy and phylogenetic relationships of the theropod dinosaur *Microvenator celer* from the Lower Cretaceous of Montana. *American Museum novitates; no 3240*.

Makovicky PJ, Zanno LE, and Gates TA. 2015. The Advent of North America's Late Cretaceous Fauna Revisited: Insights from New Discoveries and Improved Phylogenies. *Journal of Vertebrate Paleontology Program Abstract*:172-173.

Martínez AM, and Kak AC. 2001. Pca versus lda. *IEEE transactions on pattern analysis and machine intelligence* 23:228-233.

Mayr G, Pohl B, Hartman S, and Peters DS. 2007. The tenth skeletal specimen of *Archaeopteryx*. *Zoological Journal of the Linnean Society* 149:97-116.

McDonald AT, Gates TA, Zanno LE, and Makovicky PJ. 2017. Anatomy, taphonomy, and phylogenetic implications of a new specimen of *Eolambia caroljonesa* (Dinosauria: Ornithopoda) from the Cedar Mountain Formation, Utah, USA. *PLOS One* 12:e0176896.

McDonald AT, Kirkland JI, DeBlieux DD, Madsen SK, Cavin J, Milner ARC, and Panzarin L. 2010a. New basal iguanodonts from the Cedar Mountain Formation of Utah and the evolution of thumb-spiked dinosaurs. *PLOS One* 5:11. 10.1371/journal.pone.0014075

McDonald AT, Wolfe DG, and Kirkland JI. 2010b. A new basal hadrosauroid (Dinosauria: Ornithopoda) from the Turonian of New Mexico. *Journal of Vertebrate Paleontology* 30:799 - 812.

Moody R. 1984. The relative importance of cranial/postcranial characters in the classification of sea turtles. *Studia Geologica Salmanticensia Volumen Especial* 1:205-213.

Neilson RP. 1986. High-resolution climatic analysis and southwest biogeography. *Science* 232:27-34.

Nelson ME, and Crooks DM. 1987. Stratigraphy and paleontology of the Cedar Mountain Formation (Lower Cretaceous), eastern Emery County, Utah. In: Averett WR, ed. *Paleontology and Geology of the Dinosaur Triangle: Guidebook for 1987 Field Trip*. Grand Junction: Museum of Western Colorado, 55-63.

Norman DB. 2004. Basal Iguanodontia. In: Weishampel DB, Dodson P, and Osmólska H, eds. *The Dinosauria, Second Edition*. Berkeley: University of California Press, 413-437.

Nydam RL. 1999. Polyglyphanodontinae (Squamata: Teiidae) from the medial and Late Cretaceous: new records from Utah, U.S.A. and Baja California del Norte, Mexico. *Vertebrate Paleontology in Utah, Utah Geological Survey, Salt Lake City* 99:303-317 in D. D. Gillette (ed.).

Nydam RL. 2000a. New records of Early, Medial, and Late Cretaceous lizards and the evolution of the Cretaceous lizard fauna of North America PhD. University of Oklahoma.

Nydam RL. 2000b. A new taxon of helodermatid-like lizard from the Albian–Cenomanian of Utah. *Journal of Vertebrate Paleontology* 20:285-294.

Nydam RL. 2002. Lizards of the Mussentuchit local fauna (Albian-Cenomanian boundary) and comments on the evolution of the Cretaceous lizard fauna of North America. *Journal of Vertebrate Paleontology* 22:645-660.

Nydam RL, and Cifelli RL. 2002. A new teiid lizard from the Cedar Mountain Formation (Albian-Cenomanian boundary) of Utah. *Journal of Vertebrate Paleontology* 22:276-285.

Nydam RL, Rowe TB, and Cifelli RL. 2013. Lizards and snakes of the Terlingua Local Fauna (late Campanian), Aguja Formation, Texas, with comments on the distribution of paracontemporaneous squamates throughout the Western Interior of North America. *Journal of Vertebrate Paleontology* 33:1081-1099. 10.1080/02724634.2013.760467

Nydam RL, Rowe TB, and Cifelli RL. 2013. Lizards and snakes of the Terlingua Local Fauna (late Campanian), Aguja Formation, Texas, with comments on the distribution of paracontemporaneous squamates throughout the Western Interior of North America. *Journal of Vertebrate Paleontology* 33:1081-1099. 10.1080/02724634.2013.760467

Oreska MPJ, Carrano MT, and Dzikiewicz KM. 2013. Vertebrate paleontology of the Cloverly Formation (Lower Cretaceous), I: faunal composition, biogeographic relationships, and sampling. *Journal of Vertebrate Paleontology* 33:264-292. 10.1080/02724634.2012.717567

Osmólska H, and Barsbold R. 1990. Troodontidae. *The Dinosauria* 2:259-268.

Ostrom JH. 1970. Stratigraphy and paleontology of the Cloverly Formation (Lower Cretaceous) of the Bighorn Basin area, Wyoming and Montana. *Peabody Museum of Natural History Yale University Bulletin* 35:234.

Pomes M. 1988. Stratigraphy, paleontology, and paleobiogeography of lower vertebrates from the Cedar Mountain Formation (lower Cretaceous), Emery County, Utah. *Unpublished Master's thesis Fort Hays State University, Fort Hays, Kansas.*

Puértolas-Pascual E, Rabal-Garcés R, and Canudo JI. 2015. Exceptional crocodylomorph biodiversity of" La Cantalera" site (lower Barremian; Lower Cretaceous) in Teruel, Spain. *Palaeontologia Electronica* 18:1-16.

Rasband WS, ImageJ U, and Health NIo. 2011. Bethesda, Maryland, USA, 1997–2014. *URL:* http://imagej *nih gov/ij/(16 4 2013)*.

Rauhut OW. 2002. Dinosaur teeth from the Barremian of Uña, province of Cuenca, Spain. *Cretaceous Research* 23:255-263.

Rauhut OW, Milner AC, and Moore-Fay S. 2010. Cranial osteology and phylogenetic position of the theropod dinosaur *Proceratosaurus bradleyi* (Woodward, 1910) from the Middle Jurassic of England. *Zoological Journal of the Linnean Society* 158:155-195.

Rensberger JM, and Krentz HB. 1988. Microscopic effects of predator digestion on the surfaces of bones and teeth. *Scanning Microscopy* 2:1541-1551.

Rogers RR, Carrano MT, Rogers KAC, Perez M, and Regan AK. 2017. Isotaphonomy in concept and practice: an exploration of vertebrate microfossil bonebeds in the Upper Cretaceous (Campanian) Judith River Formation, north-central Montana. *Paleobiology* 43:248-273.

Russell DA. 1993. The role of Central Asia in dinosaurian biogeography. *Canadian Journal of Earth Sciences* 30:2002-2012.

Russell DA. 1995. China and the lost worlds of the dinosaurian era. *Historical Biology* 10:3-12.

Sankey JT. 2001. Late Campanian southern dinosaurs, Aguja Formation, Big Bend, Texas. *Journal of Paleontology* 75:208-215.

Sankey JT. 2008a. Diversity of latest Cretaceous (Late Maastrichtian) small theropods: Teeth from the Lance and Hell Creek Formations, USA. In: Sankey JT, and Baszio S, eds. *Life of the Past*. Bloomington: Indiana University Press, 117-134.

Sankey JT. 2008b. Vertebrate paleoecology from microsites, Talley Mountain, Upper Aguja Formation (Late Cretaceous), Big Bend National Park, Texas, USA. In: Sankey JT, and Baszio S, eds. *Life of the Past*. Bloomington: Indiana University Press, 61-77.

Sankey JT, Brinkman DB, Guenther M, and Currie PJ. 2002. Small theropod and bird teeth from the late Cretaceous (late Campanian) Judith River Group, Alberta. *Journal of Paleontology* 76:751-763.

Saward S. 1992. A global view of Cretaceous vegetation patterns. *Geological Society of America Special Papers* 267:17-36.

Scheyer T, Pérez-García A, and Murelaga X. 2015. Shell bone histology of solemydid turtles (stem Testudines): palaeoecological implications. *Organisms Diversity & Evolution* 15:199-212.

Scheyer TM, Sander PM, Joyce WG, Böhme W, and Witzel U. 2007. A plywood structure in the shell of fossil and living soft-shelled turtles (Trionychidae) and its evolutionary implications. *Organisms Diversity & Evolution* 7:136-144.

Scheyer TM, Syromyatnikova EV, and Danilov IG. 2017. Turtle shell bone and osteoderm histology of Mesozoic and Cenozoic stem-trionychian Adocidae and Nanhsiungchelyidae (Cryptodira: Adocusia) from Central Asia, Mongolia, and North America. *Mitteilungen aus dem Museum für Naturkunde in Berlin Fossil Record* 20:69.

Schoch RR, Ullmann F, Rozynek B, Ziegler R, Seegis D, and Sues H-D. 2018. Tetrapod diversity and palaeoecology in the German Middle Triassic (Lower Keuper) documented by tooth morphotypes. *Palaeobiodiversity and Palaeoenvironments*:1-24.

Schwarz-Wings D, Rees J, and Lindgren J. 2009. Lower cretaceous mesoeucrocodylians from Scandinavia (Denmark and Sweden). *Cretaceous Research* 30:1345-1355.

Sereno PC. 1999. The evolution of dinosaurs. *Science* 284:2137-2147.

Shannon C, and Weaver W. 1949. The mathematical theory of communication. *University of Illinois Press Urbana*.

Silva H, and Gallo V. 2011. Taxonomic review and phylogenetic analysis of Enchodontoidei (Teleostei: Aulopiformes). *Anais da Academia Brasileira de Ciências* 83:483-511.

Smith JB. 2002. An examination of dental morphology and variation in theropod dinosaurs: implications for the identification of shed teeth. *PhD Dissertation, University of Pennsylvania.*

Smith JB. 2005. Heterodonty in *Tyrannosaurus rex*: implications for the taxonomic and systematic utility of theropod dentitions. *Journal of Vertebrate Paleontology* 25:865-887.

Smith JB, Vann DR, and Dodson P. 2005. Dental morphology and variation in theropod dinosaurs: implications for the taxonomic identification of isolated teeth. *The Anatomical Record Part A: Discoveries in Molecular, Cellular, and Evolutionary Biology* 285:699-736.

Sorensen, A.E.M., 2011. Geologic mapping of exhumed, mid-Cretaceous paleochannel complexes near Castle Dale, Emery County, Utah: On the correlative relationship between the Dakota Sandstone and the Mussentuchit Member of the Cedar Mountain Formation. *Brigham Young University, Provo, UT.*

Spellerberg IF, and Fedor PJ. 2003. A tribute to Claude Shannon (1916–2001) and a plea for more rigorous use of species richness, species diversity and the 'Shannon–Wiener' Index. *Global ecology and biogeography* 12:177-179.

Stokes WL. 1944. Morrison Formation and related deposits in and adjacent to the Colorado Plateau. *Bulletin of the Geological Society of America* 55:951-992.

Stokes WL. 1952. Lower Cretaceous in Colorado Plateau. *AAPG Bulletin* 36:1766-1776.

Suarez CA, González LA, Ludvigson GA, Cifelli RL, and Tremain E. 2012. Water utilization of the Cretaceous Mussentuchit Member local vertebrate fauna, Cedar Mountain Formation, Utah, USA: Using oxygen isotopic composition of phosphate. *Palaeogeography, Palaeoclimatology, Palaeoecology* 313:78-92.

Suarez CA, González LA, Ludvigson GA, Kirkland JI, Cifelli RL, and Kohn MJ. 2014. Multi-taxa isotopic investigation of paleohydrology in the Lower Cretaceous Cedar Mountain Formation, Eastern Utah, USA: deciphering effects of the Nevadaplano Plateau on regional climate. *Journal of Sedimentary Research* 84:975-987.

Sweetman SC. 2004. The first record of velociraptorine dinosaurs (Saurischia, Theropoda) from the Wealden (Early Cretaceous, Barremian) of southern England. *Cretaceous Research* 25:353-364.

Syromyatnikova E, and Danilov I. 2009. New material and a revision of turtles of the genus *Adocus* (Adocidae) from the Late Cretaceous of Middle Asia and Kazakhstan. *Трудыы Зоологического института РАН* 313:74-94.

Tucker RT, Makovicky PJ, and Zanno LE (in press). Recent advances in temporal calibration for newly discovered dinosaurian assemblages in the Mussentuchit Member of the Cedar Mountain Formation, Central Utah, USA. *J Vert Paleontol Progr Abstr*.

Titus AL, and Loewen MA. 2013. *At the Top of the Grand Staircase: The Late Cretaceous of Southern Utah*: Indiana University Press.

Upchurch Jr G, and Wolfe J. 1987. Mid-Cretaceous to Early Tertiary vegetation and climate: evidence from fossil leaves and woods. *Origins of angiosperms and their biological consequences/edited by EM Friis, WG Chaloner, and PR Crane*.

Virág A, and Ősi A. 2017. Morphometry, microstructure and wear pattern of neornithischian dinosaur teeth from the Upper Cretaceous Iharkút locality (Hungary). *The Anatomical Record*:n/a-n/a. 10.1002/ar.23592

Vullo R, Neraudeau D, and Lenglet T. 2007. Dinosaur teeth from the Cenomanian of Charentes, Western France: evidence for a mixed Laurasican-Gondwanan assemblage. *Journal of Vertebrate Paleontology* 27:931-943.

White T, Furlong K, and Arthur M. 2002. Forebulge migration in the Cretaceous Western Interior basin of the central United States. *Basin Research* 14:43-54.

Williamson TE, and Brusatte SL. 2014. Small theropod teeth from the Late Cretaceous of the San Juan Basin, northwestern New Mexico and their implications for understanding Latest Cretaceous dinosaur evolution. *PLOS One* 9:e93190.

Wilson LE. 2008. Comparative taphonomy and paleoecological reconstruction of two microvertebrate accumulations from the Late Cretaceous Hell Creek Formation (Maastrichtian), eastern Montana. *Palaios* 23:289-297.

Wilson LE, Chin K, and Cumbaa SL. 2016. A new hesperornithiform (Aves) specimen from the Late Cretaceous Canadian High Arctic with comments on high-latitude hesperornithiform diet. *Canadian Journal of Earth Sciences* 53:1476-1483.

Winkler DA, Murry PA, and Jacobs LL. 1990. Early Cretaceous (Comanchean) vertebrates of central Texas. *Journal of Vertebrate Paleontology* 10:95-116.

Young RG. 1960. Dakota Group of Colorado Plateau. *Bulletin of the American Association of Petroleum Geologists* 44:156-194.

Zanno LE, and Makovicky PJ. 2011. On the earliest record of Cretaceous tyrannosauroids in western North America: implications for an Early Cretaceous Laurasian interchange event. *Historical Biology* 23:317-325.

Zanno LE, and Makovicky PJ. 2013. Neovenatorid theropods are apex predators in the Late Cretaceous of North America. *Nature Communications* 4(1):2827 DOI 10.1038/ncomms3827.

Zanno LE, Loewen MA, Farke AA, Kim G-S, Claessens L, and McGarrity CT. 2013. Late Cretaceous theropod dinosaurs of southern Utah. At the Top of the Grand Staircase: The Late Cretaceous of Southern Utah Edited by AL Titus and MA Loewen Indiana University Press, Bloomington:504-525.

Zanno LE, and Makovicky PJ. 2016. A new species of early diverging ornithopod increases the paleobiodiversity of herbivorous dinosaurs in late Cretaceous ecosystems in North America. *Journal of Vertebrate Paleontology, Program and Abstracts*:256.

Zelenitsky DK, Carpenter K, and Currie PJ. 2000. First record of elongatoolithid theropod eggshell from North America: The Asian oogenus *Macroelongatoolithus* from the Lower Cretaceous of Utah. *Journal of Vertebrate Paleontology* 20:130-138.

CHAPTER 2

Comparing morphometric methods for quantifying shape variation: best practices for archosaurian teeth

ABSTRACT

Isolated teeth often constitute the majority of identifiable vertebrate remains from microvertebrate fossil localities, and are therefore useful indicators of biodiversity. However, without associated skeletal material, taxonomic referrals based on isolated teeth can be tenuous. For example, although generally considered homodont, the dentitions of some theropod dinosaurs display underappreciated morphological disparity within the tooth row. Several studies have conducted multivariate statistical analyses, utilizing series of linear measurements, in order to discriminate between tooth morphologies for the purpose of taxonomic identifications. The traditional method of using linear measurements has proven relatively effective at parsing out tooth morphotypes; however, this approach often fails to account for various morphological tooth features predicted to be important indicators of similarity. For example, characteristics such as curvature, regions of convexity and concavity, carina orientation, and other nuances of shape are usually excluded from these analyses, or may require additional calculations and arbitrary measurements that may not be homologous across all samples. In contrast, geometric morphometrics offers the ability to statistically compare the shape of teeth with more refinement, potentially improving taxonomic identifications. Unfortunately, geometric morphometric analysis of isolated teeth is challenged by the simplicity of archosaurian teeth, which yield few discrete homologous points, and the often-diminutive size of specimens, which have proven difficult to capture in 3D. Here I characterized the shape of 32 archosaurian (theropod, phytosaurian, mosasaurid, mesocrocodillian) and two osteichthyan teeth using traditional linear measurements, 2D and 3D geometric morphometrics, as well as combinations of these

techniques, and analyze shape data using various multivariate techniques. I compare the effectiveness of these various protocols based on accuracy (correct placement of teeth in known taxonomic groups), data discrimination (ability to reduce convex hull overlap, identify ontogenetic differences, and account for preservation quality), amount of time and labor necessary, and complexity of the approach. Although data collection effort is significantly higher, I find optimum accuracy and data discrimination of isolated archosaurian teeth when 2D landmarks are used, and find additional value in combining linear measurements with either 2D and 3D landmarks.

INTRODUCTION

Historically, the practice of analyzing biological morphology was a descriptive field (Thompson 1917). However, the early 20th century saw a paradigm shift towards quantitative approaches, concurrent with the advent of statistical methods such as correlation coefficient (Pearson 1895), variance analysis (Fisher 1935), and principal component analysis (Hotelling 1933; Pearson 1901). The application of various morphometric methods gained increasing favor towards the later part of the century (Bookstein 1998; Adams et al. 2004), and morphometrics have been utilized in a wide array of fields such as comparative anatomy (Harvati 2003; Marugan-Lobon & Buscalioni 2003; Marugán-Lobón & Buscalioni 2009), functional morphology (Andrews 1974; Nickel et al. 2006; Kulemeyer et al. 2009), ontogeny (Fink & Zelditch 1995; Rohlf 1998), phylogenetics (Zelditch et al. 1995; Stone 2003; González-José et al. 2008; Klingenberg & Gidaszewski 2010), and taxonomy (Dodson 1976; Chapman & Brett-Surman 1990; Naylor & Marcus 1994).

Morphometric analyses are conducted using either traditional or geometric morphometrics, the former relying on a series of measured variables such as linear measurements, angles, volume, area, and ratios (Blackith & Reyment 1971; Bookstein 1978), and the latter utilizing a series of 2-dimensional or 3-dimensional landmarks, placed at homologous points along a comparable area of interest (Richtsmeier et al. 2002; Small 2012).

Isolated teeth offer an abundance of biological information, as compared to other anatomical structures, and are particularly useful for addressing paleontological questions at the community level (Brinkman 1990). Terrestrial vertebrates such as archosaurs and lizards exhibit polyphyodonty, continuously shedding their teeth into the environment throughout their lifetime. Additionally, teeth are covered in enamel, one of the strongest biological substances (Shellis et al. 1998), and are therefore particularly resistant to abrasion and decomposition, preserving much of their structural integrity and morphological information (Argast et al. 1987; Teaford 1988). Together, these factors lead to high preservation potential and underscore the usefulness of isolated teeth for understanding fossil vertebrate assemblages (e.g. Estes 1964; Dodson 1983; Dodson et al. 1987; Fiorillo 1989; Evans & Milner 1994; Hasegawa et al. 1995; Long & Murry 1995; Chinnery et al. 1998; Larsson & Sidor 1999; Lucas et al. 1999; Weishampel et al. 1999; Nydam 2000; Papazzoni 2003; Heckert 2004; Zanno & Makovicky 2011; Gates et al. 2013; Oreska et al. 2013; Gerke & Wings 2016; Frederickson et al. 2017; Schoch et al. 2018).

Until recently, the practice of assigning isolated archosaurian teeth has depended largely on traditional morphometrics (e.g., Sankey et al. 2002; Smith et al. 2005; Larson & Currie 2013; Hendrickx et al. 2014; Williamson & Brusatte 2014; Gerke & Wings 2016). This is because archosaurian teeth are simple geometric shapes, with few identifiable homologous points that can be associated with manually placed landmarks. Furthermore, until recently, capturing accurate

3D data on diminutive objects has been an impractical or impossible task, and by contrast, collecting linear measurement data is a relatively low investment in terms of time, labor, and complexity.

Prior to Smith et al. (2005) many studies using isolated teeth based taxonomic referrals on gross similarity with the teeth of other dinosaurs (e.g., Fiorillo & Currie 1994; Zinke 1998; Fiorillo & Gangloff 2000; Sankey et al. 2002; Buffetaut et al. 2004). Smith et al. (2005) was one of the first to apply a rigorous approach at discriminating theropod tooth morphologies using quantitative morphometrics. The objective was to determine if isolated theropod teeth could be correctly classified to refined taxonomic levels. The researchers created a dataset of 345 teeth, comprised of 325 insitu teeth belonging to 20 theropod clades, and 20 isolated cf. *Tyrannosaurus* teeth. Seventeen morphological variables comprised of linear measurements, curvature profiles, serration densities, and serration size densities were used in a series of different multivariate analyses.

Smith et al. (2005) performed four analyses of variance (ANOVA) tested the between-taxon comparisons of four size variables and another four ANOVAs tested the between-taxon comparisons of shape and denticle size variables. These tests showed that the individual dental characteristics of theropod teeth had high discrimination potential. Next, the authors conducted a linear discriminant analysis (LDA), which successfully classified 15 of the 20 theropod groups in every case, with the 5 remaining groups correctly classified in over 95% of the cases. Overall, 97% of specimens were said to be correctly classified. The authors noted that this high success rate was surprising, especially due to the high degree of morphological variation along the dental row in some theropod groups such as *T.rex* and *Masiakasaurus*; a result later linked to a small

sample size comprised of a restricted number of taxa with similar dentitions (Hendrickx et al 2014).

Despite the small sample size, Smith et al. (2005) showed that most isolated theropod teeth can be identified, or at least classified, within a reasonable degree of certainty to the genus level using numerical dental information. This work opened up the possibility of utilizing the previously ignored collections of abundant isolated theropod teeth to address paleoecological and biogeographic questions.

Larson & Currie (2013) sought to test if isolated coelurosaurian teeth could be reliably referred to the species level. In this study, they used teeth that were previously described from more complete skeletal material, specifically *Dromaeosaurus albertensis, Richardoestesia gilmorei, Saurornitholestes langstoni,* and *Troodon formosus.* Additionally, the authors aimed to assess the taxonomic diversity of ten western North American lithostratigraphic units, which span the last 18 million years of the Cretaceous, in order to determine if faunal turnovers could be quantifiably documented.

The authors compiled a dataset on the measurements of 1183 complete teeth. Each tooth was classified as belonging to one of ten Late Cretaceous formations and measured using three linear measurements and two denticle density variables. A canonical variate analysis (CVA) was performed on 1047 of the teeth (Figure 2.1), and a series of LDAs was performed using the entire dataset.

These analyses parsed the sample into 23 distinct tooth morphotypes, each likely representing a distinct theropod taxon from one of the ten formations. When placed in a stratigraphic context, these tooth morphotypes revealed two important diversity trends: (1) the Late Cretaceous of North America had a far greater diversity of small theropods than previously

recognized and therefore hosted multiple theropod faunal turnovers comparable to those recognized in other dinosaur lineages (Currie 2003; Ryan & Currie 2005); and (2) theropod diversity was higher during the Late Campanian and lower towards the Cretaceous–Paleogene (K–Pg) extinction event, in alignment with data derived from a number of other dinosaur clades by previous authors (Sloan et al. 1986; Barrett et al. 2009; Campione & Evans 2011; Lloyd 2011).

These results suggested that distinct taxa could be identified with high resolution from a series of different formations, even if those formations lacked other skeletal material. However, the authors noted that referring temporally or geographically isolated material to the species or genus level is unwise without quantifying similarities. Additionally, the authors noted three other concerns. Some of the difficulties involving distinguishing tooth morphologies in their analysis may be attributable to incorrect referrals based on a priori hypotheses. For example, analyses were more robust if taxonomic groups were previously described with in situ teeth (e.g., dromaeosaurids and some *Richardoestesia* taxa). Analyses performed with small sample sizes ($n<10$) were often difficult to interpret and produced inconsistent results and analyses performed on closely related taxa usually suffered from poor discrimination, due to similar dental morphologies. Nonetheless, this study highlighted the potential for similar biodiversity analyses to be conducted in other formations across the globe, especially those with poor skeletal representations. However, the potential for variation due to ontogeny and heterodonty across the tooth row should be taken into consideration, as failure to do so may result in over splitting of taxa.

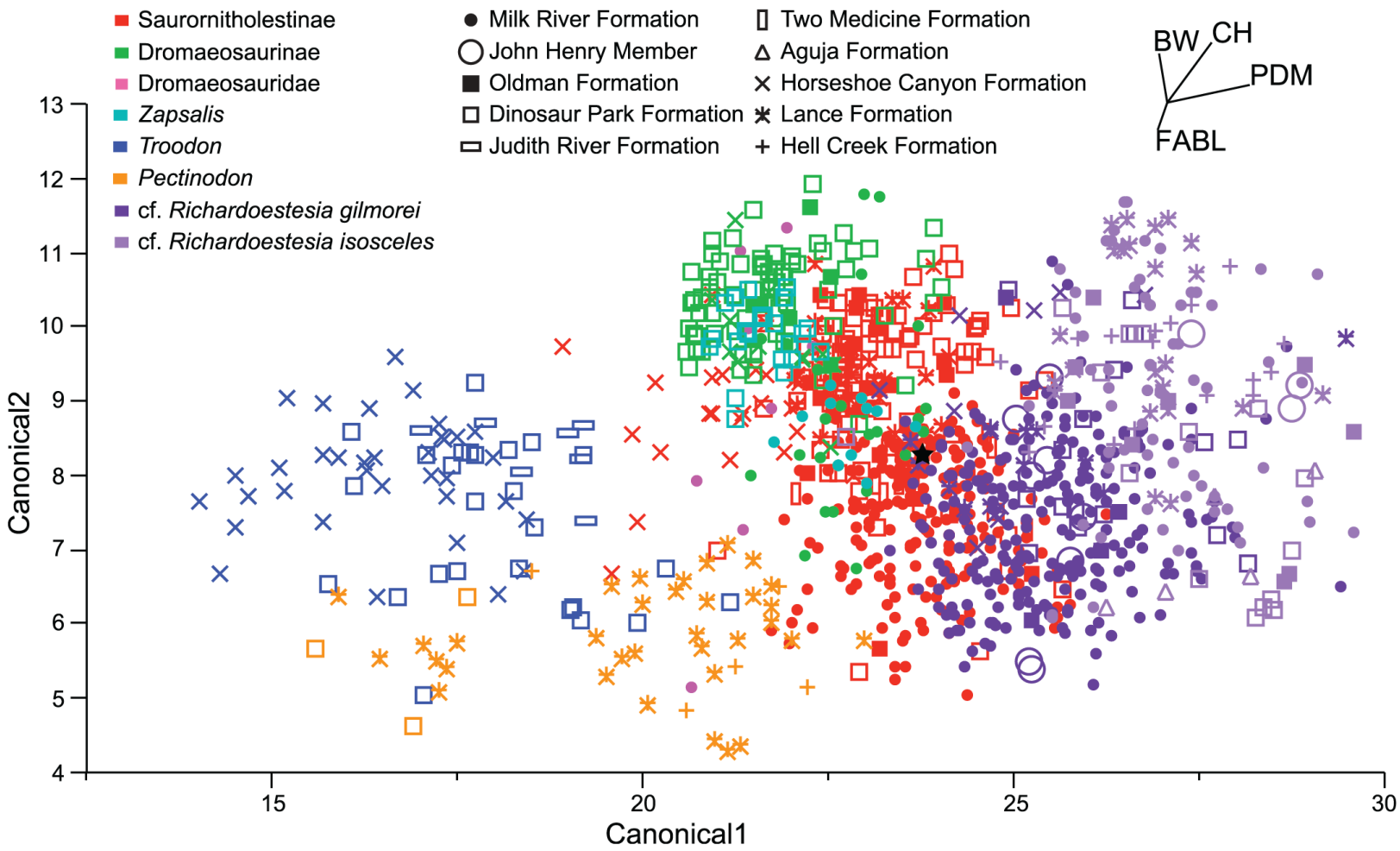

Figure 2.1: Canonical variate analysis
Canonical variate analysis (CVA) of 1047 Late Cretaceous North America theropod teeth using four linear measurements (reproduced from Larson & Currie 2013).

Williamson & Brusatte (2014) recognized that well documented studies of theropod biodiversity using isolated teeth had been primarily focused on faunas of the northern Rockies. Therefore, it was unknown whether the southern North America theropod faunas were distinct from those in the north. Furthermore, investigating the taxonomic diversity of southern faunas was paramount to a more complete understanding of the biodiversity changes occurring in North American towards the end of the Cretaceous.

The authors used the Larson & Currie (2013) dataset and added 116 isolated theropod teeth, collected from six lithostratigraphic units in the San Juan Basin of Northwestern New Mexico, spanning the Santonian, late Campanian, and late Maastrichtian. A synapomorphy-based approach was initially used to classify some of the teeth with discrete characters known to be phylogenetically distinct. Next, a PCA was performed to see if teeth from the San Juan Basin overlapped with teeth that were previously referred to specific groups from other geographic regions (Figure 2.2). Finally, a series of LDAs were performed in order to see if there was a distinction between tooth morphologies from the San Juan Basin and the better constrained tooth morphologies from the northern areas. The authors employed the same five tooth measurement variables used in Larson & Currie (2013).

The sample size of teeth from Santonian-age strata of the San Juan Basin was small and revealed the presence of tyrannosaurid and dromaeosaurid teeth. The small tyrannosaurid teeth were described as sharing a similar morphology to small tyrannosaurid teeth from the contemporaneous Milk River Formation of Alberta, whereas the dromaeosaurid teeth were described as possibly distinct from any other western North American dromaeosaurids. Similarly, the authors found the specimens from the Campanian age strata of the San Juan Basin

to be similar to those of Campanian age strata from the north, with differences being related to relative abundance of some taxa, specifically troodontids and a *Dromaeosaurus*-like taxon.

Lastly, the tooth morphotypes from the Maastrichtian age strata of the San Juan Basin were found to be similar to those of Maastrichtian age strata from the north. However, the authors noted that the recovery of an abundant troodontid tooth morphotype, which was not present in the northern latest Cretaceous faunas, suggested that some differences may indeed exist between the western American faunas of the north and south. Overall, the authors found that the San Juan Basin faunas did not seem to indicate major reductions in theropod diversity during the Campanian to the Maastrichtian, and the diversity and faunal patterns of the northern regions were largely consistent with those in the south.

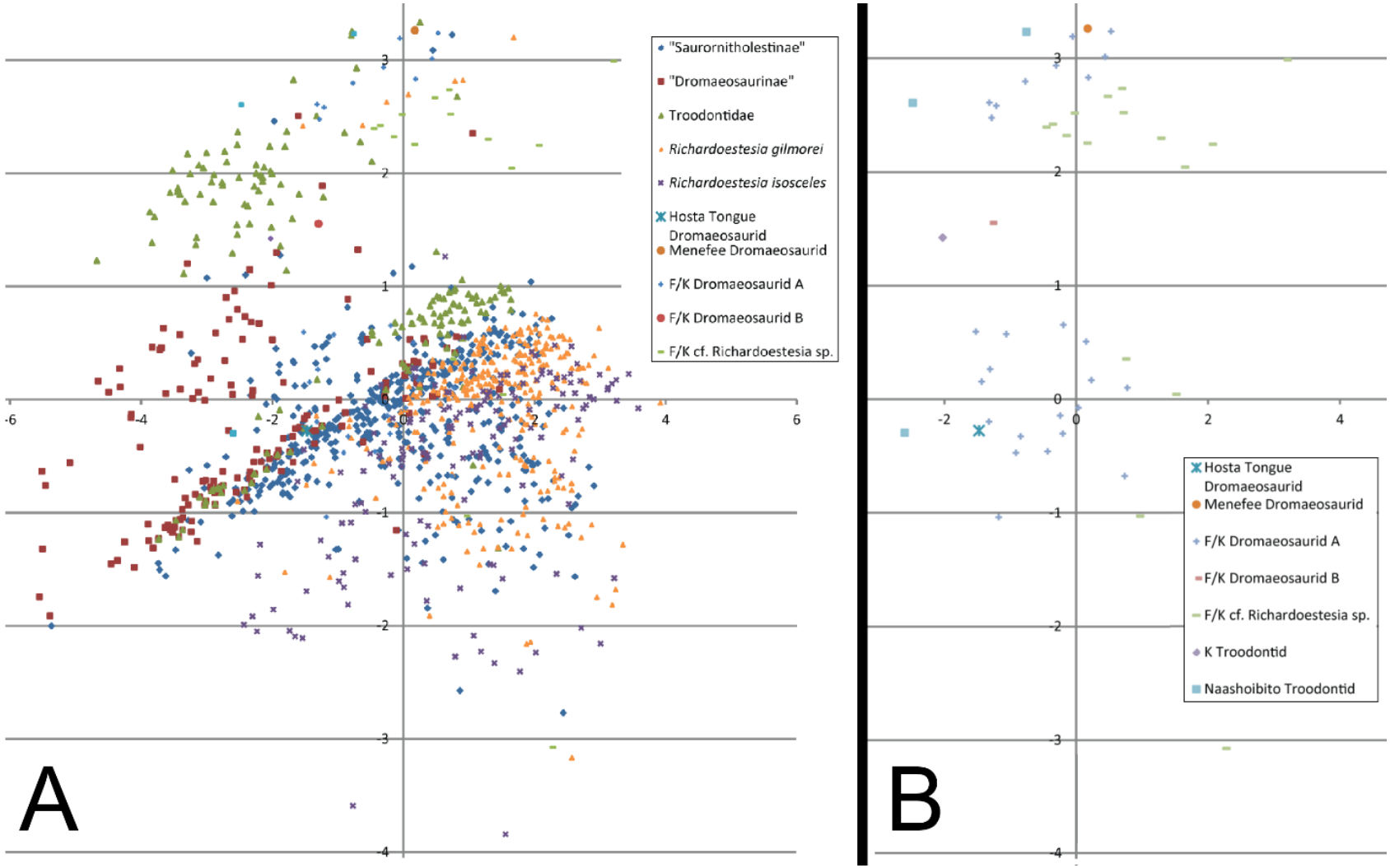

Figure 2.2: Principal component analysis

(A) Principal component analysis (PCA) of ~1163 Late Cretaceous North America theropod teeth using five linear measurements (Williamson & Brusatte 2014). **(B)** Same analysis with only the San Juan Basin specimens visualized. (reproduced from Williamson & Brusatte 2014)

Hendrickx et al. (2014) aimed to provide a comprehensive description of the dentition of Megalosauridae, a clade of large theropod dinosaurs that share a suite of dental similarities with other ziphodont theropods. Multivariate approaches were used to compare the teeth of megalosaurids to all major theropod clades in order to parse out quantitative distinctions. The authors compiled an extensive sample of theropod tooth diversity, including 995 teeth represented by 62 theropod taxa and 19 groupings, and performed a series of multivariate analyses.

Hendrickx et al. (2014) performed four linear discriminant analyses, the first of which was the most taxonomically inclusive (Figure 2.3 A). A second analysis was performed on a reduced dataset of 393 teeth, incorporating only those theropods whose dentition was most similar to Megalosauridae (Figure 2.3 B). The third analysis was performed on 232 teeth representing seven taxa and separated based on lateral or mesial dental position (Figure 2.3 C). The final analysis was performed on 81 teeth representing seven megalosaurid taxa, and one indeterminate tetanuran (Figure 2.3 D). All analyses utilized a total of eight morphological variables, except for the final analysis, which used 15 (Figure 2.3 D).

The analyses were able to effectively distinguish Megalosauridae from theropod clades with specialized dentitions, such as Coelophysoidea, Spinosauridae, and Tyrannosauroidea. However, they failed to significantly distinguish Megalosauridae teeth from other clades with morphologically similar dentition, specifically Ceratosauridae, early diverging megalosauroids, and Allosauroidea.

Table 2.1 is derived from the confusion matrix of the LDA represented in Figure 2.3 A and shows the percent of correctly identified taxa to each of their respective groupings. In the LDA using the entire tooth dataset only 71% of specimens were correctly classified to their

correct groupings, a number that dropped to 66.5% in the LDA considering only Megalosauridae teeth. Teeth belonging to early diverging theropods, troodontids, spinosaurids, *Richardoestesia,* and *Nuthetes* had the highest correct classifications at 85% – 94%. In contrast, the analysis had the most difficulty classifying ceratosaurid and megalosaurid teeth, with only 15% – 21% correctly classified.

The issues with correct classifications were explained due to the significant amount of overlap observed by teeth with similar dental morphologies, such as small teeth with small denticles and large teeth with large denticles. This is highlighted further in the LDA produced using the reduced dataset of only large ziphodont teeth (Figure 2.3 D), which shows that teeth of Megalosauridae and other large ziphodont theropods occupy the same morphospace, even when a greater number of measurement variables are incorporated. Some overlap was attributed to the degree of variation between mesial and lateral dentitions, highlighted in (Figure 2.3 C), which split taxonomic groups between mesial and lateral teeth, resulting in distinct differences in morphospace occupation.

The authors state that LDAs should be used cautiously when analyzing large ziphodont teeth due to the difficulties in distinguishing tooth dimensions and denticle quantity; suggesting quantitive identifications are only reliable for clades with distinct, easily quantified morphological characteristics such as those of Troodontidae, Spinosauridae, and Tyrannosauridae. Hendrickx et al. 2014 proposed three possibilities that may overcome the issues of poor discrimination: using additional morphological variables or measurements, increasing sample size, and utilizing geometric morphometrics.

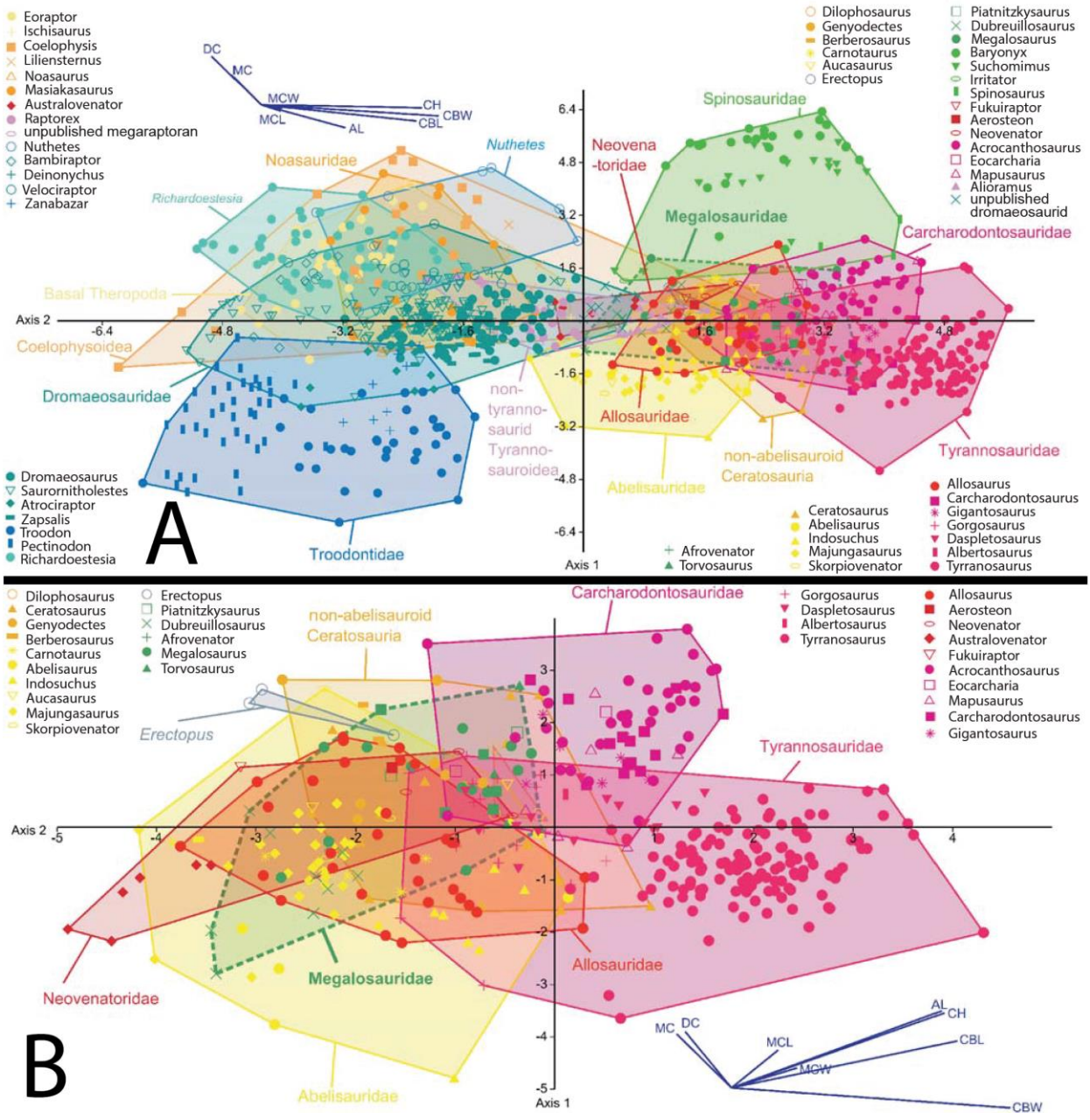

Figure 2.3: Linear discriminant analysis

(A – D) Linear discriminant analyses. **(A)** Entire dataset of 995 teeth sampled widely across the Mesozoic theropod diversity. Eigenvectors correspond to eight measurement variables. **(B)** 393 teeth representing 11 groups of large ziphodont theropods. Eigenvectors correspond to eight measurement variables.

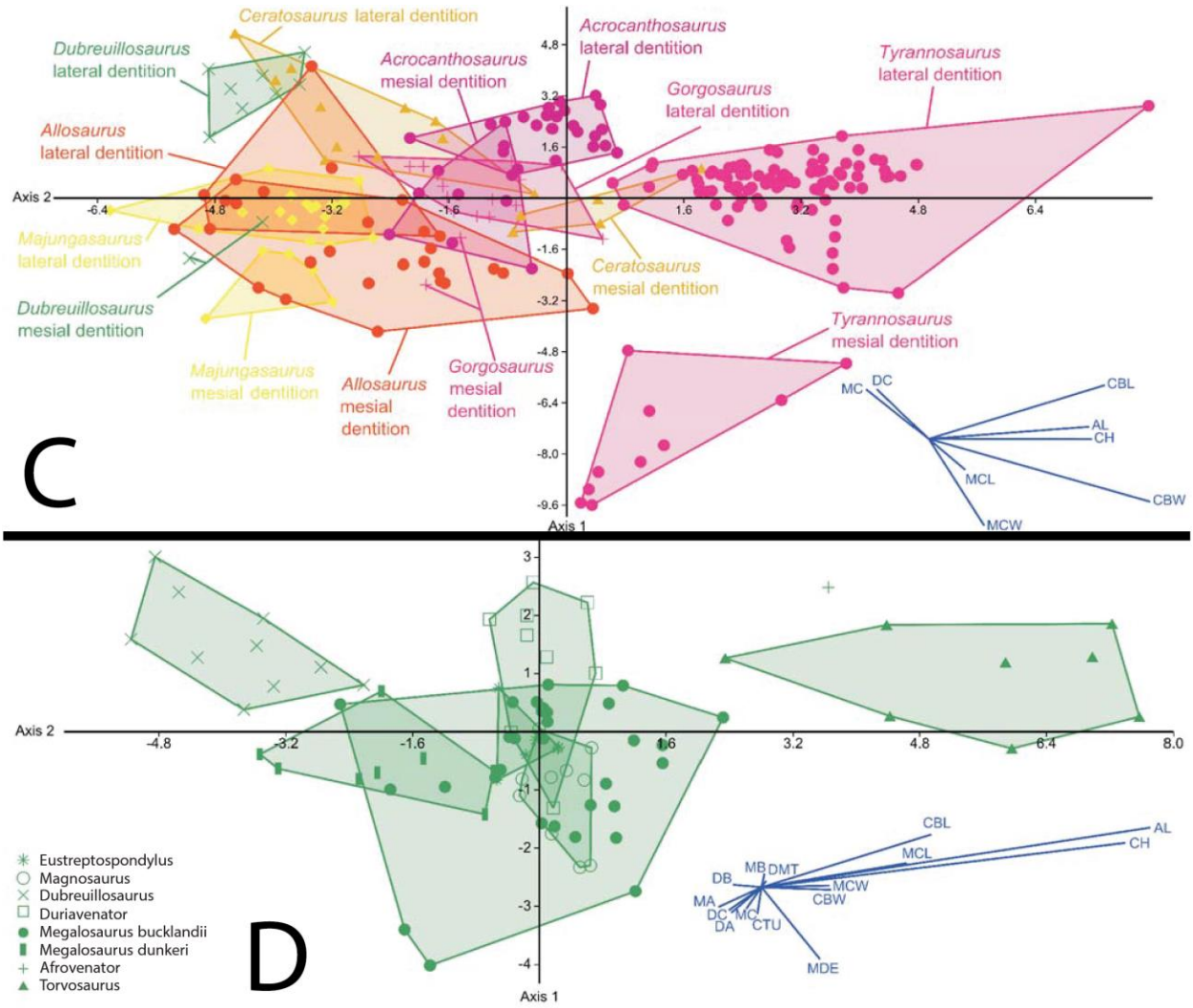

Figure 2.3 (continued): (C) 232 teeth representing 7 taxa. Groupings separated based on lateral or mesial dental position. Eigenvectors correspond to eight measurement variables. **(D)** 81 teeth representing 7 taxa of Megalosauridae, and one indeterminate tetanuran. Eigenvectors correspond to eight measurement variables. (reproduced from Hendrickx et al. 2014).

Table 2.1: Table of misclassification
Table showing the percent of correctly classified specimens to their true groupings (reproduced from Hendrickx et al. 2014).

Clades	Number of teeth correctly assigned	Total	% correctly identified
Basal Theropoda	25	29	86.2
Coelophysoidea	20	31	64.5
Ceratosauridae	4	26	15.4
Noasauridae	5	24	20.8
Abelisauridae	39	55	70.9
Erectopus	3	3	100
Piatnitzkysaurus	2	2	100
Megalosauridae	7	33	21.2
Spinosauridae	43	49	87.8
Allosauridae	18	31	58.1
Neovenatoridae	8	11	72.7
Carcharodontosauridae	47	64	73.4
Basal Tyrannosauroidea	23	39	59
Tyrannosauridae	129	164	78.7
Nuthetes	8	9	88.9
Dromaeosauridae	205	297	69
Troodontidae	77	82	93.9
Richardoestesia	42	45	93.3
Total	705	994	70.9

Per the concerns mentioned in the previous studies, I sought additional ways of reducing or eliminating the overlapping regions in multivariate analyses of tooth morphology. I initially considered increasing the number of standard measurements, in order to capture a wider breadth of morphological data, by using additional linear measurements, ratios, and angles. However, the morphology of archosaurian teeth are relatively simple geometric shapes and the lack of discrete homologous points across comparable specimens would potentially introduce a greater degree of human error due to inconsistent measurements or poorly quantified tooth features, limiting the reliability of this approach. Geometric morphometrics, by comparison, offers a more effective means to standardize morphological comparisons. Techniques in geometric morphometrics, such as generalized Procrustes superimposition of sliding semilandmarks, allow for the automatic placement of equally spaced landmarks across corresponding objects of interest (Polly 2012; Pomidor et al. 2016).

Therefore, the application of geometric morphometrics may allow for a wider breadth of morphological information to be considered in studies focusing on the quantitive analysis of archosaurian teeth, such as those mentioned previously, which may have been limited by utilizing an insufficient quantity of measurement variables. Here I employ a series of various approaches to data collection, data processing, and statistical analyses in order to compare and contrast the effectiveness of three morphometric methodological approaches, (Traditional linear measurements, 2D-landmarks, and 3D landmarks) for parsing out taxonomic referrals on archosaurian teeth. Specifically, I address the following two questions: (1) which of these three methods produce the least overlap of convex hulls (effectiveness at discriminating data); and (2) which methods require the least investment in terms of time and labor? Additionally, the effects of tooth preservation quality and variation due to dental placement (teeth with left or right

recurvature in mesial view depending on dental position) are important considerations. However, addressing these questions confidently is difficult with a sample size of only 34 teeth; where only indeterminate theropod tooth #2 and #3 represent the same tooth with different preservation quality, and only three troodontid theropod and three dromaeosaurid theropod teeth display significant recurvature in mesial view. Nonetheless, the effects of these preservational and morphological factors will be addressed briefly.

Although other derivatives of these approaches exist, such as using various outline analyses instead of 2D-landmarks (e.g. Lestrel 1982; 1989; Lohmann 1983; MacLeod 1999; Joshi et al. 2011), I focus on those most commonly used by relevant studies.

MATERIALS AND METHODS

Data Collection

All analyses were performed using a sample of 34 teeth placed into one of nine groups (Figure 2.4). Due to long data collection times required for 3D-landmark approaches, a sample size of only 34 teeth was constructed in order to maintain consistent comparisons between all analyses. The sample is composed of 18 theropod dinosaur teeth (grouped into sub-categories [three dromaeosaurid teeth, three troodontid teeth, three cf. spinosaurid teeth, and nine indeterminate theropods]), five phytosaurian teeth, five mosasaurid teeth, four mesocrocodillian teeth, and two osteichthyan (*Enchodus*) teeth. The teeth included in the sample were selected because they overlap in general morphology, a particular problem references by the previously discussed studies, and therefore allow me to assess which of the methodologies tested results in the greatest improvement in data discrimination.

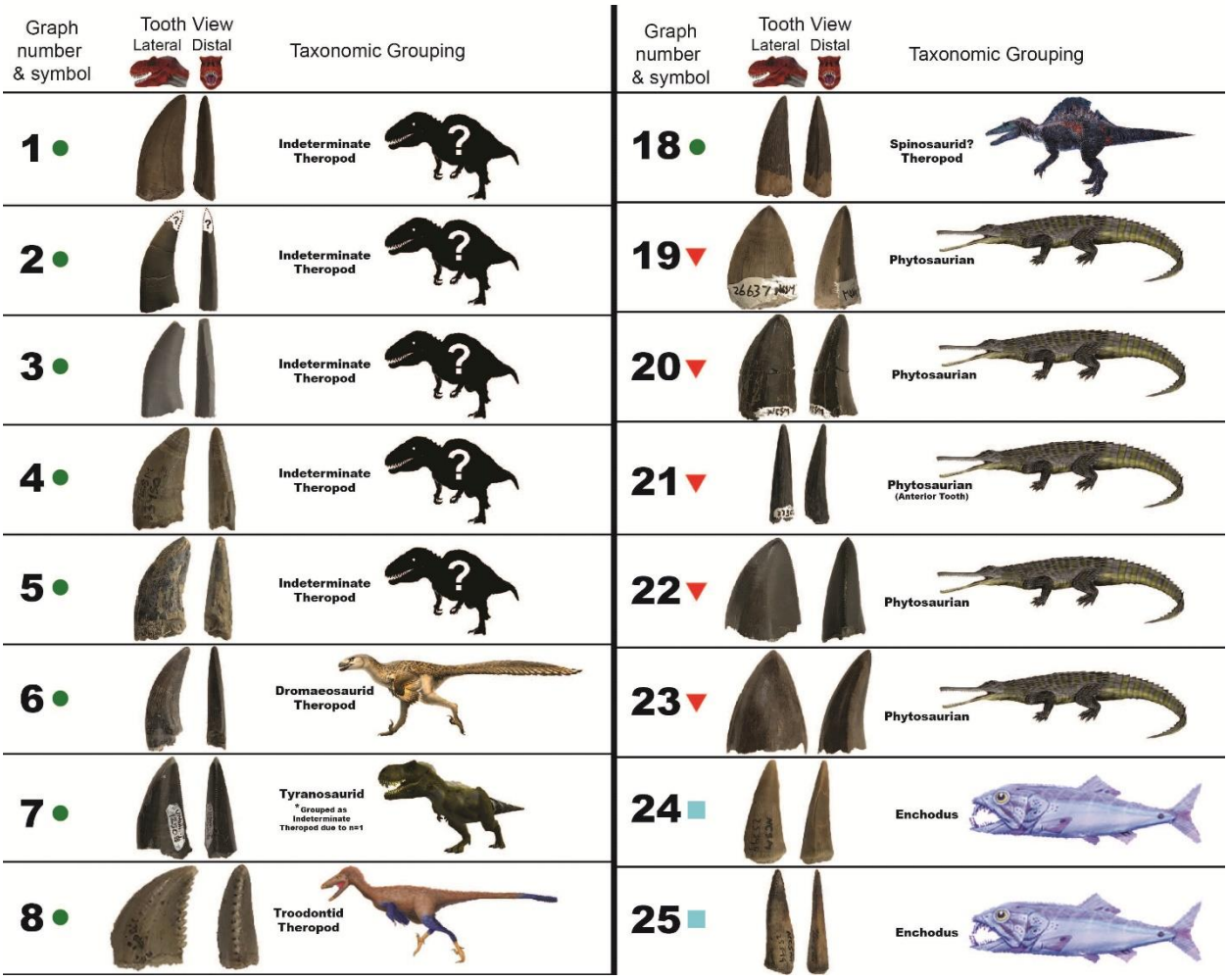

Figure 2.4: Tooth taxon chart
Chart showing taxonomic groupings of all 34 teeth and corresponding colors/symbols used in multivariate analyses. Taxon images were labeled for reuse and sourced from Creative Commons, Wikimedia Commons, and Google Images; or taken from screenshots of 3D models overlain with self-made textures.

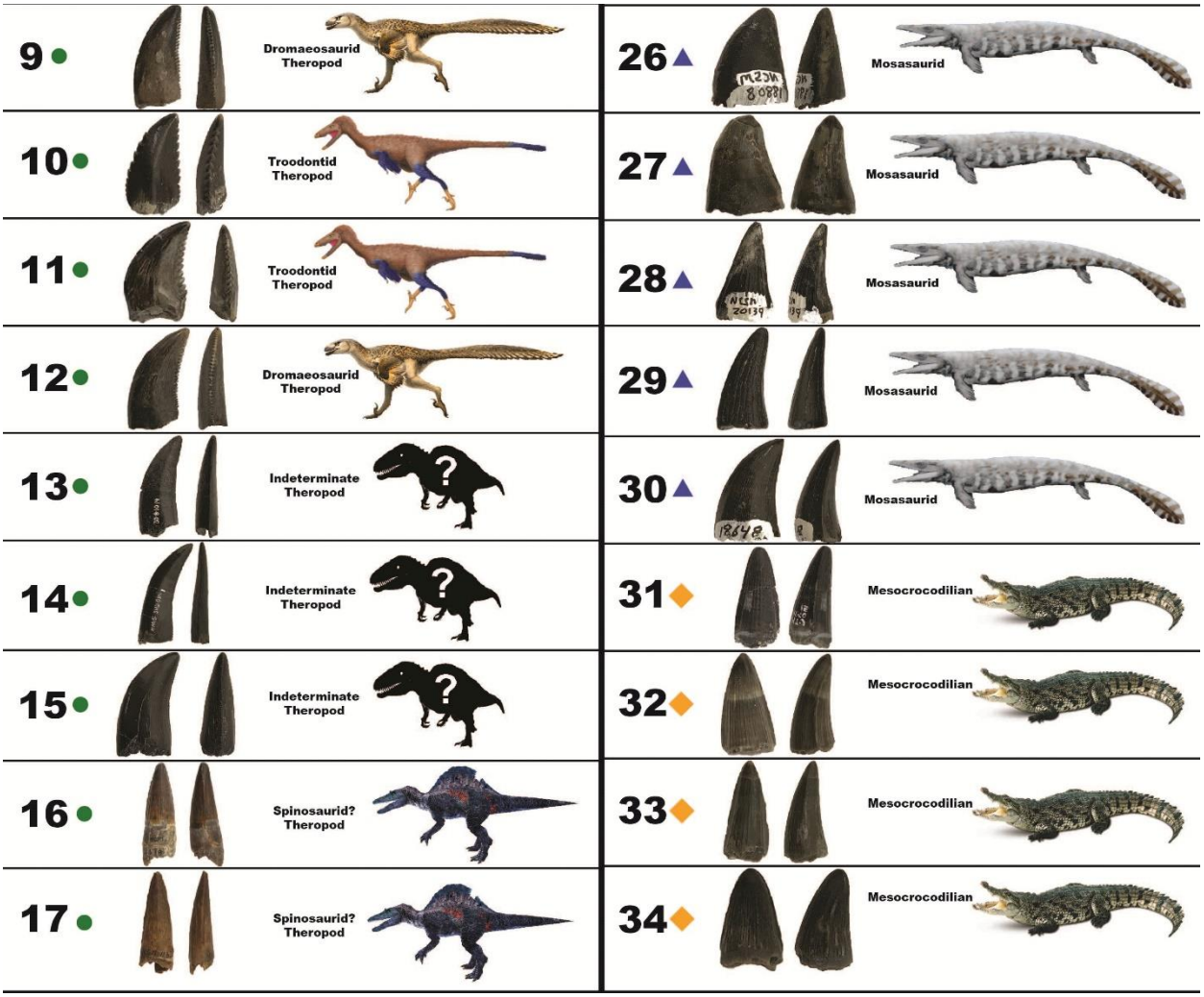

Figure 2.4: Tooth taxon chart (continued)

Linear Measurement Data Collection

Collection of linear measurements followed Hendrickx et al. (2014), resulting in a total of 11 variables corresponding to eight linear measurements and three ratios (Figure 2.5): CH = tooth crown height, CBL = crown basal length, CBW = crown basal width, AL = apical length, MCL = mid-crown length, MCW = mid-crown width, MC = mesiocentral denticle density per mm, DC = distocentral denticle density per mm, CBR = crown base ratio, CHR = crown height ratio, MCR = mid-crown ratio. Measurements were collected using Starret 798 calipers and a free digital Microsoft Windows timer was used to document the duration of each procedure (Table 2.2). In order to represent realistic data collection times, external factors influencing extended data collection times were included. These mid-data collection disruptions include factors such as technical difficulties, momentary distractions, personal hydration breaks, and confusion on how to proceed during the middle of the data collection process (e.g. determining how to collect certain measurements on fractured tooth #3). Data was opened in a Microsoft Excel document, organized and labelled, and pasted into the free statistical program PAST (Hammer et al. 2001) for analyses.

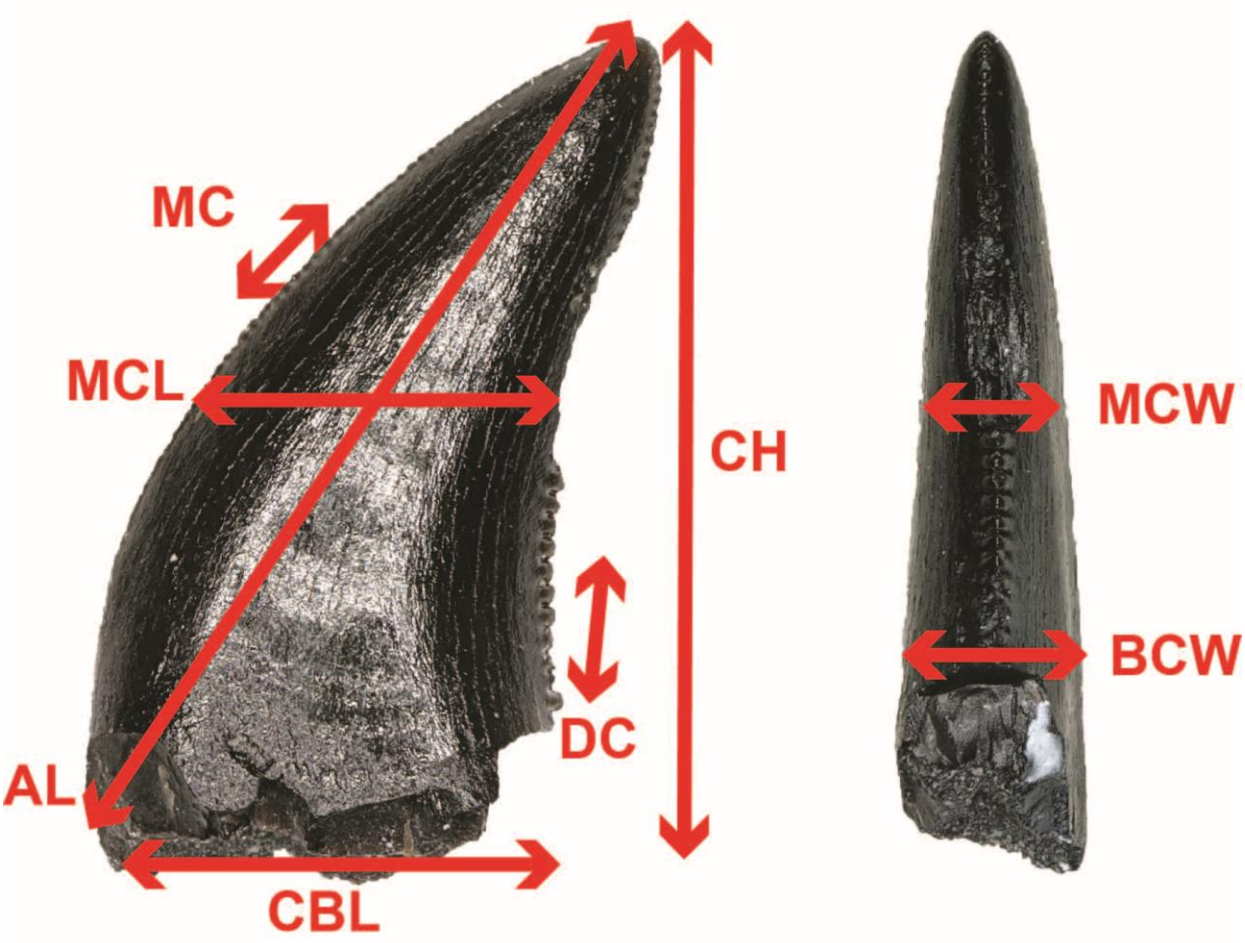

Figure 2.5: Anatomical Abbreviations
Directions of all 8 linear measurements. (**CH)** tooth crown height, (**CBL)** crown basal length, (**CBW)** crown basal width, (**AL)** apical length, (**MCL)** mid-crown length, (**MCW)** mid-crown width, (**MC**) mesiocentral denticle density per mm, (**DC)** distocentral denticle density per mm.

Table 2.2: Data collection times

Data collection times for linear measurements, 2D landmarks, and 3D landmarks for all 34 teeth in the sample.

	Linear Measurements	2D Landmarks			3D Landmarks							
	Collecting Linear Measurements	Photographing teeth 34 teeth in both views	Image modificaions using Photoshop batch processing	Using tpsDig	Video recording	Transfering video files	Converting videos to images	Photoscan Importing masks	Photoscan Aligning 2 chunks	Photoscan Building Dense Cloud	Photoscan Build Mesh	GPSA
Task Duration (miniutes)	102.6	33.2	32	28	58	17	34	51	340	272	170	3
Total time (miniutes)	102.6	93.2			945							
Total time (hours)	1.71	1.55			15.75							

2D Procrustes Landmark Data Collection

Photographing teeth

Images of all 34 teeth were digitally photographed using an iPhone 7 camera. In order to capture both dimensional planes each tooth was imaged twice, corresponding with a lateral view and a mesial view (Figure 2.6), resulting in a total of 68 images. Extra care was taken while imaging in order to maintain a consistent angle and mitigate possible deformations, as images taken at inconsistent angles will result in varying degrees of inaccurate representation and disrupt later procedures (see figure 2.7).

Figure 2.6: Tooth views with 99 landmarks
Tooth showing the two views in lateral and mesial view, with 99 landmarks plotted around the outline.

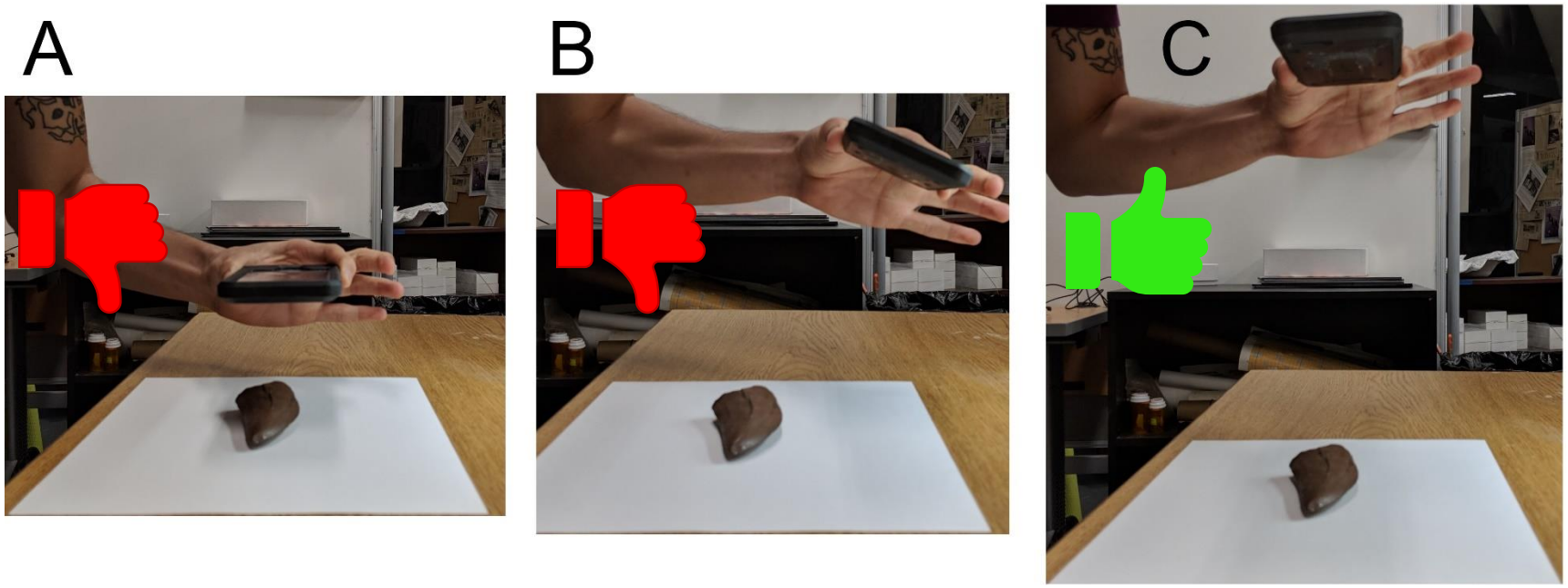

Figure 2.7: Camera position for 2D photographs
A, Camera is too close to tooth of that size. **B,** Camera is at an inappropriate angle. **C,** Camera is at an appropriate distance and angle for a tooth of that size. Smaller teeth will require the camera to be closer.

Image modification

Using the Adobe Photoshop (Photoshop 2015) batch processing with recorded actions, all images were slightly downsized (to reduce file size) and thresholded to remove artifacts such as shadows, producing an image composed of only white and black pixels (a black tooth surrounded by a white background). This was done to ensure accurate capture of outlines in later procedures, however it should be noted that this step is not necessarily required. If imaging is performed using optimal lighting in front of an appropriately contrasting background and the tpsDig outline object tool is calibrated appropriately there will be little to no need for external modification of images using accessory software.

Collecting outlines

2D landmarks were collected using the free program tpsDIG2 (Rohlf 2016), in conjunction with the free utility program tpsUtil (Rohlf 2018). Using the tpsUtil operation "build tps file from images" a TPS file was created containing all 34 tooth images in lateral view. Next, this TPS file was imported into tpsDig and XY coordinate outlines were collected on each tooth using the outline object tool.

There are three important things to consider for the previous step to be performed appropriately. First, prior to the collection of any outline, the option "outline lengths in steps" must be selected (this ensures all XY coordinates are equally spaced). Second, it is important to understand how the outline object tool operates to maintain consistent capture of comparable specimens. The outline object tool will search to the left to find the left side of the object and circle around the object until it finds its starting point (Rohlf 2016). Therefore, teeth images were rotated so that the tooth apex occupied the region of the image furthest to the left and the outline

object pointer was placed slightly to the right of the tooth apex (still within the black region of the tooth). This allows all specimens to have their first landmark occupy the tooth apex, which is arguably the most homologous point across all specimens.

Lastly, after capturing the outline, which will be denoted as a yellow border around the object, XY coordinates must be saved by right clicking on the image and selecting the save option. The program will ask for the number of coordinates to be saved, which will be transformed into corresponding landmarks in the following operation. Therefore, it would be wise to label TPS files with the desired number of landmarks whilst saving a consistent number of XY coordinates for all images within.

Creating landmarks from XY coordinates

After XY coordinates were saved for all 34 images, tpsUtil was used to convert all XY coordinates into landmarks by using the "convert tps XY outline to landmarks" operation. Next, the tpsUtil operation "delete/reorder landmarks" was used to remove the last landmark, which overlaps with the first (e.g. landmark 1 and 100 overlap when n=100) (Figure 2.6). This step is not mandatory, however, in analyses with fewer landmarks this redundancy may result in a higher chance of improperly weighted variables.

Exporting landmark data

Next, the tpsUtil operation "convert tps/nts coordinates file" was used to export a CSV file with all landmarks. Two 10-landmark files representing teeth in lateral and mesial views were exported, and two 100-landmark files representing teeth in lateral and mesial views were exported. Landmark data was opened in a Microsoft Excel document and lateral and mesial view

landmarks were combined. It should be notated that for the analyses in PAST to be performed correctly, the data must undergo a Procrustes transformation. In order to do this appropriately, landmarks corresponding to lateral and mesial views must be Procrustes transformed by rotating all landmarks to major axis and disregarding size. This must be done for each view (lateral and mesial) separately. For example, when performing an analysis using 10 landmarks in lateral view and 10 landmarks in mesial view, all 10 lateral view landmarks must be transformed simultaneously, and then all 10 mesial view landmarks must be transformed simultaneously.

3D Procrustes Landmark Analysis Workflow

Overview of utilized software

Images of teeth were extracted from video files using the free program Free Video to JPG Converter (DVDVideoSoft 2018). Adobe Photoshop (Photoshop 2015) was used for image modification, but is not necessarily required for all circumstances. 3D models were rendered using Agisoft Photoscan Professional Edition version 1.2.0.2127 (Agisoft & St Petersburg 2014) (Figure 2.8). 3D landmarks were collected using the free program Generalized Procrustes Surface Superimposition (GPSA) (Pomidor et al. 2016). Additionally, the program Checkpoint (Checkpoint 2017) was used to visually verify correct associations between landmark data and corresponding labels (Figure 2.9). 3D landmark data was opened in a Microsoft Excel document organized with desired labeling, and pasted into the free statistical program PAST (Hammer et al. 2001) for analyses.

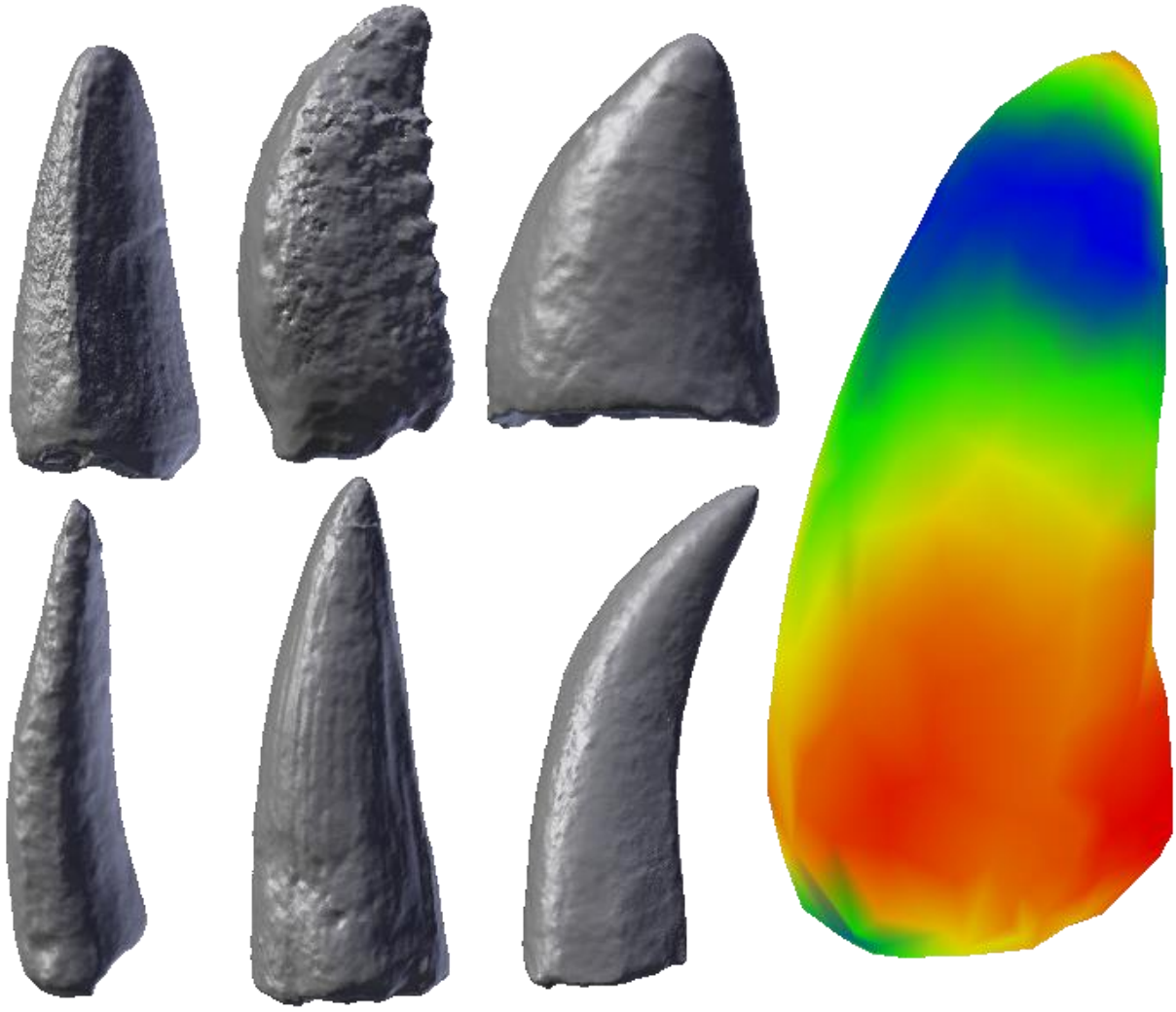

Figure 2.8: 3D models
(**Left**) Six of the 34 teeth in the sample, rendered in 3D using Agisoft Photogrammetry. Teeth display a wide range of morphological shape diversity. From top left to bottom right: Mesocrocodillian tooth #30, troodontid tooth #10, mosasaurid tooth #26, phytosaurian anterior tooth #21, spinosaurid tooth #18, and indeterminate theropod tooth #14. (**Right)** The mean tooth shape of all 34 teeth, produced using the GPSA, showing the regions accounting for the greatest variation.

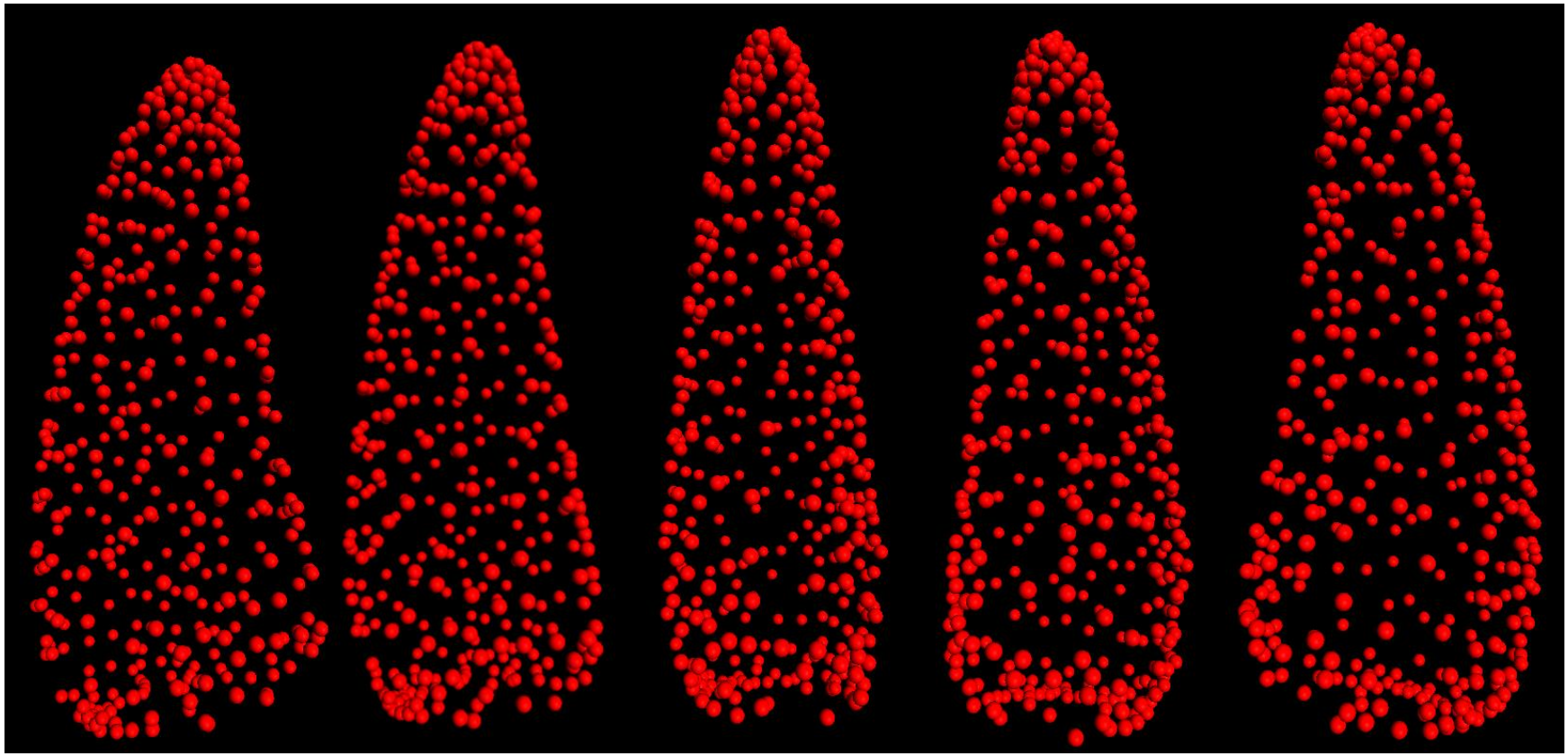

Figure 2.9: Checkpoint landmarks
Visualization of the generalized procrustes mean tooth with 402 3D landmarks using the Stratovan Checkpoint software. From left to right: lateral view, oblique view, mesial view, oblique view and lateral view.

Challenges of photographing small objects

The traditional method of creating accurate 3D models of objects using Agisoft Photoscan requires an object to be imaged from multiple sides. The program uses these images to reconstruct a 3D model by identifying and matching common points on photographs and finding the position of the camera for each picture.

An abundance of high resolution photographs usually corresponds to the production of better-quality models, as higher resolution pictures will offer more common points to be identified. Currently however, collecting high resolution images on diminutive objects in the cm to sub-cm range can be difficult because many cameras are not able to capture high resolution images at such high magnifications; and even cameras equipped with microscopes or macro lenses usually suffer from in depth of field distortion, focal length blurring, and decreased resolution at higher magnifications. Furthermore, larger objects are typically photographed at a distance, using a flat base with various symbols that act as easily identifiable common points. Photographing small scale objects requires the camera to be near the object, therefore any external symbols often fall out of focus. There are ways to remedy these challenges, such as using specialized microscopes and image stacking to correct for depth of field blur. However, I have found these approaches tenuous, laborious, impractical, and most importantly, ineffective.

It should be noted that some details of the following steps are subject to variation and modification depending on the research question, objects of interest, and accessibility to the tools, items, and software listed previously. For instance, other smartphones equipped with high-quality cameras may perform comparable to or better than an iPhone 7, and a DSLR camera, equipped with a macro lens, is likely to produce higher quality recordings than most smartphones, however large cameras offer less maneuverability when using small light boxes.

Furthermore, if one does not wish to invest in Agisoft Photoscan, other free photogrammetry programs exist such as the SterioMorph package (Olsen & Westneat 2015) for R statistics. The practice of capturing, processing, and analyzing 3D information is rapidly evolving, and it is likely that future applications will allow for many of the following steps to be simplified or eliminated altogether.

A solution: recording video of teeth

Rather than taking individual images of a stationary tooth, I employ a method using video recording of a rotating tooth. A video is essentially a series of images taken in rapid succession. This offers a distinct advantage to photographs because hundreds of images can be acquired relatively quickly.

I acquired a low rpm motor from DC Gear Motor, specifically a Bemonoc 3V high torque, low speed, reversible worm gear motor with a 6mm shaft rotating at 3rpm. This motor was placed inside of an eka Co. portable photo light box.

Next, I rolled red and green Sculpey polymer clay into two equally sized spheres, approximately the size of a pea. The purpose of different colored clay is to help Agisoft Photoscan identify camera locations during later processes. The specific colors do not necessarily matter; rather it is important that they contrast with each other, and preferably to the object of interest. The red ball was placed at the top of the motor shaft and a tooth, with its long axis oriented vertically and the apex facing upwards, was securely affixed to the top of the red clay ball (Figure 2.10). Teeth with shiny surfaces or solid textures were coated with baby powder to remove glare and mitigate lighting issues.

Using an iPhone 7 in video recording mode (set to record in 1080p at 30 fps) I distanced the camera as close to the tooth as possible without sacrificing focal clarity, increased the zoom if necessary, activated the AE/AF lock by holding one finger down on the screen, and increased the exposure slightly by swiping upwards. The motor was activated, followed by initiation of the video recording. In a slow and steady motion, the camera was raised and lowered as the tooth rotated, capturing video of the tooth from multiple angles (Figure 2.11).

After approximately one full rotation I set the phone down, without ending the recording, and removed the tooth so that the red clay ball could be replaced with the green clay ball. The tooth was then rotated 180° along its long axis and affixed to the green clay ball with its base facing upwards. Video recording resumed for an additional 1-1.5 rotations. This process was repeated for each tooth, with video durations usually lasting two to three minutes.

Procedures varied depending on tooth size. For example: the largest teeth required more clay to remain affixed to the motor shaft, whereas a Kingmas phone clip-on macro lens was necessary to record the smallest teeth (those with a CH of ~0.5-1 cm).

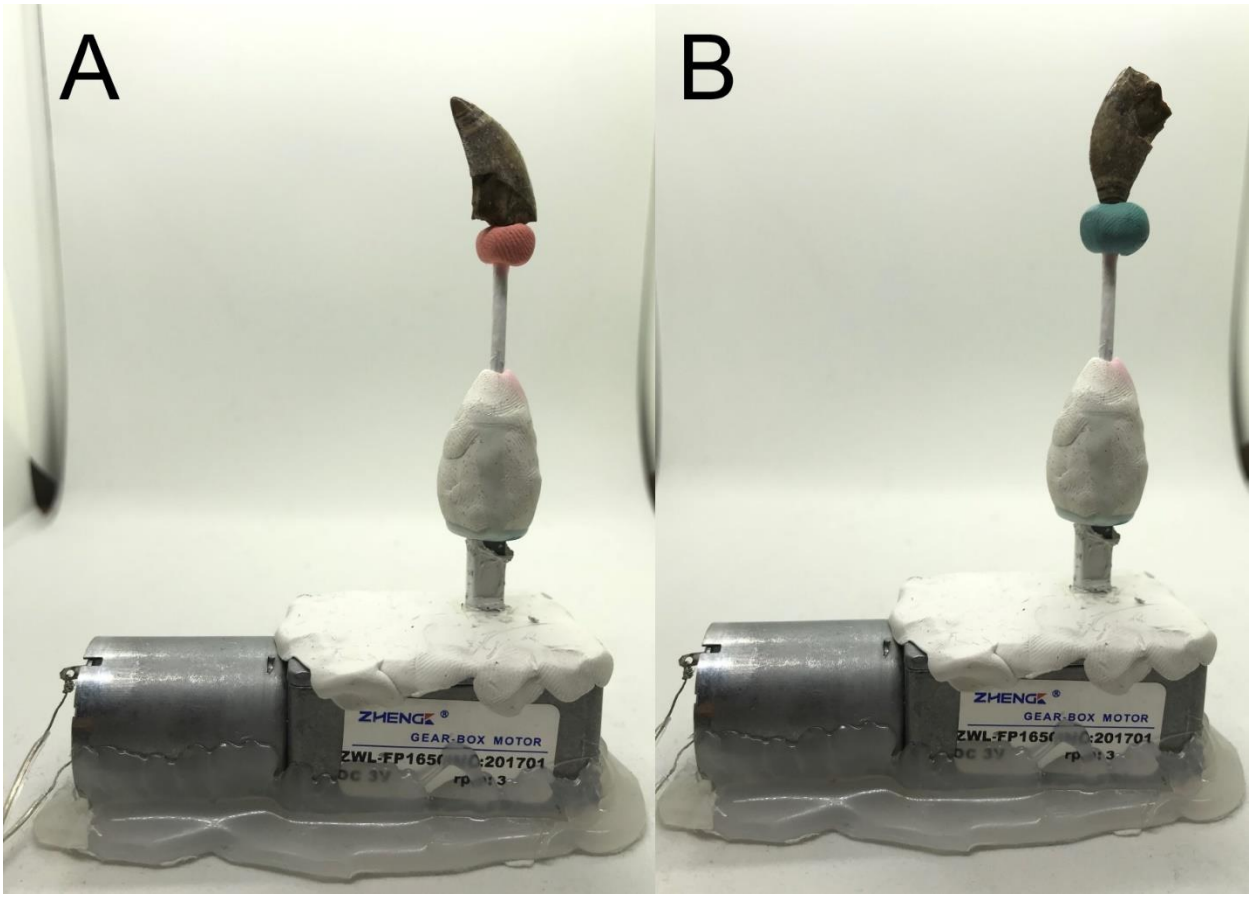

Figure 2.10: Tooth orientations and corresponding clay color for video recording
A, Red clay corresponding to a tooth oriented apex up and base down. **B,** Green clay corresponding to a tooth oriented apex down and base up.

Figure 2.11: Camera motion during video recording
Arrows show relative motion of camera during video recording. During recording process camera can turn and spin in multiple directions as long as all regions of the tooth stay in frame. Phone camera is shown with clip on macro lens, however not necessary for a tooth of this size. Motor and tooth should be placed deeper into light box than shown.

Extracting video frames

Currently, Agisoft Photoscan does not support video formats and will only accept still images. Therefore, I used the Free Video to JPG Converter (DVDVideoSoft 2018) to convert videos into jpg image files. Videos files were transferred from my iPhone 7 to my Windows computer and uploaded into the program. The program was configured to extract every 15 frames and export them to a specific file directory.

Depending on the video length, this can result in 100-400 images. Therefore, it is up to the investigator to determine the appropriate number of frames to extract. For example, video durations will be longer if motor shaft rotation is slower than 3rpm. In this circumstance extracting every 30 (or more) frames may be preferable, otherwise Agisoft Photoscan processes may take longer than necessary. In contrast, video durations will be shorter if motor shaft rotation is greater than 3rpm. In this circumstance extracting every ten (or less) frames may be preferable, otherwise there may not be enough overlap between images for Agisoft Photoscan to operate effectively.

Lastly, images were visually inspected in the file browser, and those that do not include the tooth in frame (unnecessary images correspond to the halfway point of each video recording, when the clay spheres were exchanged and the tooth was reoriented) were deleted.

Creating masks using batch processing in Photoshop

For Agisoft Photoscan to operate properly, it must be able to discern the background from the object of interest, otherwise dense clouds and meshes may include numerous artifacts. There are two methods to creating effective masks, both with advantages and disadvantages.

Agisoft Photoscan can import masks directly from a background by selecting an image without the object of interest included. Photoscan will then use this image to discern between the tooth and the background. I found this method to result in long import times and variable reliability.

Alternatively, masks can be imported from alpha layers. Using Adobe Photoshop batch processing. In Photoshop the action window was opened and a tooth image file was imported. In the action pane, a new action was created, which I named Background Remover, and began recording. First, I unlocked the main layer and created a new layer below it. Then using the wand tracing tool, set with a tolerance of 50, I clicked on all four corners of the top layer image, and deleted the selection. Next, I saved the image in a new file location as a PNG, which preserves the alpha layer. Lastly, I closed the image and ended the action recording.

Using the batch processing operation, I selected the Background Remover action and chose the file location of the jpg images. This process was repeated for all 34 tooth image folders, with the save destination for PNG images as the only modification to the Background Remover action between operations.

Constructing 3D models using Agisoft Photoscan

To build 3D models of all 34 teeth, I used batch processing following the steps outlined in the Agisoft Photoscan user manual (Agisoft & St Petersburg 2014). This process is relatively straightforward. First, images are imported into Photoscan in two separate chunks, corresponding to the clay colors/tooth orientation. There should be between 30-150 images for each chunk, as a higher quantity of images will cause the program to proceed slowly and too few images may not provide enough image overlap, resulting in misalignment. Sometimes it may be easier to run the

entire process in a single chunk. However, this will require detailed manual removal of points representing the clay, after the dense cloud is constructed.

Next, the batch processing window was opened and masks were imported as step one. If image modification was not performed in Photoshop, then masks were imported from background using a tolerance around 50-80, and applied to all images in the workspace. If tolerance is set too high, portions of the tooth perimeter will be cropped out and excluded from the following operations. This effect is greater with smaller teeth, where image resolution is lower and there may be considerable blur around tooth perimeters. If tolerance it too low, artifacts from the background may be included during alignment and may result in a deformed model or require extra maintenance to clean up the dense field. If images were modified in Photoshop to remove backgrounds, then masks were imported from alpha and applied to the entire workspace.

Next, the job title “Align Photos” was selected as the second operation, applied to all chunks and with the constrain features by mask setting set to yes. The third job type included in the batch process was “Align Chunks”, applied to all chunks, followed by “Build Dense Cloud” as the fourth and final operation in the series.

After the four operations concluded, both dense clouds were inspected to confirm that an accurate representation was constructed. Using the free-form selection tool, both clay balls were removed from their corresponding dense clouds, and then the two chunks were merged together. Lastly, a mesh was built from the merged chunk and the model was exported in the Stanford PLY format. This process was repeated for all 34 teeth.

GPSA

After 3D models of all 34 teeth were created, the GPSA program (Pomidor et al. 2016), was started. First, a prototype file must be selected. The number of vertices that a prototype model has will correspond to the number of landmarks created. Therefore, a separate model of tooth six was exported from Photoscan and decimated to a target face count of 18, resulting in 11 vertices. This model was used as the prototype file in GPSA. Next, all 34 tooth models were selected as the surface files, and the GPSA was initiated. After approximately three minutes, a data file titled "_gpsa_homologized_points.dat" was created in the same folder as the surface files. This data file was opened with a text editor, specifically Notepad++, and all values (3D landmarks) were copied into a Microsoft Excel document. Data was organized according to desired specifications and labeling, and pasted into PAST for analyses.

Combining traditional and geometric morphometrics

The 2D and 3D landmark analyses disregard size, however size can be an important biological feature that should not necessarily be disregarded. Additionally, the abundance of measurement data that has been collected on thousands of teeth from various studies offers a great deal of comparative biological information that would necessarily be disregarded in studies only utilizing geometric morphometrics. It is possible that analyses combining traditional and geometric morphometrics could improve data discrimination. However, there are challenges with combining these datasets.

The greatest challenge involved with combing measurement variables and landmark data is that the numerical information differs greatly. Analyses performed with a combination of non-transformed linear measurements and landmark data often result in complete failure or

inappropriately loadings and most data transformations are not possible across all three morphometric approaches in this study. Log-transforming all data simultaneously is not possible because 3D-landmark data contains negative numbers. Likewise, transforming all 11 linear measurements into 2D or 3D landmarks is not possible for this study because 2D Procrustes transformation requires an even number of variables and 3D Procrustes transformation requires variables to be ordered in multiples of three. Nonetheless, preliminary tests did produce favorable results when linear measurements were Procrustes transformed into landmark data. However, this required some linear measurements to be either completely removed, or temporarily removed, transformed separately, and reincluded into the dataset; a labor-intensive task that did not allow consistent comparisons between analyses.

Two transformations included in PAST (converting to ranks and Box-Cox transformation) were found to be consistently reliable across all datasets. Converting data to ranks is a transformation that replaces numerical and ordinal values with a corresponding rank after the data is sorted. This transformation initially seemed to produce the best separation potential and balance between the two datatypes, and therefore all PCAs and LDAs combining traditional and geometric morphometrics reported here were performed with rank converted data.

Multivariate Approaches

Although a wide array of multivariate approaches has been utilized in archosaurian tooth studies (Sankey et al. 2002; Smith et al. 2005; Larson & Currie 2013; Hendrickx et al. 2014; Williamson & Brusatte 2014; Gerke & Wings 2016; de Oliveira & Pinheiro 2017), the most widely used are PCAs, LDAs, and CVAs. Complications arise when trying to run LDAs or CVAs with some of the geometric morphometric approaches. CVAs are not possible with some

datasets because they are unable to handle a large quantity of landmark data without significant transformation to the data. LDAs are not possible with some datasets because they require more cases than variables. In other words, since the same sample of 34 teeth is used for each analysis, each analysis must contain 33 or fewer variables, making an LDA with a large number of landmarks impossible. Nonetheless, LDAs have the advantage of providing a confusion matrix, which indicates the number of cases that have been misclassified into other groups. Therefore, for the purposes of this study, only PCAs and a few LDAs will be performed and primarily reported.

All analyses were performed in PAST version 3.5 (Hammer et al. 2001). Every PCA was performed twice, using either disregard-group or between-group. Disregarding groups is useful for determining the accuracy (correct placement of the tooth in a known taxonomic group) of each morphometric method. In disregard-group only morphological data is considered. Therefore, the more isolated and densely packed a group is from other convex hulls, the greater the accuracy. For between-group, the eigenanalysis is performed on the group means and usually results in better separation. This is more likely to be useful when attempting to estimate the correct placement of uncategorized data (i.e. identifying taxonomic referrals of isolated teeth) in a dataset with samples belonging to predetermined groups.

Several graphs contain an associated biplot. The biplot shows the projection of the eigenvector principal loadings. The length of an eigenvector (green line) corresponds to the magnitude of influence that variable contributes to the analysis. The orientation of an eigenvector represents the direction of influence that variable has on the graphical projection. Biplots are excluded from analyses that incorporate many variables because the high density of eigenvectors is difficult to decipher and manipulate during post-analysis modifications.

RESULTS

PCA Analyses

Linear Measurements

Two disregard-group and two between-group analyses were performed using either raw measurement data or log-transformed measurement data (Figure 2.12). Data was log-transformed to better reflect a normally distributed multivariate dataset. When data is not transformed (Figure 2.12 A and B), the results are nearly identical for both disregard groups and between-groups analysis. Both analyses show seven of the nine groups overlapping with one or more groups. Troodontid theropods are densely clustered together, whereas the indeterminate theropod convex hull spans the length of the x-axis.

Group overlap is reduced when data is log-transformed. The most effective separation of convex hulls occurs when groups are disregarded, with troodontid theropod, dromaeosaurid theropod, and mesocrocodillian completely isolated from other groups. However, mosasaurid teeth overlap with both phytosaurian and spinosaurid theropod teeth, and two *Enchodus* teeth and the phytosaurian anterior tooth plot within the indeterminate theropod hull. In both disregard-group and between-group analyses, indeterminate theropod teeth #2 and #3 plot in close proximity to each other. The greatest overlap between sampled teeth occurs in the log-transformed between-group analysis (Figure 2.12 D), where only troodontid theropod teeth and the phytosaurian anterior tooth are completely isolated and the indeterminate theropod group overlaps with dromaeosaurid theropod, mesocrocodillian, spinosaurid theropod, mosasaurid, and *Enchodus* teeth.

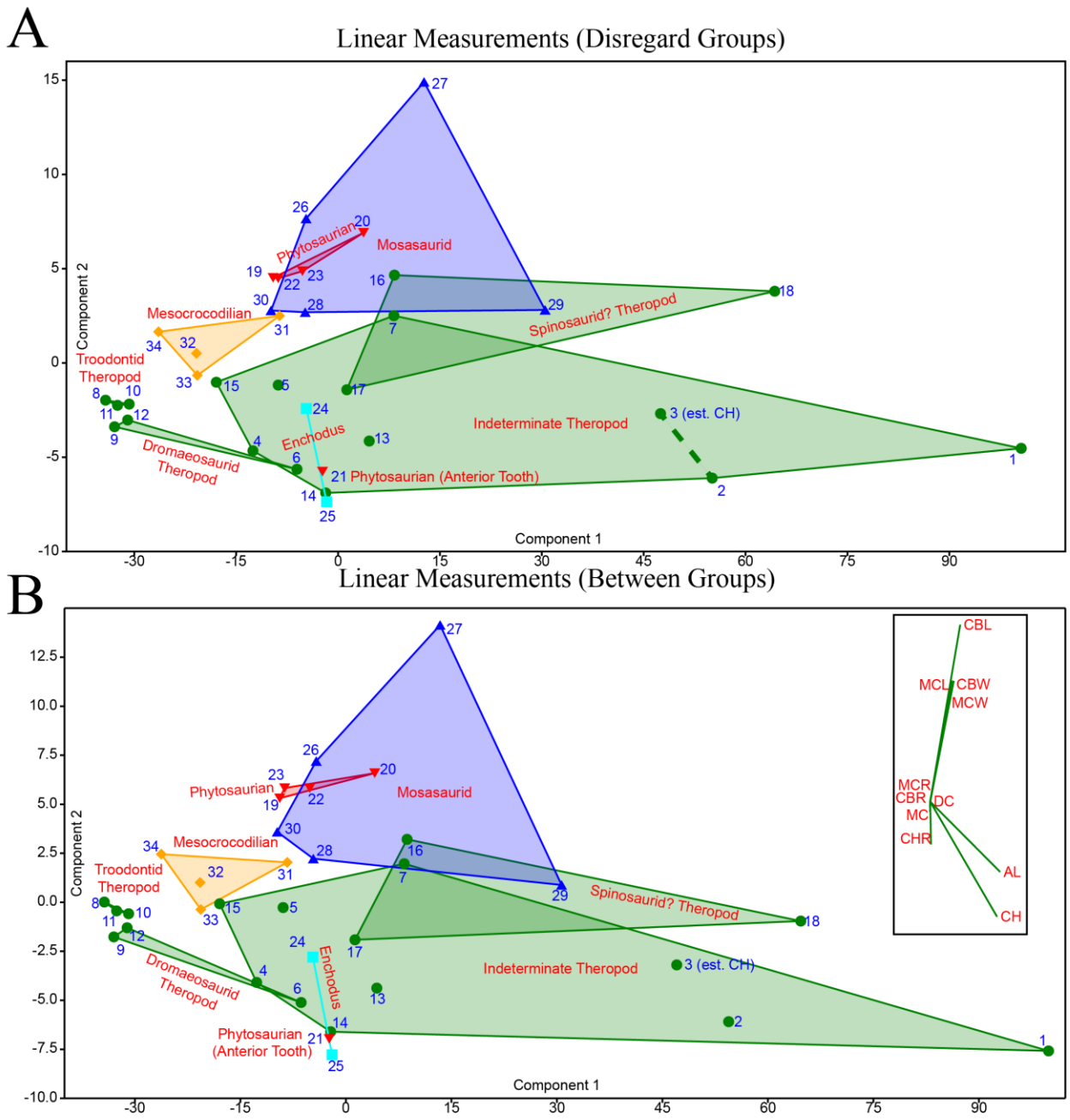

Figure 2.12: PCAs using linear measurement data
(A) PCA of non-transformed linear measurement data (disregard groups). **(B)** PCA of non-transformed linear measurement data (between groups).

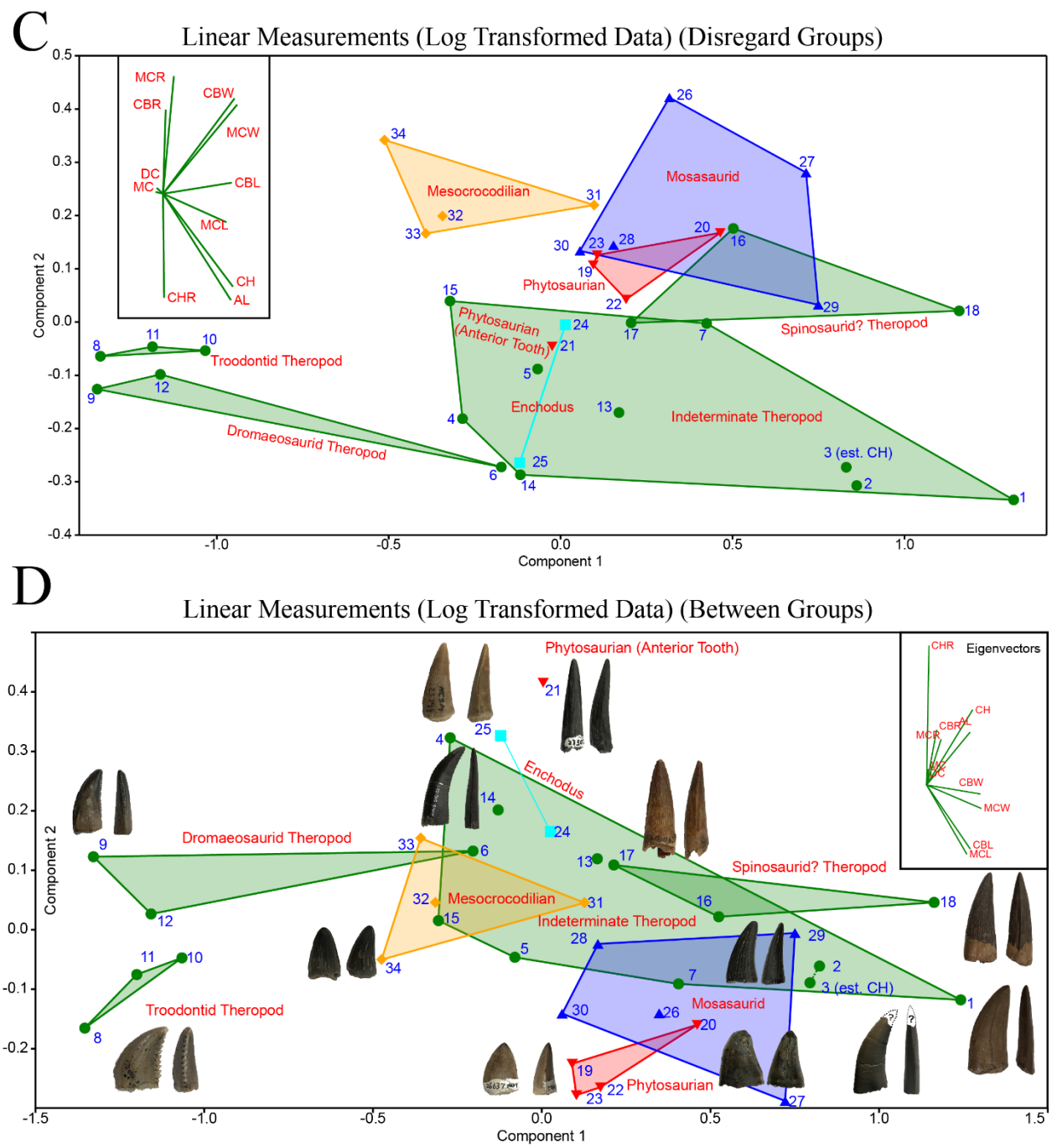

Figure 2.12 (continued): PCAs using linear measurement data
(C) PCA of log-transformed linear measurement data (disregard groups). **(D)** PCA of log-transformed linear measurement data (between groups).

2D-Landmarks

Two disregard-group and two between-group analyses were performed each using either 20 2D landmarks (Figure 2.13 A-B) or 200 2D landmarks (Figure 2.13 C-D). As previously stated, each analysis contains an equal number of landmarks from both lateral and mesial views (i.e., the 20 landmark analyses combine 10 landmarks in lateral view with 10 landmarks in mesial view). All graphical outputs show similar results. Troodontid theropod teeth occupy a wide, isolated convex hull, with all three teeth showing an equal distance of separation and tooth #10 slightly overlapping into the indeterminate theropod hull. Dromaeosaurid theropod teeth always overlap with (and is usually contained within) the indeterminate theropod hull. Phytosaurian teeth #20 and #19 always overlaps into mosasaurid, except in the 200 2D-landmark analysis between-group, where phytosaurian tooth #22 plots slightly outside of mosasaurid. The spinosaurid theropod convex hull always overlaps slightly with mesocrocodillian because tooth #16 plots closer to mesocrocodillian teeth than the other two spinosaurid teeth. The two *Enchodus* teeth and the phytosaurian anterior tooth never overlap with any other group. Mosasaurid teeth always display the widest convex hull, followed by indeterminate theropods teeth (an expected result due to these groups containing teeth with the greatest morphological diversity). Indeterminate theropod teeth #2 and #3 are always significantly separated from each other, plotting closer to Dromaeosaurid tooth #6 and indeterminate theropod tooth #1 respectively, than to each other.

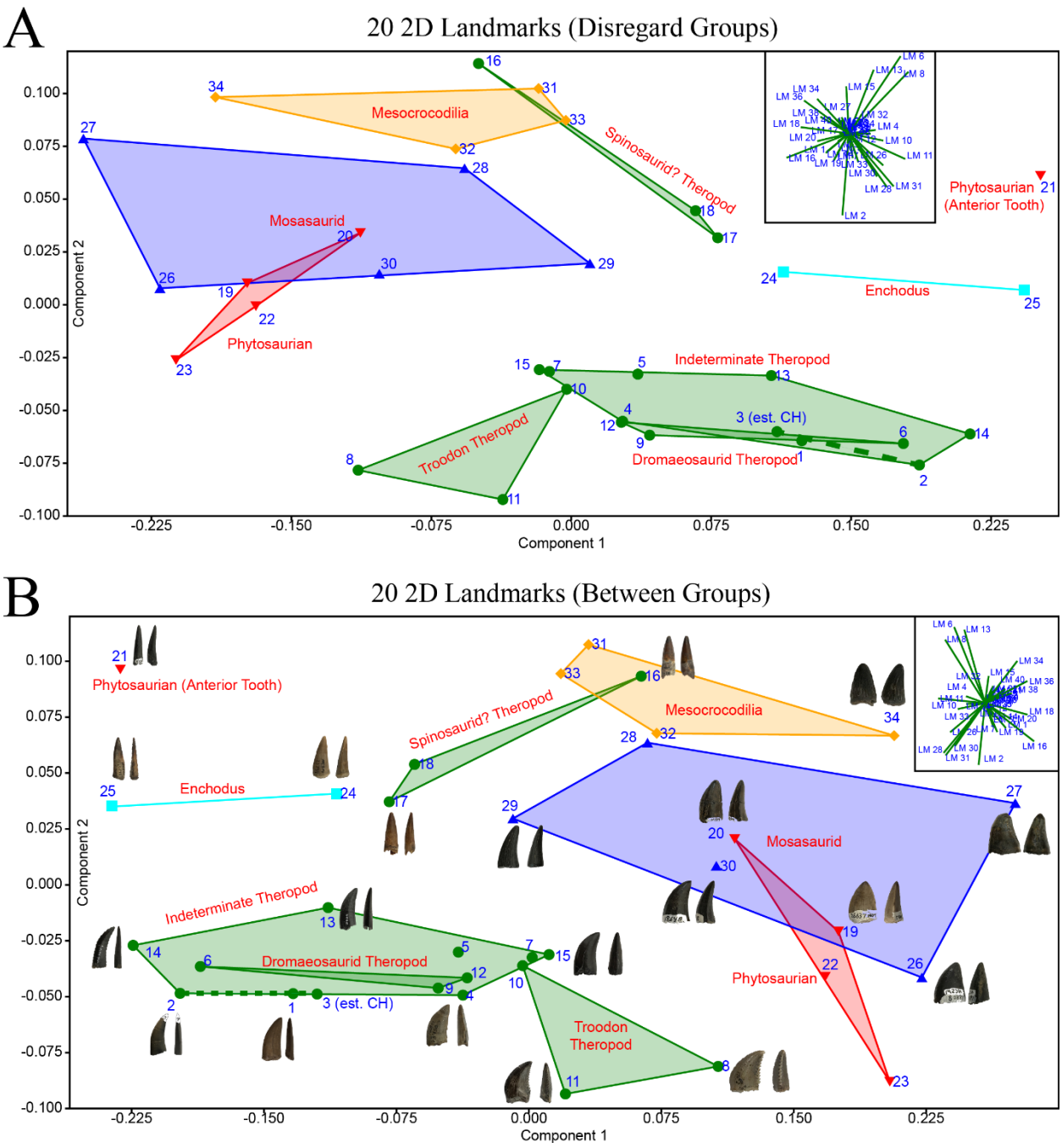

Figure 2.13: PCAs using 2D landmark data
(A) PCA of 20 2D landmarks (disregard groups). **(B)** PCA of 20 2D landmarks (between groups). **(C)** PCA of 200 2D landmarks (disregard groups). **(D)** PCA of 200 2D landmarks (between groups)

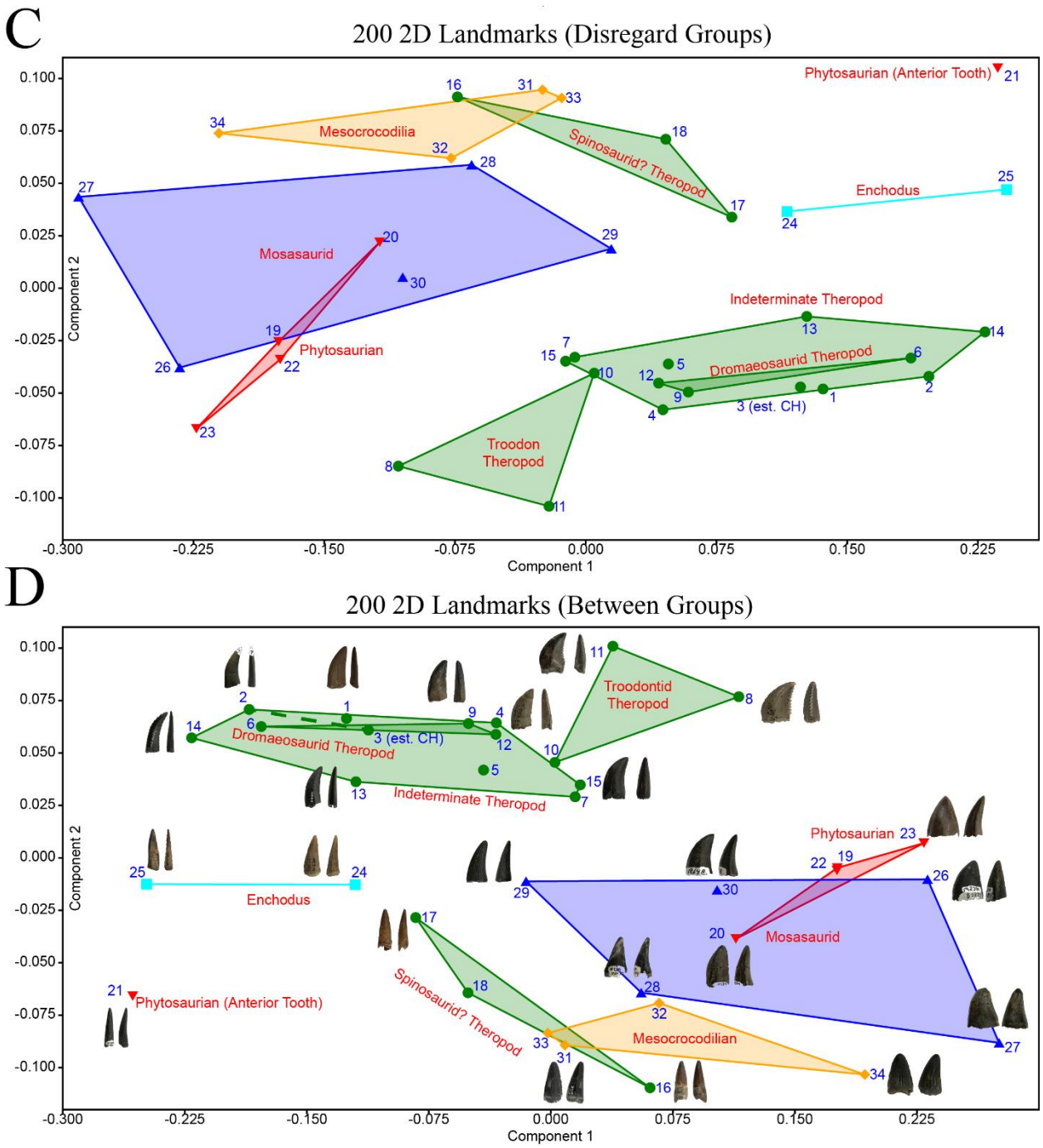

Figure 2.13 (continued): PCAs using 2D landmark data
(C) PCA of 200 2D landmarks (disregard groups). (**D)** PCA of 200 2D landmarks (between groups)

3D-Landmarks

Three disregard-group and three between-group analyses were performed each using a sample of 11, 53, or 402 3D landmarks (Figure 2.14). The results of each analysis vary considerably; however, there are several consistent themes. Except for the 402 3D-landmark between group analysis, tooth mosasaurid tooth #27 consistently plots far from all other teeth, enlarging the mosasaurid convex hull. The phytosaurian anterior tooth consistently plots at the furthest regions of morphospace, usually nearest to *Enchodus* tooth #25 and indeterminate theropod tooth #14. Indeterminate theropod teeth #2 and #3 plot relatively close to each other; however, they are usually more proximal to other teeth in the sample than they are to each other. *Enchodus* tooth #24 and #25 plot far from each other, with tooth #24 usually overlapping with the indeterminate theropod convex hull.

The analyses of 11 3D-landmarks result in a substantial amount of overlap between all groups except the phytosaurian anterior tooth (Figure 2.14 A-B). The 53 3D-landmark analysis (Figure 2.14 C-D) shows only slightly reduced convex hull overlap compared to the 11 3D-landmark analyses. The disregard-group analysis (Figure 2.14 C) results in a significant overlap between every group except the phytosaurian and mesocrocodillian convex hulls. The troodontid theropod convex hull is small and overlaps slightly with mosasaurid teeth. Indeterminate theropod teeth overlap with spinosaurid theropod teeth, dromaeosaurid theropod teeth, and *Enchodus* tooth #24. The between-group analysis (Figure 2.14 D) is similar; however, mesocrocodillian teeth overlap slightly with mosasaurid teeth, whereas phytosaurian teeth, troodontid theropod teeth, and spinosaurid theropod teeth do not overlap with other groups. The 402 3D-landmark analysis (Figure 2.14 E-F) results in a similar amount of convex hull separation as the 53 3D-landmark analysis, with overlap between every group except spinosaurid

theropod in the disregard-group analysis, and overlap between every group except spinosaurid theropod and mesocrocodillian in the between-group analysis.

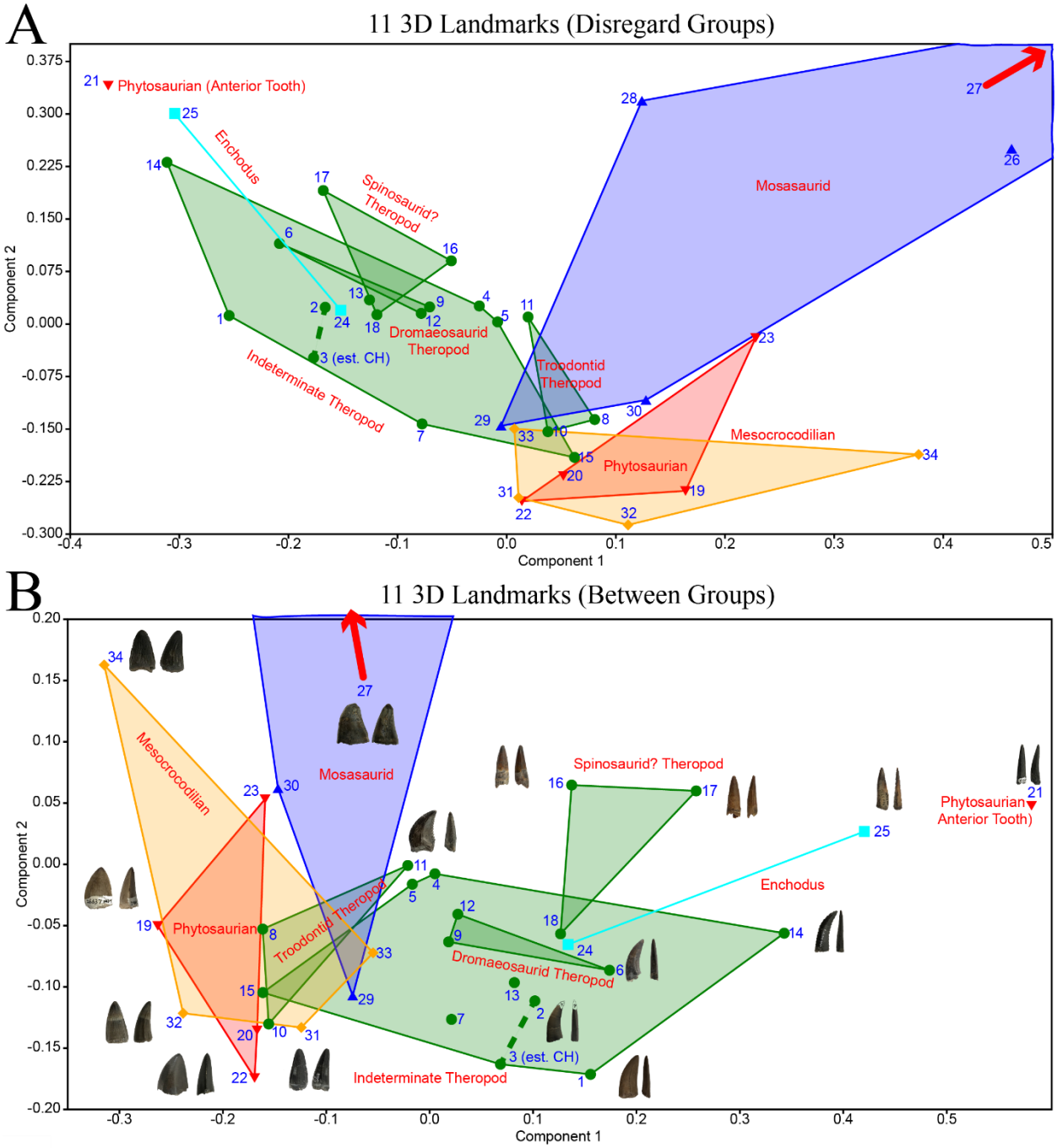

Figure 2.14: PCAs using 3D landmark data
(A) PCA of 11 3D landmarks (disregard groups). **(B)** PCA of 11 3D landmarks (between groups).

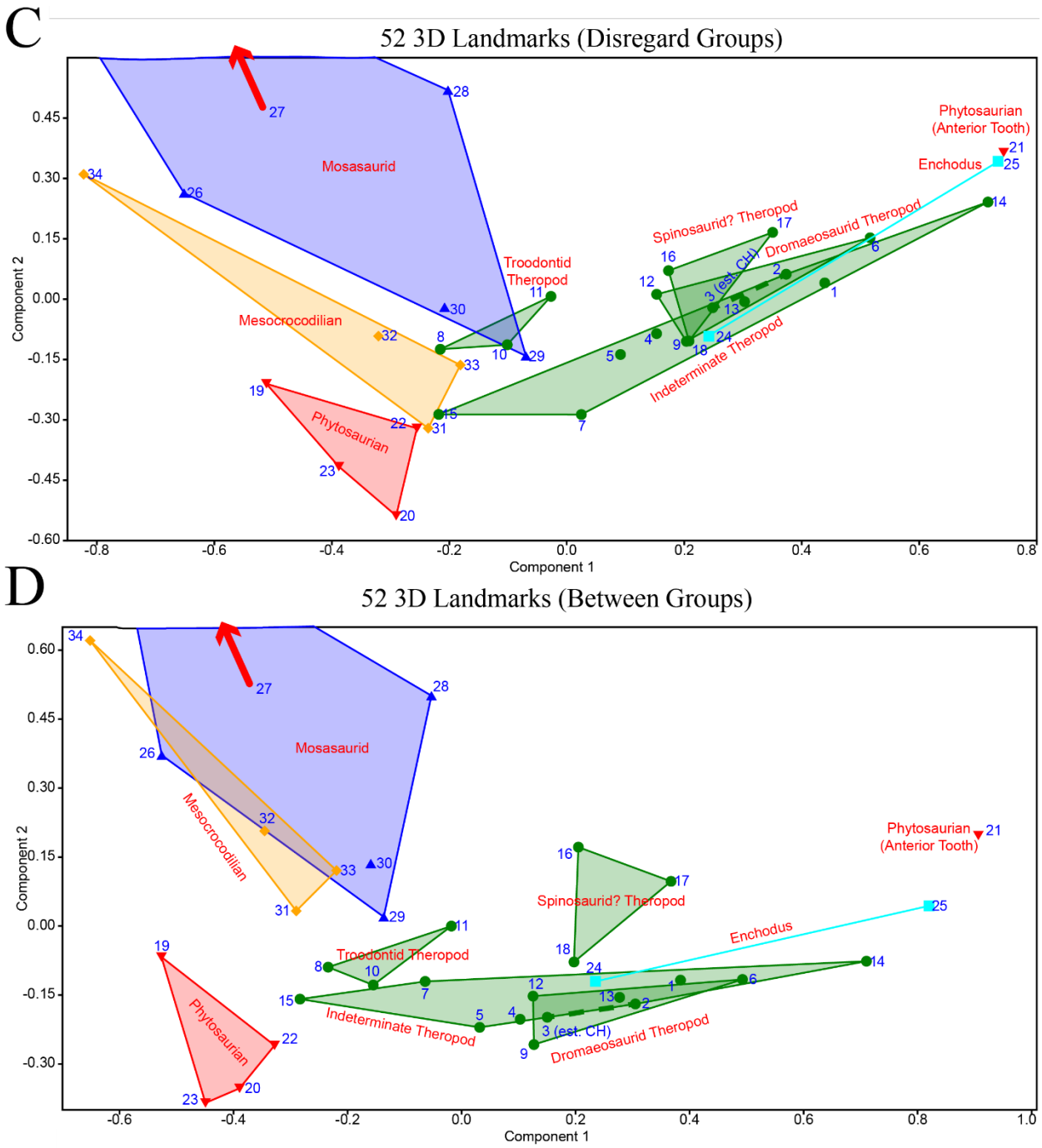

Figure 2.14 (continued): PCAs using 3D landmark data
(C) PCA of 53 3D landmarks (disregard groups). (**D)** PCA of 53 3D landmarks (between groups).

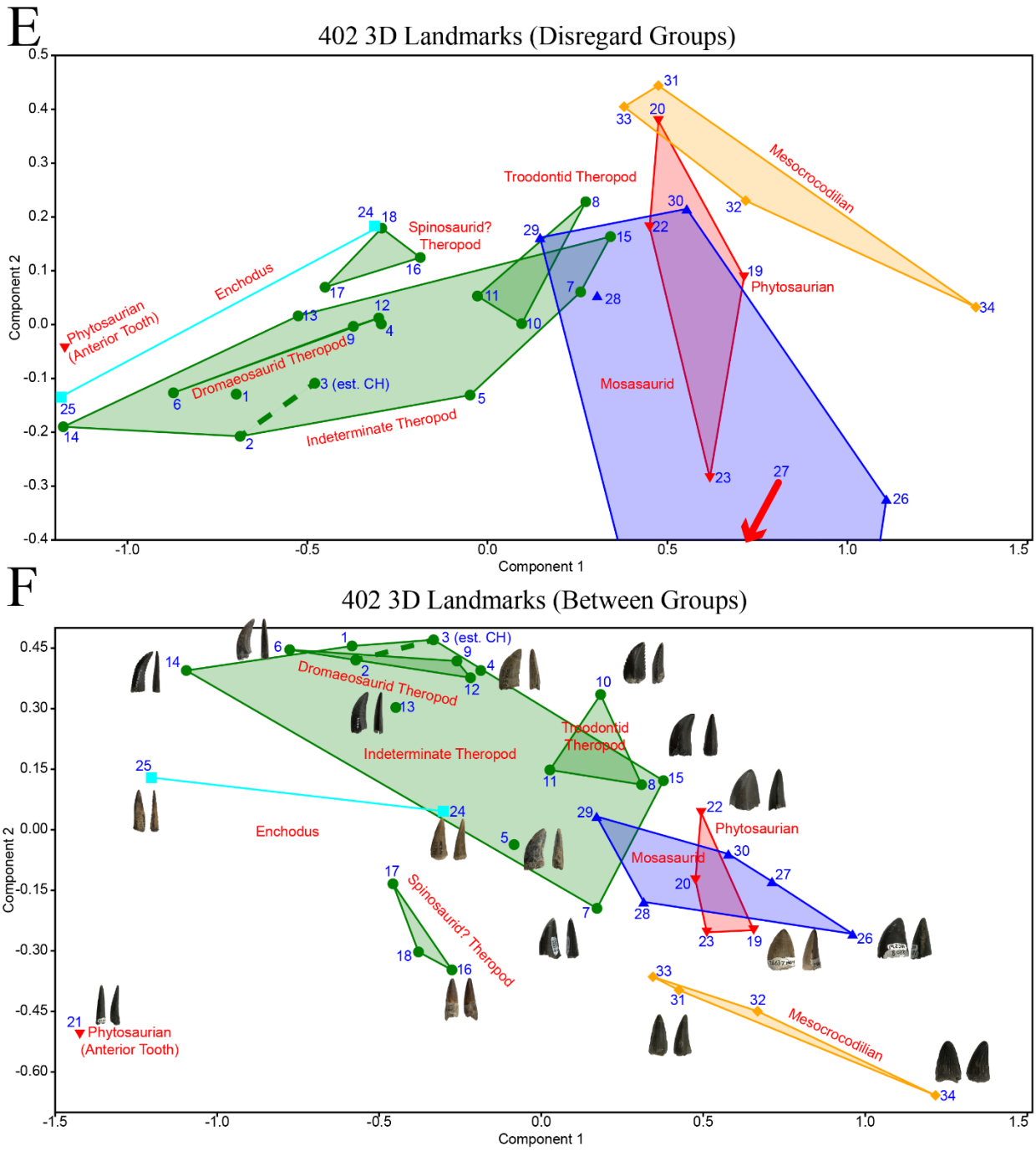

Figure 2.14 (continued): PCAs using 3D landmark data
(E) PCA of 402 3D landmarks (disregard groups). **(F)** PCA of 402 3D landmarks (between groups).

Combining linear measurements and 2D-Landmarks

Two disregard-group and two between-group analyses were performed using linear measurement combined with either 20 or 200 2D landmarks (Figure 2.15). The results of each analysis are similar in the amount of separation of taxonomic groups. The analysis combining linear measurements and 20 2D-landmarks (Figure 2.15 A-B) completely separate all theropod groups from each other, whereas phytosaurian, and mesocrocodillian overlap with mosasaurid. When groups are disregarded (Figure 2.15 A), *Enchodus* overlaps with indeterminate theropod, whereas in the between-group analysis *Enchodus* is separated from indeterminate theropod.

Separation seems to increase slightly in the analyses combining linear measurements with 200 2D-landmarks (Figure 2.15 C-D) compared to the combined linear measurements and 20 2D-landmarks. In the disregard group analysis (Figure 2.15 C) spinosaurid teeth and mesocrocodillian teeth slightly overlap with each other, phytosaurian teeth overlap with mosasaurid teeth, and troodontid theropod teeth slightly overlap with indeterminate theropod. In the between-group analysis (Figure 2.15 D), nearly all taxonomic groups are separated from each other, with only phytosaurian teeth and mesocrocodillian teeth slightly overlapping with mosasaurid teeth.

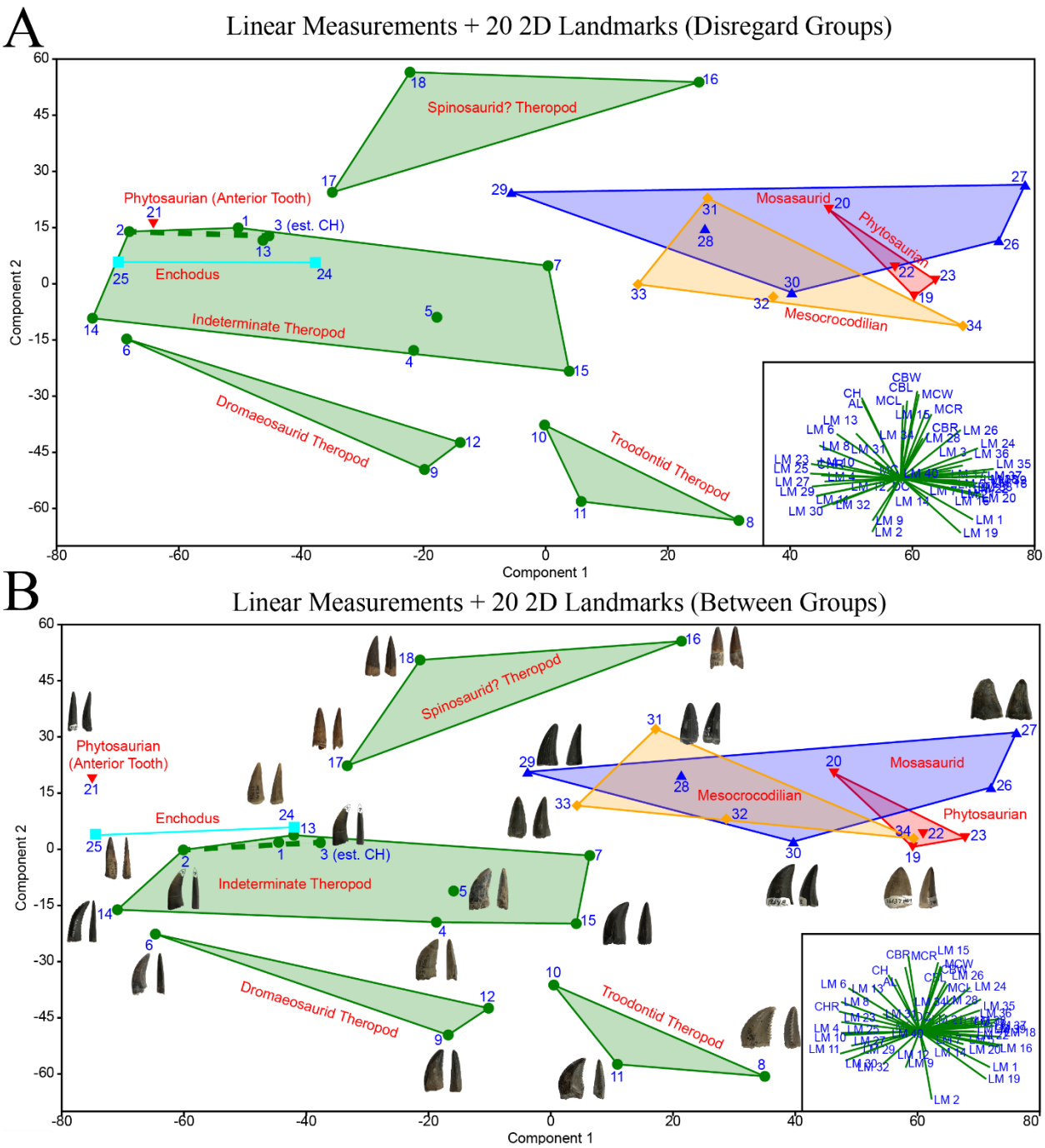

Figure 2.15: PCAs using linear measurements combined with 2D landmark data
(A) PCA of linear measurements combined with 20 2D landmarks (disregard groups). (**B)** PCA of linear measurements combined with 20 2D landmarks (between groups). All data converted to ranks.

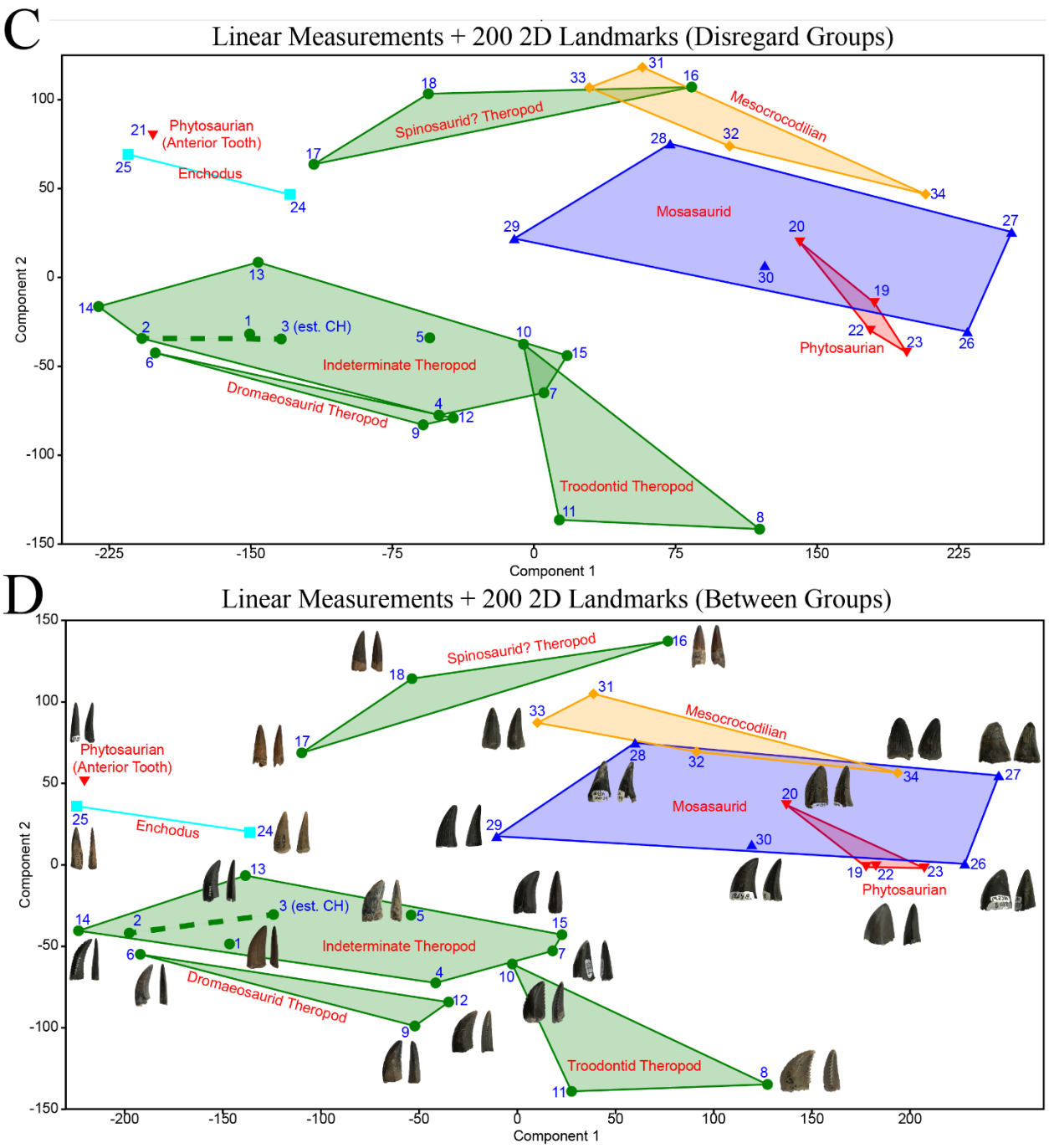

Figure 2.15 (continued): PCAs using linear measurements combined with 2D landmark data

(C) PCA of linear measurements combined with 200 2D landmarks (disregard groups). **(D)** PCA of linear measurements combined with 200 2D landmarks (between groups). All data converted to ranks.

Combining linear measurements and 3D-Landmarks

Three disregard-group and three between-group analyses were performed using linear measurement combined with either 11, 52 or 402 3D-landmarks (Figure 2.16). The results of each analysis show varying degrees of separation. The disregard group and between group analyses combining linear measurements and 11 3D-landmarks (Figure 2.16 A-B) are similar to each other, however the disregard group analysis (Figure 2.16 A) plots the *Enchodus* teeth and the phytosaurian anterior tooth within indeterminate theropod. The between-group analysis (Figure 2.16 B) is slightly more effective at separating all theropod groups from each other, whereas phytosaurian teeth and mesocrocodillian teeth overlap with each other, and both slightly overlap with mosasaurid teeth. Indeterminate theropod teeth #2 and #3 plot in close proximity to each other and the troodontid theropod teeth #8 and #10 (recurved to the right in mesial view) plot closer to each other than #11 (recurved to the left in mesial view).

Separation seems to decrease in the analyses combining linear measurements with 52 3D-landmarks (Figure 2.16 C-D). In the disregard group analysis (Figure 2.16 C) all groups overlap with one or more other groups except for the phytosaurian anterior tooth. However, separation increases greatly in the between-group analysis (Figure 2.16 D). Nearly all taxonomic groups are separated from each other, except for indeterminate theropod teeth, which overlaps with troodontid theropod teeth and slightly with mosasaurid teeth, and mesocrocodillian teeth, which overlaps slightly with mosasaurid teeth.

Group separation in the analyses combining linear measurements with 402 3D-landmarks (Figure 2.16 C-D) seems to be greater compared to the analyses with linear measurements combined with 52 3D-landmarks, but less than the analyses with linear measurements combined with 11 3D-landmarks. In the disregard group analysis (Figure 2.16 E) most groups overlap with

one or more other groups except for *Enchodus* teeth, spinosaurid theropod teeth, and the phytosaurian anterior tooth. However, in the between-group analysis (Figure 2.16 F) all taxonomic groups are separated from each other, except for troodontid theropod teeth, which overlaps slightly with indeterminate theropod teeth.

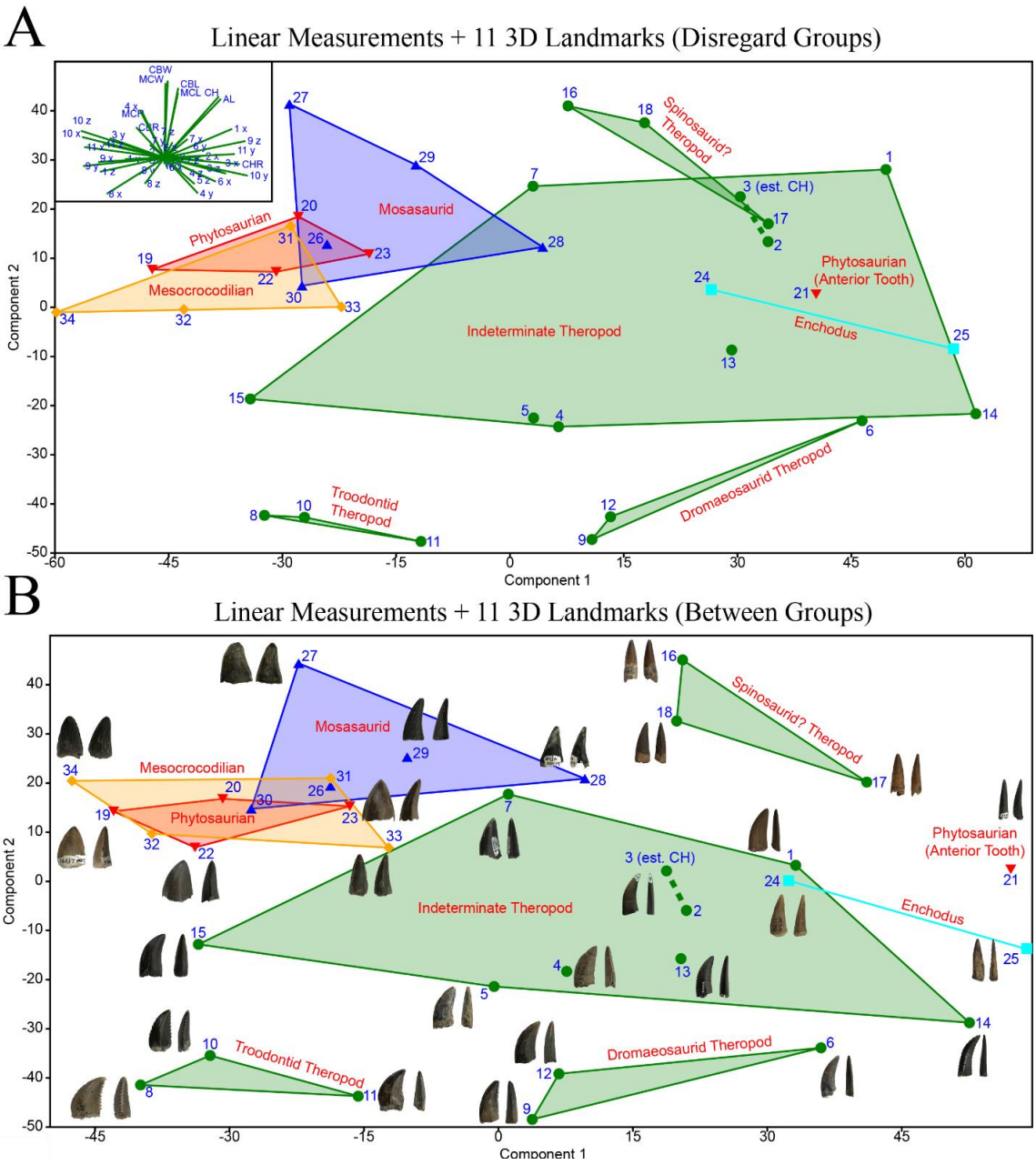

Figure 2.16: PCAs using linear measurements combined with 3D landmark data **(A)** PCA of linear measurements combined with 11 3D landmarks (disregard groups). (**B)** PCA of linear measurements combined with 11 3D landmarks (between groups). All data converted to ranks.

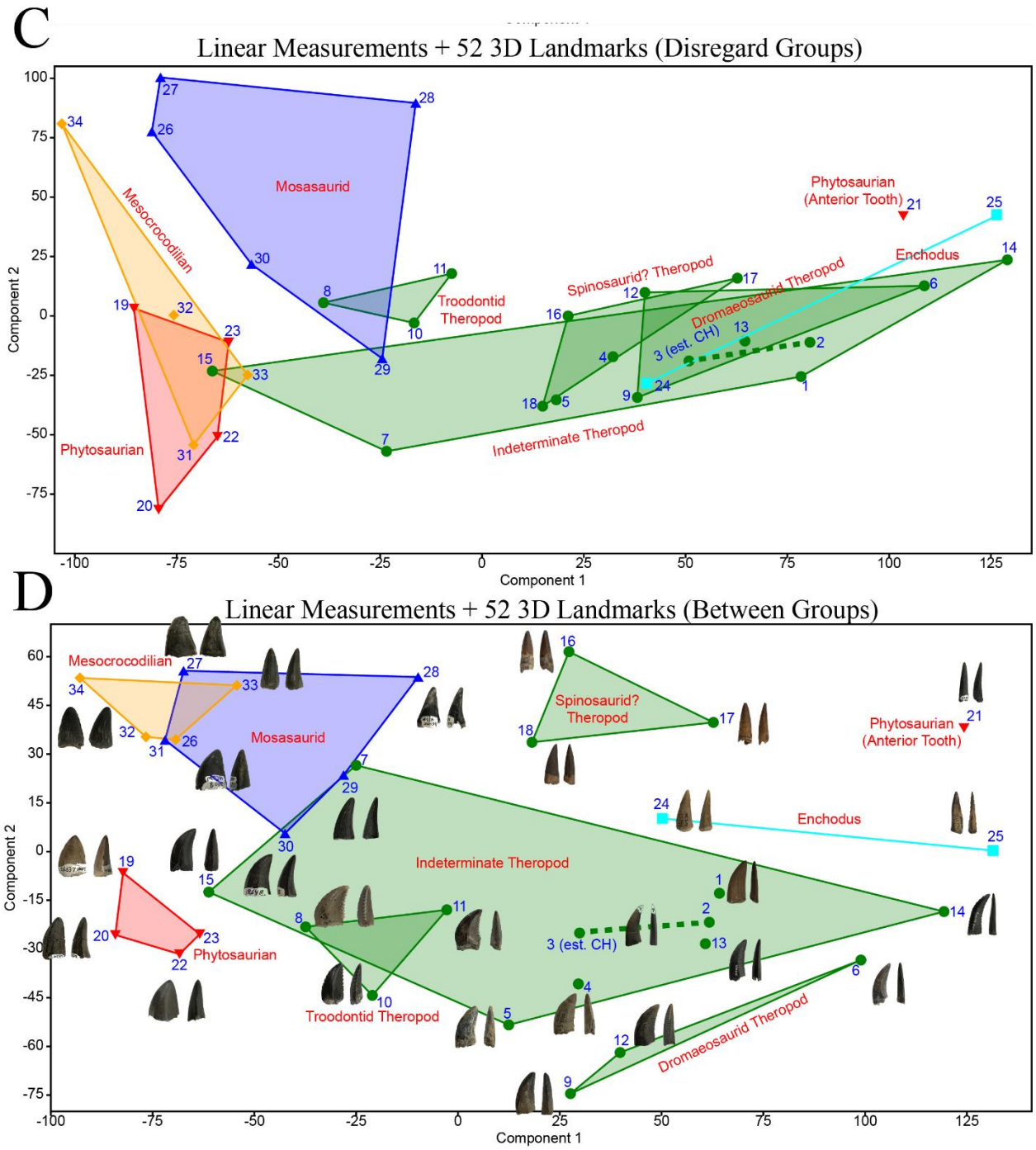

Figure 2.16 (continued): PCAs using linear measurements combined with 3D landmark data

(C) PCA of linear measurements combined with 52 3D landmarks (disregard groups). (**D)** PCA of linear measurements combined with 53 3D landmarks (between groups). All data converted to ranks.

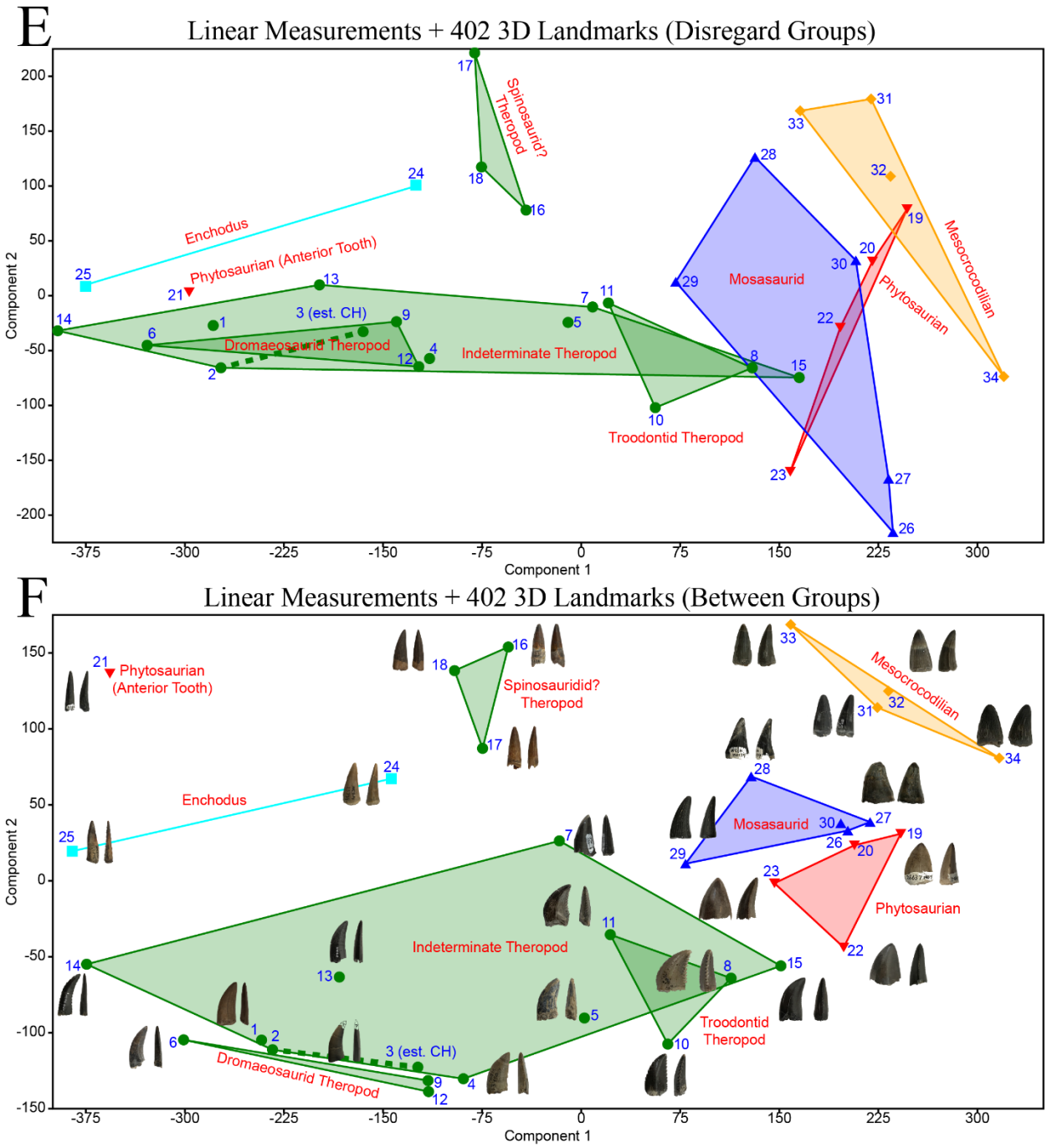

Figure 2.16 (continued): PCAs using linear measurements combined with 3D landmark data

(E) PCA of linear measurements combined with 402 3D landmarks (disregard groups). **(F)** PCA of linear measurements combined with 402 3D landmarks (between groups). All data converted to ranks.

Linear discriminant analyses

Only four LDAs were performed due to the requirement that specimens must outnumber variables (Figure 2.17). All LDAs produced convex hulls with little to no overlap, separation is most pronounced when linear measurements are combined with 11 lateral view 2D-landmarks (Figure 2.17 D), however these results do not necessarily represent effective classification of teeth into their correct groups. Table 2.3, shows which approaches (linear measurements, 2D, 3D, or combination) worked best for classifying teeth with an LDA approach.

The highest correct classifications occurred when using only measurement variables or when using ten 2D landmarks. When linear measurements were used alone, 88.24% of specimens were correctly classified; increasing to 94.1% and 97.06% when data was converted to ranks and log transformed, respectively. The 2D landmark LDA used a total of 10 landmarks for each specimen. A higher number of landmarks was not used because every 2D landmark is represented by an X and Y coordinate variable, therefore the analysis consisted of 20 total variables. This approach showed the highest degree of classification, with 100% of specimens correctly classified when data was left untransformed and 100% when data was converted to ranks.

In contrast, the 3D approaches showed the worst classification, with 0% of specimens correctly classified when data was left untransformed and 0% when data was converted to ranks. When linear measurements were combined with ten 2D landmarks only 29.41% of specimens were correctly classified, dropping to 0% when data was converted to ranks.

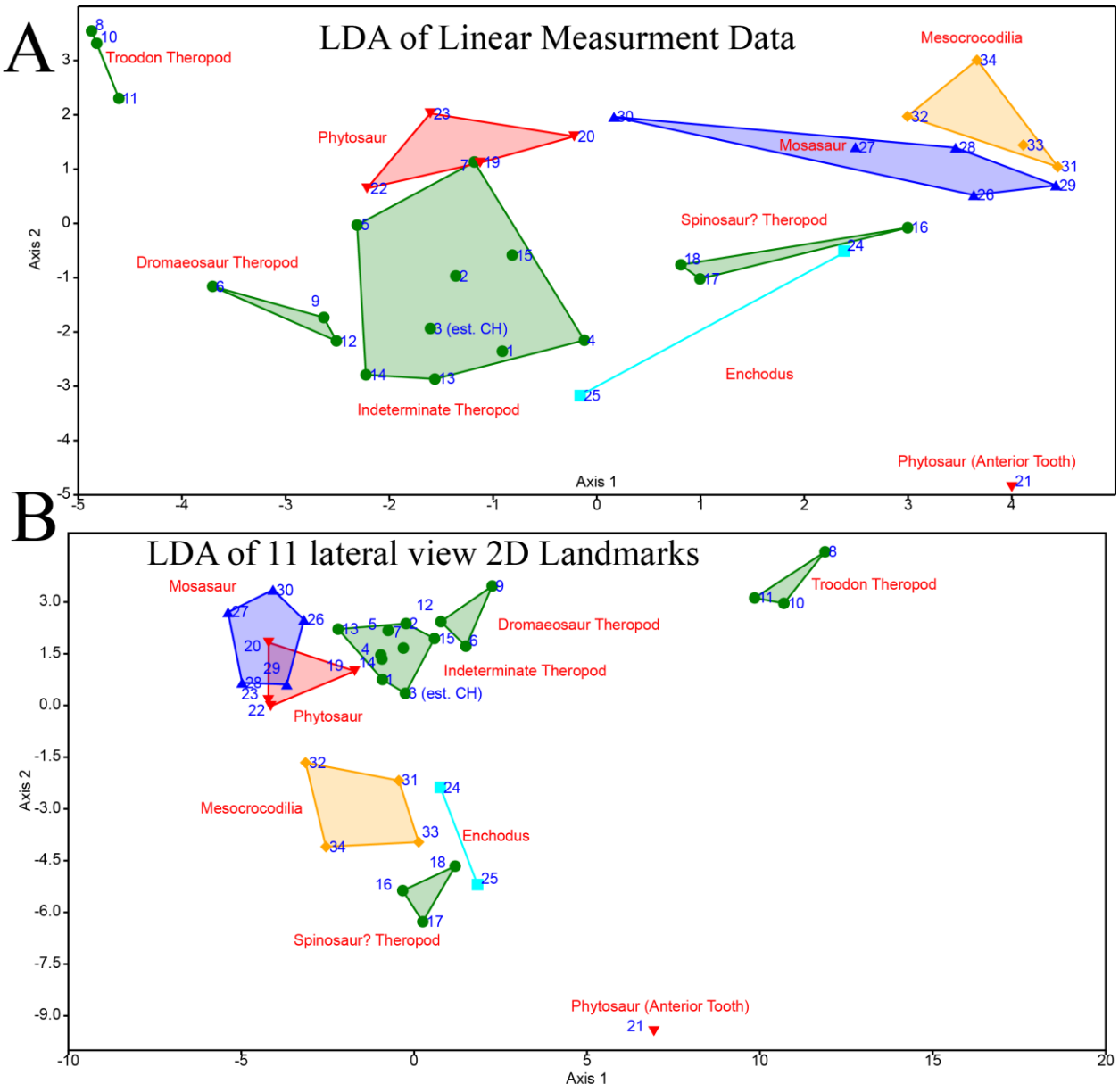

Figure 2.17 (continued): Linear discriminant analyses
(A) LDA of linear measurements. (**B)** LDA of 11 lateral view 2D-landmarks.

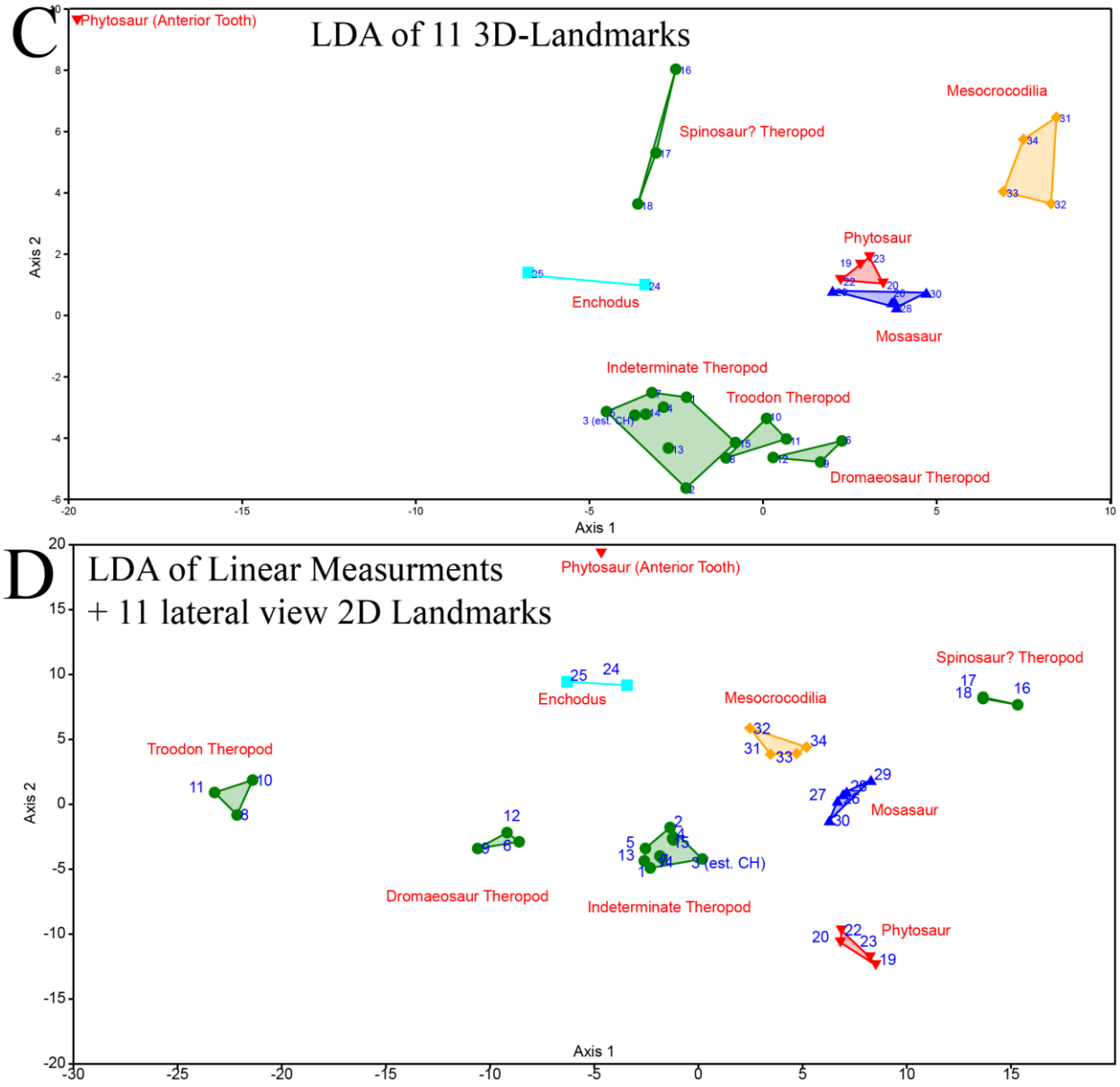

Figure 2.17 (continued): Linear discriminant analyses
(C) LDA of 11 3D landmarks. (**D)** LDA of linear measurements combined with 11 lateral view 2D landmarks (data converted to ranks).

Table 2.3: Confusion matrices

LDA confusion matrices showing the degree of misclassification for each morphometric approach. Ideally a highlighted box should contain the total number of teeth from its respective taxonomic group. Unhighlighted boxes indicate the degree of failure of classification.

Only measurement variables. correctly classified = 88.24%	Indeterminate Theropod	Dromaeosaur Theropod	Troodon Theropod	Spinosaur? Theropod	Phytosaur	Phytosaur (Anterior Tooth)	Enchodus	Mosasaur	Mesocrocodilia	Total
Indeterminate Theropod	7	1	0	0	1	0	0	0	0	9
Dromaeosaur Theropod	0	3	0	0	0	0	0	0	0	3
Troodon Theropod	0	0	3	0	0	0	0	0	0	3
Spinosaur? Theropod	0	0	0	2	0	0	1	0	0	3
Phytosaur	0	0	0	0	4	0	0	0	0	4
Phytosaur (Anterior Tooth)	0	0	0	0	0	1	0	0	0	1
Enchodus	0	0	0	0	0	0	2	0	0	2
Mosasaur	0	0	0	0	1	0	0	4	0	5
Mesocrocodilia	0	0	0	0	0	0	0	0	4	4
Total	7	4	3	2	6	1	3	4	4	34
Only measurement variables (data rank converted). correctly classified = 94.12%	Indeterminate Theropod	Dromaeosaur Theropod	Troodon Theropod	Spinosaur? Theropod	Phytosaur	Phytosaur (Anterior Tooth)	Enchodus	Mosasaur	Mesocrocodilia	Total
Indeterminate Theropod	9	0	0	0	0	0	0	0	0	9
Dromaeosaur Theropod	0	3	0	0	0	0	0	0	0	3
Troodon Theropod	0	0	3	0	0	0	0	0	0	3
Spinosaur? Theropod	0	0	0	3	0	0	0	0	0	3
Phytosaur	0	0	0	0	3	0	0	1	0	4
Phytosaur (Anterior Tooth)	0	0	0	0	0	1	0	0	0	1
Enchodus	0	0	0	0	0	0	2	0	0	2
Mosasaur	0	0	0	0	1	0	0	4	0	5
Mesocrocodilia	0	0	0	0	0	0	0	0	4	4
Total	9	3	3	3	4	1	2	5	4	34
Only measurement variables (data log transformed). correctly classified = 97.06%	Indeterminate Theropod	Dromaeosaur Theropod	Troodon Theropod	Spinosaur? Theropod	Phytosaur	Phytosaur (Anterior Tooth)	Enchodus	Mosasaur	Mesocrocodilia	Total
Indeterminate Theropod	8	0	0	0	1	0	0	0	0	9
Dromaeosaur Theropod	0	3	0	0	0	0	0	0	0	3
Troodon Theropod	0	0	3	0	0	0	0	0	0	3
Spinosaur? Theropod	0	0	0	3	0	0	0	0	0	3
Phytosaur	0	0	0	0	4	0	0	0	0	4
Phytosaur (Anterior Tooth)	0	0	0	0	0	1	0	0	0	1
Enchodus	0	0	0	0	0	0	2	0	0	2
Mosasaur	0	0	0	0	0	0	0	5	0	5
Mesocrocodilia	0	0	0	0	0	0	0	0	4	4
Total	8	3	3	3	5	1	2	5	4	34
10 2D landmarks. correctly classified = 100%	Indeterminate Theropod	Dromaeosaur Theropod	Troodon Theropod	Spinosaur? Theropod	Phytosaur	Phytosaur (Anterior Tooth)	Enchodus	Mosasaur	Mesocrocodilia	Total
Indeterminate Theropod	9	0	0	0	0	0	0	0	0	9
Dromaeosaur Theropod	0	3	0	0	0	0	0	0	0	3
Troodon Theropod	0	0	3	0	0	0	0	0	0	3
Spinosaur? Theropod	0	0	0	3	0	0	0	0	0	3
Phytosaur	0	0	0	0	4	0	0	0	0	4
Phytosaur (Anterior Tooth)	0	0	0	0	0	1	0	0	0	1
Enchodus	0	0	0	0	0	0	2	0	0	2
Mosasaur	0	0	0	0	0	0	0	5	0	5
Mesocrocodilia	0	0	0	0	0	0	0	0	4	4
Total	9	3	3	3	4	1	2	5	4	34
10 2D landmarks (data rank converted). correctly classified = 100%	Indeterminate Theropod	Dromaeosaur Theropod	Troodon Theropod	Spinosaur? Theropod	Phytosaur	Phytosaur (Anterior Tooth)	Enchodus	Mosasaur	Mesocrocodilia	Total
Indeterminate Theropod	9	0	0	0	0	0	0	0	0	9
Dromaeosaur Theropod	0	3	0	0	0	0	0	0	0	3
Troodon Theropod	0	0	3	0	0	0	0	0	0	3
Spinosaur? Theropod	0	0	0	3	0	0	0	0	0	3
Phytosaur	0	0	0	0	4	0	0	0	0	4
Phytosaur (Anterior Tooth)	0	0	0	0	0	1	0	0	0	1
Enchodus	0	0	0	0	0	0	2	0	0	2
Mosasaur	0	0	0	0	0	0	0	5	0	5
Mesocrocodilia	0	0	0	0	0	0	0	0	4	4
Total	9	3	3	3	4	1	2	5	4	34

Table 2.3 (continued): Confusion matrices

10 3D landmarks. correctly classified = 0%	Indeterminate Theropod	Dromaeosaur Theropod	Troodon Theropod	Spinosaur? Theropod	Phytosaur	Phytosaur (Anterior Tooth)	Enchodus	Mosasaur	Mesocrocodilia	Total
Indeterminate Theropod	0	0	0	0	9	0	0	0	0	9
Dromaeosaur Theropod	0	0	0	0	3	0	0	0	0	3
Troodon Theropod	0	3	0	0	0	0	0	0	0	3
Spinosaur? Theropod	0	0	0	0	3	0	0	0	0	3
Phytosaur	0	4	0	0	0	0	0	0	0	4
Phytosaur (Anterior Tooth)	0	0	0	0	1	0	0	0	0	1
Enchodus	0	0	0	0	2	0	0	0	0	2
Mosasaur	0	0	0	0	5	0	0	0	0	5
Mesocrocodilia	0	4	0	0	0	0	0	0	0	4
Total	0	11	0	0	23	0	0	0	0	34
10 3D landmarks (data rank converted). correctly classified = 0%	Indeterminate Theropod	Dromaeosaur Theropod	Troodon Theropod	Spinosaur? Theropod	Phytosaur	Phytosaur (Anterior Tooth)	Enchodus	Mosasaur	Mesocrocodilia	Total
Indeterminate Theropod	0	0	9	0	0	0	0	0	0	9
Dromaeosaur Theropod	0	0	0	0	0	0	3	0	0	3
Troodon Theropod	0	0	0	0	0	0	3	0	0	3
Spinosaur? Theropod	0	0	0	0	3	0	0	0	0	3
Phytosaur	0	0	0	0	0	0	4	0	0	4
Phytosaur (Anterior Tooth)	0	0	0	0	1	0	0	0	0	1
Enchodus	0	0	0	0	2	0	0	0	0	2
Mosasaur	0	0	0	0	0	0	5	0	0	5
Mesocrocodilia	0	0	0	0	0	0	4	0	0	4
Total	0	0	9	0	6	0	19	0	0	34
Measurement variables + 20 2D lateral face landmarks. correctly classified = 29.41%	Indeterminate Theropod	Dromaeosaur Theropod	Troodon Theropod	Spinosaur? Theropod	Phytosaur	Phytosaur (Anterior Tooth)	Enchodus	Mosasaur	Mesocrocodilia	Total
Indeterminate Theropod	0	0	9	0	0	0	0	0	0	9
Dromaeosaur Theropod	0	0	3	0	0	0	0	0	0	3
Troodon Theropod	0	0	0	0	0	0	0	3	0	3
Spinosaur? Theropod	0	0	0	0	0	3	0	0	0	3
Phytosaur	0	0	0	0	4	0	0	0	0	4
Phytosaur (Anterior Tooth)	0	0	0	1	0	0	0	0	0	1
Enchodus	0	0	0	0	0	0	2	0	0	2
Mosasaur	0	0	5	0	0	0	0	0	0	5
Mesocrocodilia	0	0	0	0	0	0	0	0	4	4
Total	0	0	17	1	4	3	2	3	4	34
Measurement variables + 20 2D lateral face landmarks. correctly classified = 0%	Indeterminate Theropod	Dromaeosaur Theropod	Troodon Theropod	Spinosaur? Theropod	Phytosaur	Phytosaur (Anterior Tooth)	Enchodus	Mosasaur	Mesocrocodilia	Total
Indeterminate Theropod	0	0	0	0	0	0	0	0	9	9
Dromaeosaur Theropod	0	0	0	0	0	0	0	0	3	3
Troodon Theropod	0	0	0	0	3	0	0	0	0	3
Spinosaur? Theropod	0	3	0	0	0	0	0	0	0	3
Phytosaur	0	4	0	0	0	0	0	0	0	4
Phytosaur (Anterior Tooth)	0	0	0	0	0	0	0	0	1	1
Enchodus	0	2	0	0	0	0	0	0	0	2
Mosasaur	0	0	0	0	0	0	0	0	5	5
Mesocrocodilia	0	4	0	0	0	0	0	0	0	4
Total	0	13	0	0	3	0	0	0	18	34

Time Investment

Collecting 2D landmarks offered the fastest approach, at 102.6 minutes or approximately 1.55 hours. Tooth imaging duration took 33.2 minutes and individual operations ranged between 25 seconds and 2 minutes 25 seconds. Image downsizing and turning all backgrounds white for of all 34 teeth (68 total images for both views) was performed simultaneously using Photoshop batch processing and took 32 minutes. Using tpsDig and tpsUtil to collect and export landmarks for all 34 teeth (68 total images for both views) took 28 minutes (Table 2.2).

Collection of linear measurements took 102.6 minutes or approximately 1.71 hours with a range between 1 and 6 minutes per tooth, depending on the size of the tooth; larger teeth were easier to measure with calipers than smaller teeth (Table 2.2).

Collection of 3D landmarks took 945 minutes or approximately 15.75 hours. Video recording of each tooth took 58 minutes and individual operations ranged between 1.5 and 3 minutes. Importing video files from the iPhone 7 to the computer took 17 minutes. Extracting video frames from video files took 34 minutes. Importing masks into Photoscan took 51 minutes, with individual operations averaging 1.5 minutes. Aligning both chunks in Photoscan took 340 minutes, with individual operations averaging 10 minutes. Building dense clouds in Photoscan took 272 minutes, with individual operations averaging 8 minutes. Building 3D meshes in Photoscan and exporting models took 170 minutes, with individual operations averaging 5 minutes. Running the GPSA analysis for all 34 models took 3 minutes (Table 2.2).

DISCUSSION

Traditional and geometric morphometric approaches

Effectiveness at data discrimination and reduction of group overlap

If only one approach to data collection is taken (disregarding analyses combining traditional and geometric morphometrics), the most effective and consistent method of separating taxonomic groups is 2D-landmark analyses. These PCAs reliably separate nearly all taxonomic groups, with slightly improved results for between-group analyses, and nearly identical results when a higher quantity of landmarks are incorporated (200 vs. 20).

In contrast, linear measurements seem relatively ineffective at discriminating some tooth features such as conicality (quantified by MCL and MCW) and curvature (quantified by AL) (exampled by the *Enchodus* and anterior phytosaurian teeth overlapping with indeterminate theropod teeth in Figure 2.12 A – C, despite clear shape differences because these differences are not picked up by the linear measurements). Nonetheless, linear measurements appear best at disregarding preservation quality (when poor preservation is represented by a missing tooth apex, as with indeterminate theropod teeth #2 and #3).

3D landmark analyses show considerable variation in their ability to effectively discriminate taxonomic tooth groups. Although the higher landmark analyses appear to be slightly more effective at separating tooth groups than linear measurements, they are not as effective as any of the 2D-landmark analyses. Furthermore, they often plot a number of mosasaurid teeth well outside the bounds of the graph. These inconsistencies are likely the result of complications during the GPSA procedure. For example, the GPSA sometimes incorrectly aligned and rotated 3D tooth models, and despite attempts to correct these errors, it is possible that some anomalies made it into the final multivariate analyses. Furthermore, the GPSA

transforms 3D model vertices into landmarks, and this process often produced a greater number of landmarks near the basal regions of teeth. Therefore, the basal regions are more heavily weighted during analyses. Although the basal regions of teeth may display important biological variation, such as the dimensions of pulp cavities, for different taxonomic groups, much of the variation may be attributable to factors related to the life cycle (ontogeny) of the tooth. Additionally, analyses performed on datasets that exclude or underweight basal regions may produce improved results.

The most effective separation occurred when geometric data was combined with linear measurements. However, the confidence of this approach is unclear due to the ambiguity of how data transformations effects biological information, which may raise concerns on how the multivariate analyses make quantitative assumptions. For example, when 3D-landmark data was converted to ranks and inspected using Checkpoint, landmark data appeared to be completely corrupted. Nonetheless, this approach seemed to produce unparalleled results in the ability to effectively separate taxonomic groups, in both disregard-group and between-group analyses.

When linear data was combined with 2D landmarks and data was transformed by converting to ranks, there was effective separation of nearly every taxonomic group. These analyses appear ineffective at distinguishing preservation quality (evidenced by distance between indeterminate theropod teeth #2 and #3) and they are unable to differentiate between dental position (evidenced by the equal distance between troodontid teeth #8, #10 and #11). However, due to the small sample size, these interpretations on the effects of preservation quality and dental position should be held with low confidence.

Separation is most pronounced in the analysis combining linear measurements with eleven 3D-landmarks. This analysis may appear effective at disregarding preservation quality

(evidenced by the minimum separation between indeterminate theropod teeth #2 and #3), however it is unclear whether the analyses is in fact disregarding the discrepancy in preservation or if other morphological factors are influencing the close proximity of indeterminate theropod teeth #2 and #3. Similarly, this analysis may appear moderately effective at differentiating between dental position (evidenced by the moderate proximity of troodontid teeth #10 and #8, which both curve to the right in mesial view, unlike troodontid tooth #11 which curves to the left), however, whether this effect is in fact the result of effective discrimination is unclear.

Methods requiring the least investment in terms of time and labor

The amount of time required to collect tooth data on all 34 teeth for the three analyses was widely variable (Table 2.2). Unexpectedly, collecting 2D landmarks offered the fastest approach, at approximately 1.5 hours. These times can be reduced even further, to only an hour, if image modifications are not used. Similarly, collecting linear measurements took approximately 1.71 hours.

In contrast, collecting 3D data was substantially longer than both other methods, at 15.75 hours. This is largely due in part to long processing times when using Agisoft Photogrammetry to build 3D models. However, these long durations are merely representative of a process that proceeds in a linear fashion from one step to the next step; this does not reflect a realistic workflow, where several steps, such as Photoshop batch processing, Photoscan batch processing, and video recording, can be conducted simultaneously. In addition, processing times are significantly faster when they are run on computers with higher performance capabilities. The majority of Agisoft Photoscan operations were performed on a Dell Inspiron 15-5547 laptop with an Intel Core i3 and 6gb of Ram. The longest procedure in the Photoscan process is the initial

alignment of both chunks, which usually takes between eight and twelve minutes. When operations were conducted on an iMac with a 3GHz 8-Core Intel Xeon E5 processor and 125 GB 1066 MHz DDR3 of Ram, these operation times were often reduced by more than half.

Linear discriminant analyses

The linear discriminant analyses show promising results, with dramatic separation of taxonomic groups. However, it should be noted that the majority of separation in these analyses is influenced by the pre-determined groupings, and the LDA fails dramatically when non-associated teeth are included. For example, when one tooth from each category is disassociated from its group, teeth are more likely to plot far outside the bounds of the morphospace, than close to their true corresponding group.

Additionally, the results of the confusion matrices (Table 2.3) show both promising results, with 100% correct classifications in the ten 2D landmarks LDA and discouraging results with the 0% correct classifications in the ten 3D landmarks LDA. However, these results should not be considered with high confidence, as most analyses were constrained to use only 34 or fewer variables. The 3D analysis likely failed with a classification rate of 0% since every 3D landmark is represented by a X, Y, and Z coordinate, and ten landmarks represented by 30 variables is not enough to adequately represent a tooth in 3D. It is also likely that the classification failure highlights the need for software that can quickly and effectively place constant, equally distanced landmarks across the outer surface of 3D models (see section “Issues and improvements to the 3D data collection methods” for an expanded discussion of this issue).

In contrast to the 3D landmark LDA, it was surprising that the 2D landmark LDA produced 100% correct classification rate. Nonetheless, with larger sample sizes, beyond 34

teeth and improvements to landmark data collection, the effectiveness of both LDAs and between-group PCAs will likely improve dramatically. For example, a sample consisting of over 156 teeth would allow nearly every PCA in this study to be performed as an LDA.

If a similar approach was carried out with the Hendrickx et al. (2014) database, which consists of 995 teeth, one could combine the eight linear measurements with either 489 2D-landmarks or 322 3D-landmarks. It is unknown exactly how this type of data integration would result. However, it is possible that the rate of group misclassification and the overlap of convex hulls could be significantly reduced.

Issues and improvements to the 3D data collection methods

While the GPSA is effective at quickly processing multiple models, it was not intended for simple shapes such as teeth and had issues with correctly aligning models and placing too many landmarks near basal regions. Additionally, Checkpoint, which is arguably the best software currently available for managing and placing 3D landmarks, is unable to effectively and quickly distribute landmarks across certain shapes, specifically tall teeth with strong curvature.

Ideally, software should be developed that would produce a floating sphere, cylinder, stacked lattice, or cloud of available landmarks, which would envelop the object of interest. This software should allow for non-sliding landmarks to be manually or automatically anchored to one or more homologous anatomical areas, such as the crown apex, basal center, and/or the mid-length position along the mesial and/or distal carinae. Then, like an object being air sealed in plastic wrap, the floating landmarks would move inward toward the object's centroid or a median axis, stopping once they strike the surface. This would allow for multitudes of comparable 3D objects to be consistently processed at the same speeds as the linear measurement

and 2D landmark data collection methods. Additionally, the software should allow for 3D models to be mirrored prior to landmark placement, in order to eliminate some of the variation due to dental position, specifically recurvature in mesial view.

Concerns with data transformations

As discussed previously, all experimental analyses in which traditional and geometric morphometrics were combined required data transformations. When data was not transformed, PCAs did not consider landmark data as significant, and graphical outputs were identical to analyses produced with only measurement variables. While this may be a true reflection of how the analyses considers variables accounting for the greatest variation, it does not allow for the landmark data to contribute to analyses.

The converting to ranks transformation was initially used because it is capable of handling negative numbers and seemed to show the most promising results, by significantly reducing group overlap in morphospace and producing biplots with equally distanced eigenvectors. However, I began to question the true effectiveness of this transformation after rank converted landmark data was imported into 3D landmark visualizers, which showed the 3D models to be completely corrupted into amorphous clouds of landmarks. Additionally, rank conversions seemed to have conflicting results regarding the correct classification of specimens in the four LDAs; where rank conversions improved correct classification of the linear measurement LDA by 6%, lowered correct classification from 30% to 0% in the combination dataset, and did not affect classification success rates for the 2D or 3D LDAs.

These concerns led me to explore Box-Cox transformation, which finds the lowest number, raises it to 1, applies the same addition to the entire dataset, and then standardizes the

data by maximizing the log likelihood function (Hammer et al. 2001). This produced promising results by preserving 3D landmark data in a way that it could be visualized, however some artifacts of the transformation did develop, causing several scattered and out of place landmarks.

A final test was performed on the effects of rank conversion, in relation to the large tooth dataset from Hendrickx et al. (2014), which consisted of eleven measurement variables, measured across 995 teeth belonging to 62 theropod taxa and 19 groupings. The LDAs showed a correct classification rate of 64.12% for non-transformed data, 69.05% for logged data, 67.94% for Box-Cox transformed data, and 69.75% when data was converted to ranks. This shows that at least for measurement variables, converting to ranks does not negatively affect data, but in fact seems the best method transforming data.

Broader Implications

The results of this study suggest that quantifying the morphology of isolated archosaurian teeth using geometric morphometrics has advantages over linear measurements, specifically in the ability to discriminate different tooth shapes. Yet these improvements must be considered wisely in how they are applied to different biological and ecological questions, especially when assigning isolated teeth and/or undiagnosed skeletal material to previously described genera or species (e.g. Baszio 1997; Eaton et al. 1999a; Eaton et al. 1999b; Lucas et al. 2000; Sullivan & Lucas 2000; Sankey 2001; Sullivan 2006; Sullivan & Lucas 2006; Fanti & Miyashita 2009; Oreska et al. 2013; Sues & Averianov 2013; Schoch et al. 2018).

A number of studies have shown that the morphology of isolated theropod teeth have taxonomic utility (Currie et al. 1990; Fiorillo & Currie 1994; Sankey 2001; Sankey et al. 2002; Samman et al. 2005; Smith 2005; Larson 2008; Longrich 2008; Hendrickx & Mateus 2014;

Gerke & Wings 2016), however these studies focused primarily on (1) referring isolated teeth from specific stratigraphic units to previously described species from the same formation based on similarities, or (2) the morphological variability of teeth due to ontogeny or dental position.

Although theropod teeth have been used to document broad scale geographical and temporal patterns (e.g. Larson & Currie 2013; Williamson & Brusatte 2014), the confidence of tooth referrals in these studies may come into question when considering arguments against the taxonomic utility of isolated theropod teeth. For example, the morphologies of isolated dromaeosaurid teeth have been shown to display considerable overlap with different genera (Farlow et al. 1991; Currie & Varricchio 2004; Hendrickx et al. 2014), and Samman et al. (2005) was unable to identify 35 isolated tyrannosaurid teeth from the Judith River Group to the even the genus level.

Additionally, isolated troodontid teeth from the Kaiparowits Formation were originally referred to as *Troodon sp.* (Eaton et al. 1999), however the discovery of *Talos sampsoni* from the Kaiparowits Formation (Zanno et al. 2011) shows that the practice of assigning isolated material to the genus or species level across broad geographic regions can be dubious. These concerns are further highlighted by data arguing against the assumption that dinosaur taxa from the Western Interior Basin had wide geographical ranges spanning Laramidia. In contrast to this assumption, dinosaur faunas from contemporary upper Campanian formations show limited geographic ranges (Smith et al. 2003; Sampson et al. 2004; Smith et al. 2004; Gates & Evans 2005; Zanno et al. 2005b; Sampson et al. 2010; Zanno et al. 2005a; Lucas et al. 2006; Gates & Sampson 2007; Zanno 2007; Wagner & Lehman 2009; Gates et al. 2010; Sampson et al. 2010; Sampson et al. 2013; Zanno et al. 2013).

Dentigerous theropod skeletal material displays moderate to significant morphological tooth variability due to ontogeny and/or heterodonty along the tooth row (Buckley 2009; Buckley et al. 2010). Moderate to extreme dental changes are documented to occur within multiple theropod clades (Carr 1999; Rauhut & Fechner 2005; Kundrát et al. 2008; Bever & Norell 2009; Wang et al. 2017). If similar patterns are consistent among other theropod clades, it is possible that referrals of disparate teeth may in fact belong to the same species. For example, the morphological parameters defining *Richardoestesia* and *Paronychodon* are consistent with the variation of tooth dimensions observed along the dental row for many theropods (Longrich 2008). Therefore, isolated teeth representing multiple theropod groups may be inappropriately lumped into a single genus or species.

Even with vastly improved discrimination methods and analyses, assigning teeth to existing taxa or using teeth to name new species may be unwise. Unless teeth exhibit autapomorphic morphology and can be linked via these traits to teeth associated with identifiable skeletal materials, teeth should be considered as morphotypes and referred to the supergeneric level.

Nonetheless, the results of this study suggest that geometric morphometrics and combinations of linear measurement data with landmark data could have profound implications for studies of paleobiodiversity, paleobiogeography, and species abundance. With improvements in the ability to accurately discriminate tooth morphotypes, we can build more complete pictures of ancient ecosystems and improve our ability to reconstruct biodiversity and species abundances trends.

Lastly, these morphometric methods have the potential to improve studies of other biologically and anatomically significant features that display a relatively simple geometric

shape, such as avian beaks (Button 2018) or theropod claws (Birn-Jeffery et al. 2012; Lautenschlager 2014), further widening the breadth of these morphometric approaches.

CONCLUSION

Studies quantifying archosaurian tooth morphology have overwhelmingly depended on traditional morphometrics. However, the application of geometric morphometrics offers a suite of advantages including reduced data collection time, consideration of subtle tooth shape features during analyses, and improved discrimination of teeth occupying a wide spectrum of morphological diversity. Comparing traditional linear morphometrics with geometric morphometric methods indicates that 2D geometric morphometric approaches are best at discriminating tooth morphology, reducing overlap between taxonomic groups, and offer the fastest data collection times. Linear measurements offer similar data collection times as 2D landmark approaches, however appear limited in their ability to discriminate morphological data and produce moderate to significant overlap between groups. In contrast, 3D geometric morphometric approaches display significant variability in their ability to discriminate morphological data and reduce overlap between groups, and data collection takes approximately 10 times longer than the other approaches.

Additionally, combining traditional and geometric morphometrics may further improve the discrimination potential of analyses with large sample sizes. Utilizing geometric morphometrics instead of, or in conjunction with, traditional morphometrics may aid future studies, such as those focusing on: the identification of novel tooth morphotypes from isolated teeth, biodiversity changes through time, and the effects of dental variation due to ontogeny. Although the collection of 2D landmarks has been popular for decades, the practice of

constructing high resolution 3D representations of real-world objects is still in its infancy, and diminutive objects such as fossil teeth present an additional challenge. The methodology designed for this study offers a means to capture and evaluate 3D data for diminutive objects that can be utilized by researchers; however, improvements in the ability to quickly construct accurate 3D models of diminutive objects and collect 3D landmarks will greatly improve the practical utilization of 3D geometric morphometrics. Utilizing geometric morphometrics for quantifying and analyzing simple biological and anatomical objects such as teeth, beaks, and claws has the potential to greatly improve our understanding of biodiversity, paleobiogeography, ecological modeling, and ontogeny, throughout Earth's history.

REFERENCES

Adams DC, Rohlf FJ, and Slice DE. 2004. Geometric morphometrics: ten years of progress following the ‘revolution’. *Italian Journal of Zoology* 71:5-16.

Agisoft L, and St Petersburg R. 2014. Agisoft photoscan. *Professional Edition*.

Andrews HE. 1974. Morphometrics and functional morphology of Turritella mortoni. *Journal of Paleontology* 48:1126-1140.

Araújo R, Castanhinha R, Martins RMS, Mateus Ov, Hendrickx C, Beckmann F, Schell N, and Alves LC. 2013. Filling the gaps of dinosaur eggshell phylogeny: Late Jurassic Theropod clutch with embryos from Portugal. *Scientific Reports* 3:1-8.

Argast S, Farlow JO, Gabet RM, and Brinkman DL. 1987. Transport-induced abrasion of fossil reptlian teeth: Implications for the existence of Tertiary dinosaurs in the Hell Creek Formation, Montana. *Geology* 15:927-930.

Barrett PM, McGowan AJ, and Page V. 2009. Dinosaur diversity and the rock record. *Proceedings of the Royal Society B* 276:2667-2674.

Baszio S. 1997. Systematic palaeontology of isolated dinosaur teeth from the latest Cretaceous of south Alberta, Canada. *Courier Forschungsinstitut Senckenberg* 196:33-77.

Bever GS, and Norell MA. 2009. The perinate skull of Byronosaurus (Troodontidae) with observations on the cranial ontogeny of paravian theropods. *American Museum Novitates*:1-52.

Birn-Jeffery AV, Miller CE, Naish D, Rayfield EJ, and Hone DWE. 2012. Pedal claw curvature in birds, lizards and Mesozoic dinosaurs, complicated categories and compensating for mass-specific and phylogenetic control. *PLOS One* 7:e50555.

Blackith RE, and Reyment RA. 1971. *Multivariate morphometrics*.

Bookstein F. 1978. Measurement of biological shape change using biorthogonal grids. Biometrics: International Biometric Society. p 154-154.

Bookstein FL. 1998. A hundred years of morphometrics. *Acta Zoologica Academiae Scientiarum Hungaricae* 44:7-59.

Brinkman DB. 1990. Paleooecology of the Judith River Formation (Campanian) of Dinosaur Provincial Park, Alberta, Canada: Evidence from vertebrate microfossil localities. *Palaeogeography, Palaeoclimatology, Palaeoecology* 78:37-54.

Buckley LG. 2009. Individual and ontogenetic variation in theropod dinosaur teeth: a case study of *Coelophysis bauri* (Theropoda: Coelophysoidea) and implications for identifying isolated theropod teeth. University of Alberta.

Buckley LG, Larson DW, Reichel M, and Samman T. 2010. Quantifying tooth variation within a single population of *Albertosaurus sarcophagus* (Theropoda: Tyrannosauridae) and implications for identifying isolated teeth of tyrannosaurids. *Canadian Journal of Earth Sciences* 47:1227-1251. 10.1139/e10-029

Buffetaut E, Martill D, and Escuillié F. 2004. Pterosaurs as part of a spinosaur diet. *Nature* 430:33.

Button KA. 2018. Soft Tissue Reconstruction and Ecomorphology of Beaks in Extant and Extinct Theropod Dinosaurs.

Campione NE, and Evans DC. 2011. Cranial growth and variation in edmontosaurs (Dinosauria: Hadrosauridae): Implications for latest Cretaceous megaherbivore diversity in North America. *PLOS One* 6:e25186.

Carr TD. 1999. Craniofacial ontogeny in Tyrannosauridae (Dinosauria, Coelurosauria). *Journal of Vertebrate Paleontology* 19:497-520.

Chapman RE, and Brett-Surman MK. 1990. Morphometirc observations on hadrosaurid ornithopods. In: Carpenter K, and Currie PJ, eds. *Dinosaur systematics: Approaches and perspectives*. Cambridge: Cambridge University Press, 163-178.

Checkpoint. 2017. Stratovan Corporation. *https://wwwstratovancom/products/checkpoint*.

Chinnery BJ, Lipka TR, Kirkland JI, Parrish JM, and Brett-Surman MK. 1998. Neoceratopsian teeth from the Lower to middle Cretaceous of North America. *Bulletin of the New Mexico Museum of Natural History and Science* 14:297-302.

Currie PJ. 2003. Cranial anatomy of tyrannosaurid dinosaurs form the Late Cretaceous of Alberta, Canada. *Palaeontologica Polonica* 48:191-226.

Currie PJ, Rigby JK, Jr., and Sloan RE. 1990. Theropod teeth from the Judith River Formation of southern Alberta, Canada. In: Carpenter K, and Currie PJ, eds. *Dinosaur systematics: Approaches and perspectives*. Cambridge: Cambridge University Press, 108-125.

Currie PJ, and Varricchio DJ. 2004. A new dromaeosaurid from the Horseshoe Canyon Formation (Upper Cretaceous) of Alberta, Canada. In: Currie PJ, Koppelhus EB, Shugar MA, and Wright JL, eds. *Feathered Dragons: Studies on the Transition from Dinosaurs to Birds*. Bloomington: Indiana University Press, 112-132.

de Oliveira TM, and Pinheiro FL. 2017. Isolated Archosauriform Teeth From The Upper Triassic Candelária Sequence (Hyperodapedon Assemblage Zone, Southern Brazil). *Revista Brasileira de Paleontologia* 20:155-162.

Dodson P. 1976. Quantitative aspects of relative growth and sexual dimorphism in *Protoceratops*. *Journal of Paleontology* 50:929-940.

Dodson P. 1983. A faunal review of the Judith River (Oldman) Formation, Dinosaur Provincial Park, Alberta. *Mosasaur* 1:89-118.

Dodson P, Currie P, and Koster E. 1987. Microfaunal studies of dinosaur paleoecology, Judith River Formation of southern Alberta. Fourth Symposium on Mesozoic Terrestrial Ecosystems, Short Papers Occasional Papers of the Tyrrell Museum of Palaeontology. p 71-75.

DVDVideoSoft. 2018. Free Video to JPG Converter. *Digital Wave Ltd https://wwwdvdvideosoftcom/faqhtm*.

Eaton JG, Cifelli RL, Hutchison JH, Kirkland JI, and Parrish JM. 1999a. Cretaceous vertebrate faunas from the Kaiparowits Plateau, south-central Utah. In: Gillette DD, ed. *Vertebrate paleontology in Utah*. Salt Lake City: Utah Geological Survey, 345-353.

Eaton JG, Diem S, Archibald JD, Schierup C, and Munk H. 1999b. Vertebrate paleontology of the Upper Cretaceous rocks of the Markagunt Plateau, southwestern Utah. In: Gillette DD, ed. *Vertebrate paleontology in Utah*. Salt Lake City: Utah Geological Survey, 323-333.

Estes R. 1964. Fossil vertebrates from the Late Cretaceous Lance Formation, eastern Wyoming. *California University Publications on Geological Sciences* 49:180.

Evans SE, and Milner AR. 1994. Middle Jurassic microvertebrate assemblages from the British Isles. In: Fraser NC, and Sues H-D, eds. *In the Shadow of the Dinosaurs*. Cambridge: Cambridge University Press, 303-321.

Fanti F, and Miyashita T. 2009. A high latitude vertebrate fossil assemblage from the Late Cretaceous of west-central Alberta, Canada: evidence for dinosaur nesting and vertebrate latitudinal gradient. *Palaeogeography, Palaeoclimatology, Palaeoecology* 275:37-53.

Farlow JO, Brinkman D, Abler WL, and Currie PJ. 1991. Size, shape, and serration density of theropod dinosaur lateral teeth. *Modern Geology* 16:161-198.

Fink WL, and Zelditch ML. 1995. Phylogenetic analysis of ontogenetic shape transformations: a reassessment of the piranha genus Pygocentrus (Teleostei). *Systematic Biology* 44:343-360.

Fiorillo A. 1989. The vertebrate fauna from the Judith River Formation (Late Cretaceous) of Wheatland and Golden Valley Counties, Montana. *The Mosasaur* 4:127-142.

Fiorillo AR, and Currie PJ. 1994. Theropod teeth from the Judith River Formation (Upper Cretaceous) of south-central Montana. *Journal of Vertebrate Paleontology* 14:74-80.

Fiorillo AR, and Gangloff RA. 2000. Theropod teeth from the Prince Creek Formation (Cretaceous) of northern Alaska, with speculations on Arctic dinosaur paleoecology. *Journal of Vertebrate Paleontology* 20:675-682.

Fisher RA. 1935. The logic of inductive inference. *Journal of the Royal Statistical Society* 98:39-82.

Frederickson JA, Cohen JE, Hunt TC, and Cifelli RL. 2017. A new occurrence of Dakotasuchus kingi from the Late Cretaceous of Utah, USA, and the diagnostic utility of postcranial characters in Crocodyliformes. *Acta Palaeontologica Polonica* 62:279-286.

Gates T, and Evans D. 2005. Biogeography of Campanian hadrosaurid dinosaurs from western North America. Dinosaur Park Symposium short papers, abstracts, and programs Royal Tyrrell Museum of Paleontology, Drumheller, Alberta. p 33-39.

Gates T, Sampson S, Zanno L, Roberts E, Eaton J, Nydam R, Hutchison J, Smith J, Loewen M, and Getty M. 2010. The fauna of the Late Cretaceous Kaiparowits Formation: testing previous ideas about late Campanian vertebrate biogeography in the Western Interior Basin: Paleogeography. *Paleoclimatology, and Paleoecology* 291:371-387.

Gates TA, and Sampson SD. 2007. A new species of *Gryposaurus* (Dinosauria: Hadrosauridae) from the late Campanian Kaiparowits Formation, southern Utah, USA. *Zoological Journal of the Linnean Society* 151:351-376.

Gates TA, Zanno LE, and Makovicky PJ. 2013. Theropod teeth from the upper Maastrichtian Hell Creek Formation "Sue" quarry: morphotypes and faunal comparisons. *Acta Palaeontologica Polonica* 60:131-139.

Gerke O, and Wings O. 2016. Multivariate and cladistic analyses of isolated teeth reveal sympatry of theropod dinosaurs in the Late Jurassic of Northern Germany. *PLOS One* 11:e0158334.

González-José R, Escapa I, Neves WA, Cúneo R, and Pucciarelli HM. 2008. Cladistic analysis of continuous modularized traits provides phylogenetic signals in Homo evolution. *Nature* 453:775.

Hammer Ø, Harper D, and Ryan P. 2001. Paleontological statistics software: Package for education and data analysis. *Palaeontologia Electronica*.

Harvati K. 2003. Quantitative analysis of Neanderthal temporal bone morphology using three-dimensional geometric morphometrics. *American Journal of Physical Anthropology* 120:323-338.

Hasegawa Y, Manabe M, Isaji S, Ohkura M, Shibata I, and Yamaguchi I. 1995. Terminally Resorbed Iguanodontid Teeth from the Neocomian Tetori Group, Ishikawa and Gifu Prefecture, Japan. *Bulletin of the National Science Museum Toykyo Series C* 21:35-49.

Heckert AB. 2004. Late Triassic microvertebrates from the lower Chinle Group (Otischalkian-Adamanian: Carnian), southwestern U.S.A. *New Mexico Museum of Natural History and Science Bulletin* 27:1-170.

Hendrickx C, and Mateus O. 2014. Abelisauridae (Dinosauria: Theropoda) from the Late Jurassic of Portugal and dentition-based phylogeny as a contribution for the identification of isolated theropod teeth. *Zootaxa* 3759.

Hendrickx C, Mateus O, and Araújo R. 2014. The dentition of megalosaurid theropods. *Acta Palaeontologica Polonica* 60:627-642.

Hendrickx C, Mateus O, and Araújo R. 2015. A proposed terminology of theropod teeth (Dinosauria, Saurischia). *Journal of Vertebrate Paleontology* 35:e982797.

Hotelling H. 1933. Analysis of a complex of statistical variables into principal components. *Journal of educational psychology* 24:417.

Joshi SH, Prieto-Marquez A, and Parker WC. 2011. A landmark-free method for quantifying biological shape variation. *Biological Journal of the Linnean Society* 104:217-233.

Klingenberg CP, and Gidaszewski NA. 2010. Testing and quantifying phylogenetic signals and homoplasy in morphometric data. *Systematic Biology* 59:245-261.

Kulemeyer C, Asbahr K, Gunz P, Frahnert S, and Bairlein F. 2009. Functional morphology and integration of corvid skulls–a 3D geometric morphometric approach. *Frontiers in Zoology* 6:2.

Kundrát M, Cruickshank AR, Manning TW, and Nudds J. 2008. Embryos of therizinosauroid theropods from the Upper Cretaceous of China: diagnosis and analysis of ossification patterns. *Acta Zoologica* 89:231-251.

Larson DW. 2008. Diversity and variation of theropod dinosaur teeth from the uppermost Santonian Milk River Formation (Upper Cretaceous), Alberta: a quantitative method supporting identification of the oldest dinosaur tooth assemblage in Canada. *Canadian Journal of Earth Sciences* 45:1455-1468. 10.1139/e08-070

Larson DW, and Currie PJ. 2013. Multivariate analyses of small theropod dinosaur teeth and implications for paleoecological turnover through time. *PLOS One* 8:e54329.

Larsson H, and Sidor C. 1999. Unusual crocodyliform teeth from the Late Cretaceous (Cenomanian) of southeastern Morocco. *Journal of Vertebrate Paleontology* 19:398-401.

Lautenschlager S. 2014. Morphological and functional diversity in therizinosaur claws and the implications for theropod claw evolution. *Proceedings of the Royal Society of London B: Biological Sciences* 281:20140497.

Lestrel PE. 1982. A Fourier analytic procedure to describe complex morphological shapes. *Progress in clinical and biological research* 101:393-409.

Lestrel PE. 1989. Method for analyzing complex two-dimensional forms: Elliptical Fourier functions. *American Journal of Human Biology* 1:149-164.

Lloyd GT. 2011. A refined modelling approach to assess the influence of sampling on palaeobiodiversity curves: new support for declining Cretaceous dinosaur richness. *Biology Letters* 8:123-126.

Lohmann G. 1983. Eigenshape analysis of microfossils: a general morphometric procedure for describing changes in shape. *Journal of the International Association for Mathematical Geology* 15:659-672.

Long RA, and Murry PA. 1995. Late Triassic (Carnian and Norian) tetrapods from the southwestern United States. *New Mexico Museum of Natural History and Science Bulletin* 4:254 p.

Longrich N. 2008. Small theropod teeth from the Lance Formation of Wyoming, USA. In: Sankey JT, and Baszio S, eds. *Life of the Past*. Bloomington: Indiana University Press, 135-158.

Lucas SG, Estep JW, Heckert AB, and Hunt AP. 1999. Cynodont teeth from the Upper Triassic of New Mexico, U.S.A. *Neues Jahrbuch für Geologie und Paläontologie Monatshefte* 1999:331-344.

Lucas SG, Heckert AB, and Sullivan RM. 2000. Cretaceous dinosaurs in New Mexico. *New Mexico Museum of Natural History and Science Bulletin* 17:83-90.

Lucas SG, Spielmann JA, Sullivan RM, Hunt AP, and Gates T. 2006. *Anasazisaurus*, a hadrosaurian dinosaur from the Upper Cretaceous of New Mexico. *New Mexico Museum of Natural History and Science Bulletin* 35:293-297.

MacLeod N. 1999. Generalizing and extending the eigenshape method of shape space visualization and analysis. *Paleobiology* 25:107-138.

Marugan-Lobon J, and Buscalioni AD. 2003. Disparity and geometry of the skull in Archosauria (Reptilia: Diapsida). *Biological Journal of the Linnean Society* 80:67-88.

Marugán-Lobón J, and Buscalioni ÁD. 2009. New insight on the anatomy and architecture of the avian neurocranium. *The Anatomical Record* 292:364-370.

Naylor GJ, and Marcus LF. 1994. Identifying isolated shark teeth of the genus Carcharhinus to species: relevance for tracking phyletic change through the fossil record. American Museum novitates; no. 3109.

Nickel M, Bullinger E, and Beckmann F. 2006. Functional morphology of Tethya species (Porifera): 2. Three-dimensional morphometrics on spicules and skeleton superstructures of T. minuta. *Zoomorphology* 125:225.

Nydam RL. 2000. New records of Early, Medial, and Late Cretaceous lizards and the evolution of the Cretaceous lizard fauna of North America PhD. University of Oklahoma.

Olsen AM, and Westneat MW. 2015. StereoMorph: an R package for the collection of 3D landmarks and curves using a stereo camera set-up. *Methods in Ecology and Evolution* 6:351-356.

Oreska MPJ, Carrano MT, and Dzikiewicz KM. 2013. Vertebrate paleontology of the Cloverly Formation (Lower Cretaceous), I: faunal composition, biogeographic relationships, and sampling. *Journal of Vertebrate Paleontology* 33:264-292. 10.1080/02724634.2012.717567

Papazzoni CA. 2003. A pliosaurid tooth from the Argille Varicolori Formation near Castelvecchio di Prignano (Modena Province, Northern Italy). *Rivista Italiana di Paleontologia e Stratigrafia (Research In Paleontology and Stratigraphy)* 109.

Pearson K. 1895. Note on regression and inheritance in the case of two parents. *Proceedings of the Royal Society of London* 58:240-242.

Pearson K. 1901. On lines and planes of closest fit to systems of points in space. *The London, Edinburgh, and Dublin Philosophical Magazine and Journal of Science* 2:559-572.

Photoshop A. 2015. User Guide. *San Jose, CA: Adobe Systems*.

Polly PD. 2012. Geometric morphometrics for Mathematica. Version.

Pomidor BJ, Makedonska J, and Slice DE. 2016. A landmark-free method for three-dimensional shape analysis. *PLOS One* 11:e0150368.

Rauhut OWM, and Fechner R. 2005. Early development of the facial region in a non-avian theropod dinosaur. *Proceedings of the Royal Society B* 272:1179-1183. 10.1098/rspb.2005.3071

Richtsmeier JT, Burke Deleon V, and Lele SR. 2002. The promise of geometric morphometrics. *American Journal of Physical Anthropology* 119:63-91.

Rohlf F. 2016. TpsDig2, Digitize Landmarks and Outlines v2.32. *Stony Brook, NY: Department of Ecology and Evolution, State University of New York*.

Rohlf FJ. 1998. On applications of geometric morphometrics to studies of ontogeny and phylogeny. *Systematic Biology* 47:147-158.

Rohlf FJ. 2018. tpsUtil, file utility program, version 1.76. *Department of Ecology and Evolution, State University of New York at Stony Brook*.

Ryan MJ, and Currie PJ. 2005. Ornithischian dinosaurs. In: Currie PJ, and Koppelhus EB, eds. *Dinosaur Provincial Park: A spectacular ancient ecosystem revealed*. Bloomington: Indiana University Press, 312-348.

Samman T, Powell GL, Currie PJ, and Hills LV. 2005. Morphometry of the teeth of western North American tyrannosaurids and its applicability to quantitative classification. *Acta Palaeontologica Polonica* 50:757-776.

Sampson S, Loewen M, Roberts E, Smith J, Zanno L, and Gates T. 2004. Provincialism in Late Cretaceous terrestrial faunas: new evidence from the Campanian Kaiparowits Formation of Utah. Journal of Vertebrate Paleontology: Soc Vertebrate Paleontology 60 Revere Dr, Ste 500, Northbrook, Il 60062 Usa. P 108a-108a.

Sampson SD, Loewen MA, Farke AA, Roberts EM, Forster CA, Smith JA, and Titus AL. 2010. New horned dinosaurs from Utah provide evidence for intracontinental dinosaur endemism. *PLOS One* 5:1-12. 10.1371/journal.pone.0012292

Sampson SD, Loewen MA, Roberts EM, and Getty MA. 2013. A new macrovertebrate assemblage from the Late Cretaceous (Campanian) of southern Utah. Indiana University Press.

Sankey JT. 2001. Late Campanian southern dinosaurs, Aguja Formation, Big Bend, Texas. *Journal of Paleontology* 75:208-215.

Sankey JT, Brinkman DB, Guenther M, and Currie PJ. 2002. Small theropod and bird teeth from the late Cretaceous (late Campanian) Judith River Group, Alberta. *Journal of Paleontology* 76:751-763.

Schoch RR, Ullmann F, Rozynek B, Ziegler R, Seegis D, and Sues H-D. 2018. Tetrapod diversity and palaeoecology in the German Middle Triassic (Lower Keuper) documented by tooth morphotypes. *Palaeobiodiversity and Palaeoenvironments*:1-24.

Shellis R, Beynon A, Reid D, and Hiiemae K. 1998. Variations in molar enamel thickness among primates. *Journal of Human Evolution* 35:507-522.

Sloan RE, Rigby JK, Van Valen LM, and Gabriel D. 1986. Gradual dinosaur extinction and simultaneous ungulate radiation in the Hell Creek Formation. *Science* 232:629-633.

Small CG. 2012. *The statistical theory of shape*: Springer Science & Business Media.

Smith J, Sampson S, Roberts E, Gates T, Getty M, and Zanno L. 2003. Fossil vertebrates from the Kaiparowits Fm, Grand Staircase-Escalante National Monument: an important window into the late Cretaceous of Utah. Journal of Vertebrate Paleontology: Taylor & Francis Inc 530 Chestnut Street, Ste 850, Philadelphia, Pa 19106 Usa. p 98A-98A.

Smith J, Sampson S, Roberts E, Getty M, and Loewen M. 2004. A new chasmosaurine ceratopsian from the Upper Cretaceous Kaiparowits Formation, Grand Staircase-Escalante National Monument, Utah. Journal of Vertebrate Paleontology: Society of Vertebrate Paleontology 60 Revere Dr, Ste 500, Northbrook, Il 60062 Usa. p 114A-114A.

Smith JB. 2005. Heterodonty in *Tyrannosaurus rex*: implications for the taxonomic and systematic utility of theropod dentitions. *Journal of Vertebrate Paleontology* 25:865-887.

Smith JB, Vann DR, and Dodson P. 2005. Dental morphology and variation in theropod dinosaurs: implications for the taxonomic identification of isolated teeth. *The Anatomical Record Part A: Discoveries in Molecular, Cellular, and Evolutionary Biology* 285:699-736.

Stone J. 2003. Mapping cladograms into morphospaces. *Acta Zoologica* 84:63-68.

Sues H-D, and Averianov A. 2013. Enigmatic teeth of small theropod dinosaurs from the Upper Cretaceous (Cenomanian-Turonian) of Uzbekistan. *Canadian Journal of Earth Sciences* 50:306-314. 10.1139/e2012-033

Sullivan RM. 2006. *Saurornitholestes robustus*, n. sp. (Theropoda: Dromaeosauridae) from the Upper Cretaceous Kirtland Formation (De-na-zin Member), San Juan Basin, New Mexico. *New Mexico Museum of Natural History and Science Bulletin* 35:253-256.

Sullivan RM, and Lucas SG. 2000. First occurrence of *Saurornitholestes* (Theropoda: Dromaeosauridae) from the Upper Cretaceous of New Mexico. *New Mexico Museum of Natural History and Science Bulletin* 17:105-108.

Sullivan RM, and Lucas SG. 2006. The pachycephalosauird dinosaur *Stegoceras validum* from the Upper Cretaceous Fruitland Formation, San Juan Basin, New Mexico. *New Mexico Museum of Natural History and Science Bulletin* 35:329-330.

Teaford MF. 1988. Scanning electron microscope diagnosis of wear patterns versus artifacts on fossil teeth. *Scanning Microscopy* 2:1167-1175.

Thompson D. 1917. On growth and form. *Cambridge: Cambridge University Press*.

Tsuihiji T, Watabe M, Tsogtbaatar K, Tsubamoto T, Barsbold R, Suzuki S, Lee AH, Ridgely RC, Kawahara Y, and Witmer LM. 2011. Cranial osteology of a juvenile specimen of *Tarbosaurus bataar* (Theropoda, Tyrannosauridae) from the Nemegt Formation (Upper Cretaceous) of Bugin Tsav, Mongolia. *Journal of Vertebrate Paleontology* 31:497 - 517.

Wagner JR, and Lehman TM. 2009. An enigmatic new lambeosaurine hadrosaur (Reptilia: Dinosauria) from the Upper Shale Member of the Campanian Aguja Formation of Trans-Pecos Texas. *Journal of Vertebrate Paleontology* 29:605-611. doi:10.1671/039.029.0208

Wang S, Stiegler J, Amiot R, Wang X, Du G-h, Clark JM, and Xu X. 2017. Extreme ontogenetic changes in a ceratosaurian theropod. *Current Biology* 27:144-148.

Weishampel DB, Mulder EW, Dortangs RW, Jagt JW, Jianu C-M, Kuypers MM, Peeters HH, and Schulp AS. 1999. Dinosaur remains from the type Maastrichtian: an update. *Geologie en Mijnbouw* 78:357-365.

Williamson TE, and Brusatte SL. 2014. Small theropod teeth from the Late Cretaceous of the San Juan Basin, northwestern New Mexico and their implications for understanding Latest Cretaceous dinosaur evolution. *PLOS One* 9:e93190.

Zanno L. 2007. A new troodontid theropod from the late Campanian Kaiparowits Formation, southern Utah. Journal of Vertebrate Paleontology: Soc Vertebrate Paleontology 60 Revere Dr, Ste 500, Northbrook, Il 60062 Usa. P 170a-171a.

Zanno L, Sampson S, Roberts E, and Gates T. 2005a. Late Campanian theropod diversity across the Western Interior Basin. Journal of Vertebrate Paleontology: Society Vertebrate Paleontology 60 Revere Dr, Ste 500, Northbrook, Il 60062 Usa. p 133A-134A.

Zanno LE, Gates T, Sampson S, Smith J, and Getty M. 2005b. Dinosaur diversity and biogeographical implications of the Kaiparowits Formation (Late Campanian), Grand Staircase-Escalante National Monument, southern Utah. Geol Soc Am Abstr Programs.

Zanno LE, Loewen MA, Farke AA, Kim G-S, Claessens L, and McGarrity CT. 2013. Late Cretaceous theropod dinosaurs of southern Utah. *At the Top of the Grand Staircase: The Late Cretaceous of Southern Utah Edited by AL Titus and MA Loewen Indiana University Press, Bloomington*:504-525.

Zanno LE, and Makovicky PJ. 2011. On the earliest record of Cretaceous tyrannosauroids in western North America: implications for an Early Cretaceous Laurasian interchange event. *Historical Biology* 23:317-325.

Zanno LE, Varricchio DJ, O'Connor PM, Titus AL, and Knell MJ. 2011. A new troodontid theropod, *Talos sampsoni* gen. et sp. nov., from the Upper Cretaceous Western Interior Basin of North America. *PLOS One* 6:e24487.

Zelditch ML, Fink WL, and Swiderski DL. 1995. Morphometrics, homology, and phylogenetics: quantified characters as synapomorphies. *Systematic Biology* 44:179-189.

Zinke J. 1998. Small theropod teeth from the Upper Jurassic coal mine of Guimarota (Portugal). *Paläontologische Zeitschrift* 72:179-189.